Universität Bremen

Fachbereich für Maschinenbau und Verfahrenstechnik
Masterstudiengang Space Engineering

Feasibility analysis of SpaceX' Starship from a mission analysis point of view

von

Mika Bauerfeind

Masterarbeit zur Erlangung des akademischen Grades

***Master of Science* (M.Sc.)**

in Space Engineering

Gutachter

1. Gutachter: Dr. Volker Maiwald, DLR Institut für Raumfahrtsysteme
2. Gutachter: Dr. Oliver Romberg, DLR Institut für Raumfahrtsysteme

Eingereicht von

Mika Bauerfeind

Matrikel-Nummer: 6017690
E-Mail: mika.bauerfeind@uni-bremen.de

Bremen, 09.12.2022

Universität Bremen

Offizielle Erklärungen von

Nachname: ____________________________ Vorname: ____________________________

Matrikelnr.: ____________________________

A) Eigenständigkeitserklärung

Ich versichere, dass ich die vorliegende Arbeit selbstständig verfasst und keine anderen als die angegebenen Quellen und Hilfsmittel verwendet habe.
Alle Teile meiner Arbeit, die wortwörtlich oder dem Sinn nach anderen Werken entnommen sind, wurden unter Angabe der Quelle kenntlich gemacht. Gleiches gilt auch für Zeichnungen, Skizzen, bildliche Darstellungen sowie für Quellen aus dem Internet.
Die Arbeit wurde in gleicher oder ähnlicher Form noch nicht als Prüfungsleistung eingereicht.
Die elektronische Fassung der Arbeit stimmt mit der gedruckten Version überein.
Mir ist bewusst, dass wahrheitswidrige Angaben als Täuschung behandelt werden.

B) Erklärung zur Veröffentlichung von Bachelor- oder Masterarbeiten

Die Abschlussarbeit wird zwei Jahre nach Studienabschluss dem Archiv der Universität Bremen zur dauerhaften Archivierung angeboten. Archiviert werden:

1) Masterarbeiten mit lokalem oder regionalem Bezug sowie pro Studienfach und Studienjahr 10 % aller Abschlussarbeiten
2) Bachelorarbeiten des jeweils ersten und letzten Bachelorabschlusses pro Studienfach u. Jahr.

☐ Ich bin damit einverstanden, dass meine Abschlussarbeit im Universitätsarchiv für wissenschaftliche Zwecke von Dritten eingesehen werden darf.

☐ Ich bin damit einverstanden, dass meine Abschlussarbeit nach 30 Jahren (gem. §7 Abs. 2 BremArchivG) im Universitätsarchiv für wissenschaftliche Zwecke von Dritten eingesehen werden darf.

☐ Ich bin nicht damit einverstanden, dass meine Abschlussarbeit im Universitätsarchiv für wissenschaftliche Zwecke von Dritten eingesehen werden darf.

C) Einverständniserklärung über die Bereitstellung und Nutzung der Bachelorarbeit / Masterarbeit / Hausarbeit in elektronischer Form zur Überprüfung durch Plagiatssoftware

Eingereichte Arbeiten können mit der Software *Plagscan* auf einen hauseigenen Server auf Übereinstimmung mit externen Quellen und der institutionseigenen Datenbank untersucht werden.
Zum Zweck des Abgleichs mit zukünftig zu überprüfenden Studien- und Prüfungsarbeiten kann die Arbeit dauerhaft in der institutionseigenen Datenbank der Universität Bremen gespeichert werden.

☐ Ich bin damit einverstanden, dass die von mir vorgelegte und verfasste Arbeit zum Zweck der Überprüfung auf Plagiate auf den *Plagscan*-Server der Universität Bremen hochgeladen wird.

☐ Ich bin ebenfalls damit einverstanden, dass die von mir vorgelegte und verfasste Arbeit zum o.g. Zweck auf dem *Plagscan*-Server der Universität Bremen hochgeladen u. dauerhaft auf dem *Plagscan*-Server gespeichert wird.

☐ Ich bin nicht damit einverstanden, dass die von mir vorgelegte u. verfasste Arbeit zum o.g. Zweck auf dem *Plagscan*-Server der Universität Bremen hochgeladen u. dauerhaft gespeichert wird.

Mit meiner Unterschrift versichere ich, dass ich die oben stehenden Erklärungen gelesen und verstanden habe. Mit meiner Unterschrift bestätige ich die Richtigkeit der oben gemachten Angaben.

____________________________ ____________________________

Datum, Ort Unterschrift

Mathematical symbols

Constants

Symbol	Description	Value
μ_E	Gravitational parameter of Earth	$3.986\,004\,418 \cdot 10^5\,\mathrm{km^3\,s^{-2}}$
μ_M	Gravitational parameter of Mars	$4.282\,837 \cdot 10^4\,\mathrm{km^3\,s^{-2}}$
μ_S	Gravitational parameter of the Sun	$1.327\,124\,400\,18 \cdot 10^{11}\,\mathrm{km^3\,s^{-2}}$
g_0	Gravitational acceleration on Earth	$9.806\,65\,\mathrm{m\,s^{-2}}$

Variables

Symbol	Description	Units
Δv	Required velocity change	$\mathrm{km\,s^{-1}}$
Δv_c	Velocity change required for TCM	$\mathrm{km\,s^{-1}}$
Δv_E	Velocity change required at Earth	$\mathrm{km\,s^{-1}}$
Δv_l	Velocity change required for landing	$\mathrm{km\,s^{-1}}$
Δv_{LMO}	Velocity change required to reach a LMO	$\mathrm{km\,s^{-1}}$
Δv_M	Velocity change required at Earth	$\mathrm{km\,s^{-1}}$
Δt	Time of flight	s
$\Psi_{m_{P/L}}$	Penalty for the maximum payload mass	t
Ψ_t	Penalty for the minimum time of flight	d
φ	True anomaly	°
ϖ	Longitude of the periapsis	°
ω	Argument of the periapsis	°
Ω	Longitude of the ascending node	°
a	Semi-major axis of an orbit	km
c	Chord of a triangle	km
e	Eccentricity of an orbit	-
E	Eccentric anomaly	°
i	Inclination of an orbit	°
I_{sp}	Specific impulse of the Raptor engine	s
L	Mean longitude	°
m_0	Mass at departure	t
m_p	Propellant mass	t
$m_{P/L}$	Payload mass	t
m_s	Structural mass	t
M	Mean anomaly	°
Ma	Mach number	-
P	Orbital period	d
r	Distance of the spacecraft to the center of gravity	km
$\vec{R}$	Position vector of the planets	km
s	Semiperimeter of a triangle	km
t	Time	s
t_m	Time of flight on the minimum energy arc	s
u_s	Speed of sound	$\mathrm{m\,s^{-1}}$
v	Velocity (absolute value)	$\mathrm{m\,s^{-1}}$
$\vec{v}$	Velocity vector of the spacecraft	$\mathrm{km\,s^{-1}}$
$\vec{V}$	Velocity vector of the planets	$\mathrm{km\,s^{-1}}$

Abbreviations

Abbreviation	Description
ESA	European Space Agency
TOF	Time of flight
IAC	International Astronautical Congress
ISRU	In-situ resource utilization
LEO	Low-Earth-Orbit
LH2	Liquid hydrogen
LMO	Low-Mars-Orbit
LOX	Liquid oxygen
MAV	Mars ascent vehicle
MOI	Mars orbit injection
NASA	National Aeronautics and Space Administration
SOI	Sphere of influence
SpaceX	Space Exploration Technologies Corporation
TCM	Trajectory correction maneuver
TOI	Transfer orbit injection
TWR	Thrust-to-weight ratio
UTC	Coordinated Universal Time

Contents

1 Introduction and statement of work **9**

2 Theoretical background **10**
2.1 Technical design and data . . . 10
2.1.1 Super Heavy . . . 10
2.1.2 Raptor engine . . . 10
2.1.3 Starship . . . 11
2.2 Mars . . . 11
2.3 Earth-Mars-Earth trajectories . . . 12

3 Mission baseline **15**
3.1 Flight to Mars . . . 15
3.1.1 Departure from Earth . . . 15
3.1.2 Trajectory correction maneuver . . . 16
3.1.3 Arrival at Mars . . . 17
3.1.4 Landing at Mars . . . 18
3.2 Refuelling on Mars . . . 20
3.2.1 In situ resource utilization . . . 21
3.2.2 Fuel production . . . 21
3.3 Return to Earth . . . 21
3.3.1 Start from Mars . . . 21
3.3.2 Trajectory Correction Maneuver . . . 22
3.3.3 Arrival & landing at Earth . . . 22
3.4 Scheduling of flights . . . 23
3.4.1 SpaceX plans . . . 23
3.4.2 Launch opportunities . . . 23

4 Model development and methodology for the trajectory analysis **25**
4.1 Modelling of the planets' movement . . . 26
4.2 Lambert's problem . . . 28
4.3 Patched conics . . . 30
4.4 Total Delta-v . . . 31
4.5 Maximum payload mass . . . 31
4.6 Free-return trajectories . . . 32
4.7 Return flight . . . 33

5 Evaluation and analysis of results **34**
5.1 Restrictions . . . 34
5.1.1 Technical restrictions . . . 34
5.1.2 Computational restrictions . . . 35
5.1.3 Fixed parameters . . . 37
5.2 2028/2029 launch opportunity . . . 37
5.2.1 Minimum Delta-v and time of flight . . . 37
5.2.2 Maximum allowable payload mass to Mars . . . 40
5.2.3 Free-return trajectories . . . 42
5.3 2031 launch opportunity . . . 42
5.3.1 Minimum Delta-v and time of flight . . . 43
5.3.2 Maximum allowable payload mass to Mars . . . 45

5.3.3 Free-return trajectories . . . 47
5.4 2033 launch opportunity . . . 47
5.4.1 Minimum Delta-v and time of flight . . . 47
5.4.2 Maximum allowable payload mass to Mars . . . 50
5.4.3 Free-return trajectories . . . 51
5.5 2035 launch opportunity . . . 52
5.5.1 Minimum Delta-v and time of flight . . . 52
5.5.2 Maximum allowable payload mass to Mars . . . 55
5.5.3 Free-return trajectories . . . 55
5.6 2037 launch opportunity . . . 56
5.6.1 Minimum Delta-v and time of flight . . . 57
5.6.2 Maximum allowable payload mass to Mars . . . 59
5.6.3 Free-return trajectories . . . 59
5.7 Summary . . . 60
5.8 Return flight from Mars to Earth . . . 61
5.8.1 Restrictions and fixed parameters . . . 61
5.8.2 Return flight in 2030/2031 . . . 62
5.8.3 Return flight in 2033 . . . 62
5.8.4 Return flight in 2035 . . . 64
5.8.5 Return flight in 2037 . . . 64
5.8.6 Return flight in 2039 . . . 64
5.8.7 Summary . . . 66
5.9 Feasibility of flight times of 30 days . . . 66

6 Sensitivity analysis 69
6.1 Departure Date . . . 69
6.1.1 2029 launch opportunity . . . 69
6.1.2 2031 launch opportunity . . . 70
6.1.3 2033 launch opportunity . . . 70
6.1.4 2035 launch opportunity . . . 71
6.1.5 2037 launch opportunity . . . 72
6.1.6 Summary . . . 72
6.2 Time of flight . . . 73
6.2.1 2029 Launch Opportunity . . . 73
6.2.2 2031 Launch Opportunity . . . 73
6.2.3 2033 Launch Opportunity . . . 74
6.2.4 2035 Launch Opportunity . . . 75
6.2.5 2037 Launch Opportunity . . . 75
6.2.6 Summary . . . 76
6.3 Specific Impulse . . . 77
6.3.1 2029 Launch Opportunity . . . 77
6.3.2 2031 Launch Opportunity . . . 77
6.3.3 2033 Launch Opportunity . . . 78
6.3.4 2035 Launch Opportunity . . . 79
6.3.5 2037 Launch Opportunity . . . 79
6.3.6 Summary . . . 80
6.4 Maximum hyperbolic periapse velocity at Mars . . . 81
6.4.1 2029 launch opportunity . . . 81
6.4.2 2031 launch opportunity . . . 83

6.4.3 2033 launch opportunity . . . 85
6.4.4 2035 launch opportunity . . . 87
6.4.5 2037 launch opportunity . . . 89
6.4.6 Summary . . . 90
6.5 Propellant mass . . . 92
6.5.1 2029 launch opportunity . . . 92
6.5.2 2031 launch opportunity . . . 95
6.5.3 2033 launch opportunity . . . 98
6.5.4 2035 launch opportunity . . . 100
6.5.5 2037 launch opportunity . . . 103
6.5.6 Summary . . . 106
6.6 Maturity of the system . . . 106
6.6.1 Aggressive approach . . . 106
6.6.2 Mean approach . . . 108
6.6.3 Conservative approach . . . 109
6.6.4 Summary . . . 110

7 Feasibility assessment **112**

8 Outlook and future work **114**

1 Introduction and statement of work

Sending humans to another celestial body in our solar system has been a target for humanity ever since the very beginning of space engineering. After this target was achieved with the moon landings during the Apollo program in the late 1960s and early 1970s, attention has shifted towards a human Mars mission. In recent years, the private company SpaceX, founded and led by Elon Musk, has become the front runner in the contest to first send humans to Mars. Probably, Elon Musk is the most controversial person in the space sector, admired by many and called overrated by many others. The same accounts for SpaceX Mars mission plans: For some people, it is only a matter of time until we land on Mars with the spacecrafts developed by SpaceX. Others can not imagine that these goals will be achieved and doubt the technical concept in general. The plan of SpaceX is to build the strongest rocket of all times, Super Heavy, with a large interplanetary spacecraft, Starship, on top. This configuration shall enable the transport of hundreds of tons of payload to Mars with every flight and hence, build up a base on Mars that in the future will be the home for millions of people.
The analysis of the feasibility of SpaceX' plans covers many different aspects, for example the propulsion system of Starship or the building of their Mars base, to name just two of them. To cover and assess the feasibility of all aspects, a team of many engineers would be needed. Therefore, I choose to limit my analysis to one single aspect of the mission plans, the mission analysis. This means that in this document, I will develop a model for the analysis of the trajectories that bring Starship from Earth to Mars and back. Afterwards, I will analyse and evaluate the results of this analysis with respect to different parameters. The other part of this work will be a sensitivity analysis of Starship and its associated components. Based on the results of the two parts of my work, I will assess the feasibility of SpaceX mission plans from the view of a mission analyst and point out steps that should be performed in the future.

2 Theoretical background

In this chapter, supplementary information that support the methodology and calculations, which are carried out at a later point, are shown.

2.1 Technical design and data

In order to examine the mission, it is necessary to first describe some parameters of the system. It is built up of two stages, the suborbital booster stage and the interplanetary cruise stage. In the following sections, the core parts of the system will be described in brief fashion and the most important data, on which the calculations will built up, are shown.

2.1.1 Super Heavy

Super Heavy is the first stage of the system, acting as a booster to bring Starship and its payload into orbit. It has a height of 69 m and measures 9 m in diameter. It is powered by a CH_4/LOX propulsion system and has a propellant capacity of 3400 t, which allows it to produce a thrust of up to 74.4 MN [1]. According to Elon Musk, SpaceX aims to lower the dry mass of Super Heavy to 200 t [2].

2.1.2 Raptor engine

The raptor engine is featured onboard of the system in two different configurations. One configuration optimized for sea-level-pressure that has a specific impulse of 330 s and one optimized for vacuum with a specific impulse of 378 s. 33 of the sea-level-optimized Raptors are built on the Super Heavy first stage and three of the vacuum optimized are featured on Starship [3]. There are efforts by SpaceX to raise the specific impulse of the vacuum specification to 380 s [2]. An artist's render of a Raptor engine is shown in figure 1.

Figure 1: Artist's render of a Raptor engine. (Source: [1])

Figure 2: Footage of Starship SN15 during flight. (Source: [1])

2.1.3 Starship

Even though the whole system is often referred to as "Starship", Starship is only the upper stage. An image of the Starship with the serial number 15 during test flight can be seen in figure 2. It is the only part of the system that actually reaches orbit and serves as a cruise stage for the travel to Mars. It can be flown either manned or unmanned. It is designed to, at a dry mass of 100 t [3], hold a propellant mass of 1200 t [1]. Just as Super Heavy, the propulsion system onboard of Starship uses methane and liquid oxygen. After Starship is separated from Super Heavy at an altitude of 70 km [4], it uses its own on-board propellant to establish an low-earth orbit. In this orbit, a Starship will dock together with a Tanker-Starship to fully refill its propellant capacity. A Tanker-Starship is similar to a "normal" Starship, but does not have any capacities for people or payload other than propellant. The refuelling allows a Starship to bring payloads in excess of 100 t to Mars [1]. The technical design of Starship influences the maximum Δv that it is able to apply. It can be calculated according to the following formula, the so-called Tsiolkovsky rocket equation:

$$\Delta v_{max} = I_{sp} \cdot g_0 \cdot \ln\left(\frac{m_s + m_p + m_{P/L}}{m_s + m_{P/L}}\right) \tag{1}$$

Where I_{sp} is the vacuum specific impulse of the Raptor engine, m_s is the structural dry mass, m_p is the mass of the propellant and $m_{P/L}$ is the payload mass.

2.2 Mars

Mars is the fourth inmost of the planets in the solar system, and orbits the Sun in a low-eccentric orbit ($e = 0.0935$) with a semi-major axis of 1.524 au. One revolution around the Sun,

i.e. one martian year, takes 686.98 Earth days. Mars is a terrestrial planet with a mean radius of 3389.5 km. It has a thin atmosphere, leading to a low surface pressure and as a result, no liquid water can exist on the surface of Mars. But it is assumed and suggested by observation and measurement data that water ice is present below the surface in polar regions [5] and also in midlatitude regions [6].
Mars' Atmosphere mainly consists of Carbon Dioxide (95.1 %), Nitrogen (2.6 %) and Argon (1.9 %). It extends to a height 250 km, where the Thermosphere ends [7]. The speed of sound in the lower martian atmosphere is $240\,\mathrm{m\,s^{-1}}$ [8].
In 2019, SpaceX published a list of 23 potential landing sites on Mars. In 2021, this list narrowed down to a remaining seven, of which four are classified as "prime" and three as "secondary" [9].

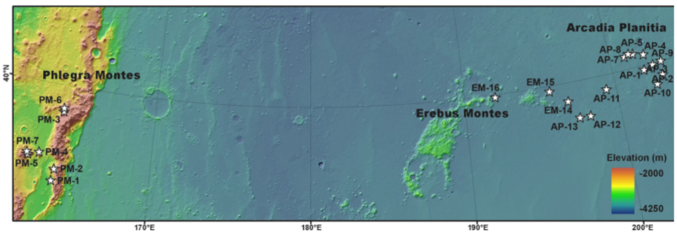

Fig. 1. Topographic map of Arcadia Planitia, Erebus and Phlegra Montes show landing sites considered for SpaceX Starship. Topography with respect to the MOLA geoid.

Table 1. Downselected prime (first 4) and secondary (last 3) landing sites

Landing Site	Latitude °N	Longitude °E	Elevation* km
PM-1	35.23	163.95	-3.2
AP-1	39.8	202.1	-3.9
AP-9	40.02	203.35	-3.9
EM-16	39.89	192.03	-3.9
AP-8	40.75	201.3	-3.9
EM-15	39.75	195.62	-3.9
PM-7	36.43	162.16	-2.3

*with respect to the MOLA geoid.

Figure 3: Overview of the potential landing sites for a SpaceX Mars mission. (Source: [9])

All of the potential landing sites are close to large amounts of water ice, close enough to the equator to ensure sufficient solar irradiation for solar panels and allow a safe landing with regard to the terrain.

2.3 Earth-Mars-Earth trajectories

In general, manned Mars mission trajectories are classified upon their stay time on Mars. One differentiates between the so-called conjunction-class and opposition-class missions. On the one hand, conjunction-class trajectories have long stay times of 400 to 600 days, short times of flight between the planets and modest propellant requirements [10]. On the other hand, opposition-class missions are characterized by short stay times of under 90 days, longer times of flight and higher propellant requirements [10]. Moreover, in most cases opposition-class trajectories require a Venus swing-by, which increases the complexity of the mission [10]. It can be seen by comparison that conjunction-class trajectories are the favorable option for manned missions. Furthermore, the boundary constraints that SpaceX describes for their mission concept only allow these type of trajectories, why I will limit the description and analysis to conjunction-class trajectories. The general concept of these trajectories will be described briefly in the following, for a optical impression, refer to figure 4.

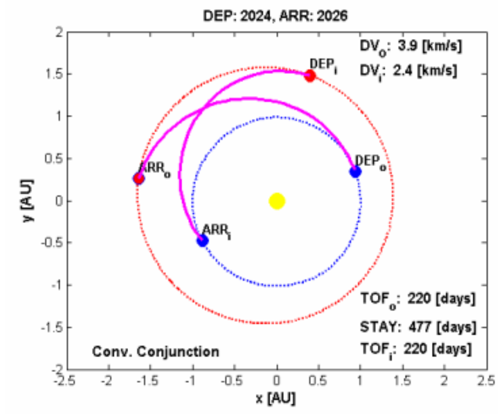

Figure 4: Schematic of a Earth-Mars-Earth conjunction-class trajectory. (Source: [10])

The spacecraft leaves Earth with a propulsive maneuver called *Transfer Orbit Injection* (TOI) and begins its cruise to Mars on a heliocentric trajectory. Upon arrival at Mars, another maneuver is required to alter the trajectory so that a landing becomes possible. This maneuver is called *Mars Orbit Insertion* (MOI). After the stay, the process is repeated to bring the spacecraft and the astronauts back to Earth. The possible trajectories and their properties will be discussed in chapter 4, but a specific trajectory concept shall be introduced now as well.
As many of the missions that feature Starship are manned and therefore the lives of humans are at stake in case of a malfunction during the cruise, it may be appropriate to develop a model for an abort during transfer and a return to Earth.
The most simple possibility to implement such a trajectory would be to use a trajectory between Earth and Mars that has a heliocentric period of two Earth years. Then, the spacecraft would return to Earth after two years and would not have to perform any propulsive maneuver other than the TOI. Such a trajectory called 2-year free return is shown schematically in figure 5.

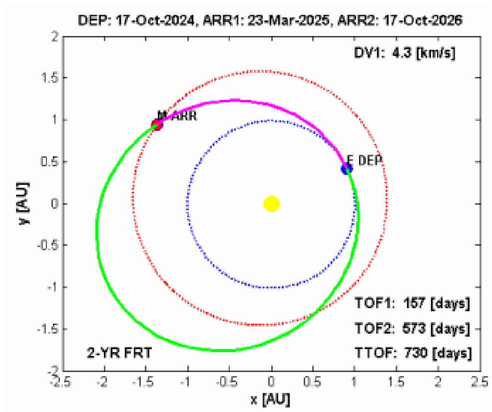

Figure 5: Schematic of a 2-year free return trajectory. (Source: [10])

Whether such an abort option should be implemented in the mission plans depends on multiple factors and is not to be discussed in this paper. For sure, a two-year travel in space would have severe negative influences on the human body. But in the most dramatic case it could be an option to save human lives. I think that this is enough motivation to at least highlight some possible trajectories in later chapters that allow such a free return.

3 Mission baseline

In this chapter, the general mission sequence of the cruise of a Starship shall be described. The mathematical models developed in chapter 4 will be based on the different steps outlined in this part.
The mission of a Starship may be divided in three different parts, the flight to Mars, the stay, and in particular the refuelling, on Mars and the flight back to Earth. In figure 6, the mission sequence as proposed by SpaceX can be seen. I decided to group every step on the upper line into the first part of the mission, the flight to Mars. The steps that take place on Mars, which is in the scope of this study only the refuelling, is grouped in the second part. And, finally, the lower line represents the flight back to Earth.

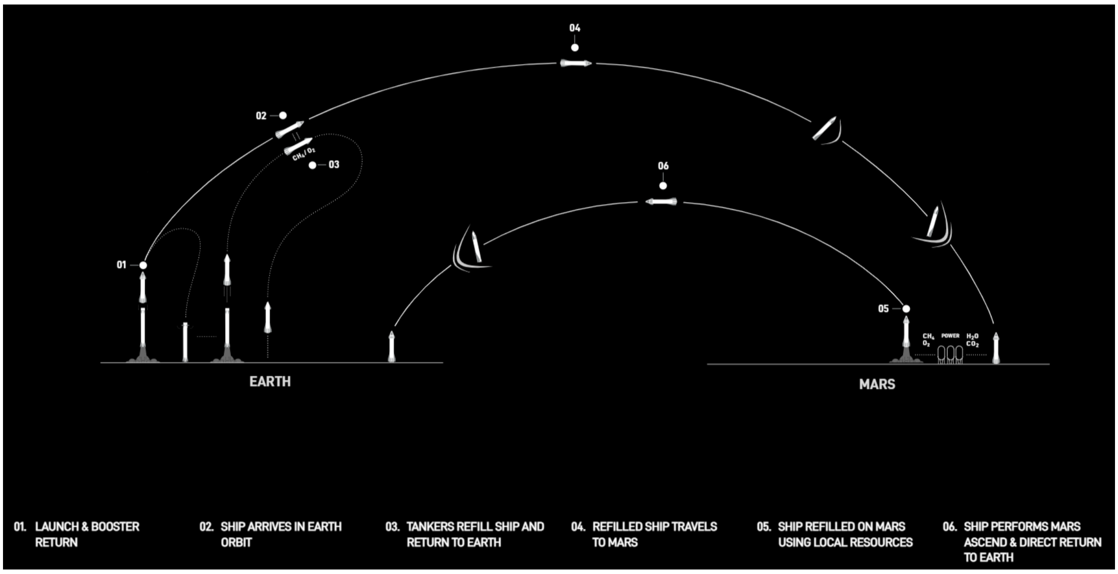

Figure 6: Mission schematic of one Starship flight to Mars and back to Earth. (Source: [11])

In the following subsections, each of the three parts is divided further into the key events and described from a mission analysis point of view.

3.1 Flight to Mars

The flight to Mars begins with the Launch of Starship and Super Heavy and ends with the landing of Starship on the surface of Mars. Between these two points, I identified three key events that I will discuss in this section. These are the refuelling of Starship in orbit, the trajectory correction maneuvers and the aerobraking in Mars' atmosphere.

3.1.1 Departure from Earth

The start of every trajectory analysis is the launch of the rocket and in particular the launch site. Currently, SpaceX is considering four potential launch sites, Kennedy Space Center, the Starbase at Boca Chica and two offshore launch platforms. The launch complex 39 at Kennedy Space Center offers every feature required to launch large rockets like Starship as it has been the launchsite for the Saturn V and the Space Shuttle in the past and will also host the SLS in the future. Nevertheless, the launch complex would still need to be adapted to the Starship as it exceeds all prior rockets in size and thrust [4]. After the launch, a manned Starship will change its orbit to perform a rendezvous with a so-called tanker Starship. These tanker Starships are unmanned versions that are filled with propellant only, in order to refill the manned Starships in orbit. Until date, no detailed technical description of the refuelling system is available to the public, so I assume the system to be thoroughly functional until the first launch. With respect to orbital mechanics, it is relevant to know the orbit in which the refuelling takes place. Most likely this will take place in a low-earth circular orbit, as this is the easiest to reach for both the crewed and uncrewed Starship. After the refuelling, the Starship will leave the circular low-earth orbit on a hyperbolic trajectory, more details on this are provided in 4.3.

3.1.2 Trajectory correction maneuver

Ideally, after the first propulsive maneuver, the spacecraft would be inserted in an orbit on which it would reach its target destination without any maneuvers upon arrival. In reality, it is impossible to insert the spacecraft in the ideal and planned trajectory. Sources of inaccuracy are for example insertion errors due to an excess in Δv implemented. To obtain the correct trajectory, it is necessary to implement multiple trajectory correction maneuvers (TCM), that alter the inaccurate trajectory to remove errors. A typical Mars mission features up to six TCM, implemented at different stages of the cruise as seen in figure 7 by the example of the trajectory of NASA's Mars 2020 mission. The first TCM, TCM-1, usually takes place 10 to 15 days after the launch and is used to remove the aforementioned errors due to the inaccurate injection. As some missions require an intentional bias to their injection maneuvers due to planetary protection means [12], the bias would also be removed in this TCM. The next two maneuvers, TCM-2 and TCM-3, are implemented to remove the errors of the prior maneuver each which are a result of inaccuracies in the firing process of the propulsive maneuver. The last three maneuvers are taking place in the approach phase of the mission and are used to target the landing site.

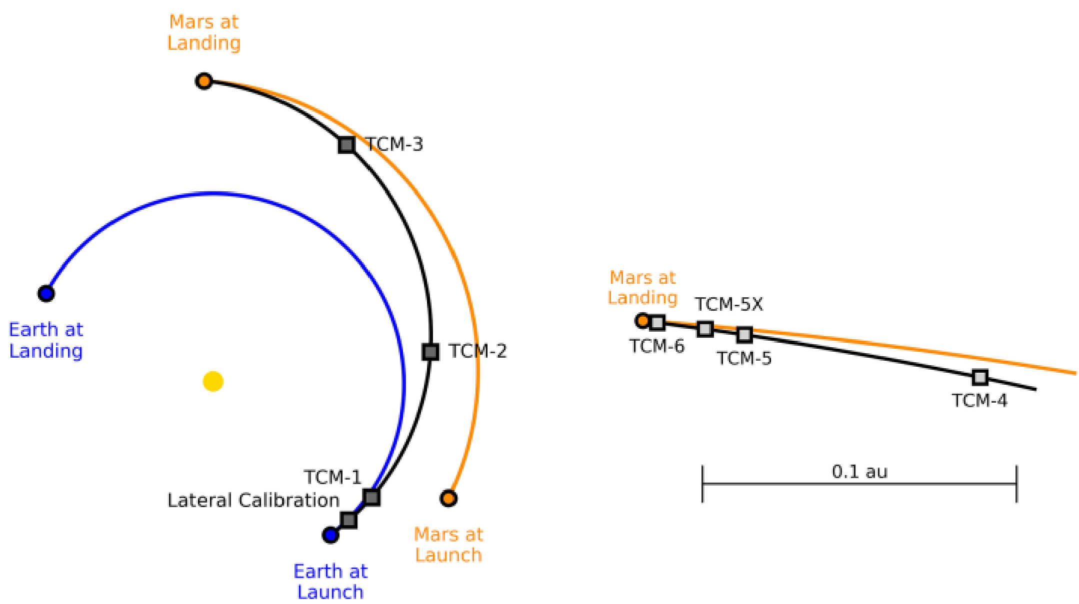

Figure 7: Schematic of the TCM of the Mars 2020 mission. (Source: [12])

In table 2, the implemented Δv for the sum of all TCM of different missions are collected and shown. It becomes evident that compared with the total required Δv for the missions, the values are almost neglectfully small.

Table 2: Overview of the required Δv for the TCM of different Mars lander missions

Mission	Δv [$\mathrm{m\,s^{-1}}$]	**Source**
Mars 2020	2.928	[12]
MSL	16.690	[13]
Insight	5.584	[14]
Pathfinder	32.939	[15]
Spirit	23.070	[16]
Opportunity	16.813	[16]

Even though these values are of no major importance for their missions, it should be considered that all of these missions have been unmanned and had, compared with the Starship mission, large target landing areas. A Starship must be able to land as precise as less than 1 km. As can be seen in table 3, none of these missions achieved an accuracy as required for Starship. In fact, most of them missed their target landing location by more than 10 km, what, however, did not pose a danger to their mission objectives.

Table 3: Overview of the achieved landing accuracy of different Mars lander missions

Mission	**Achieved distance to landing site** [km]	**Source**
Mars 2020	7.4	[12]
MSL	2.3	[17]
Insight	20.0	[14]
Pathfinder	30.0	[15]
Spirit	10.1	[18]
Opportunity	24.6	[18]

In case of Starship, an inaccuracy like this would maybe not be a problem in the first missions, but at a later stage this could lead to collisions with built structures, for example. Therefore, it seams appropriate to demand a higher accuracy when targeting the landing sites than for the other missions presented. This results in the allocation of a higher Δv for the sum of the TCM during the cruise of Starship. Taking into account the numbers from table 2 and that Starship has a retro-propulsive landing system which is able to maneuver the spacecraft accurately, it seems suitable for me to assume a Δv_c of $200\,\mathrm{m\,s^{-1}}$ for all TCM during one flight of a Starship.

3.1.3 Arrival at Mars

When approaching Mars, Starship is travelling on a hyperbolic keplerian orbit with a certain inclination with respect to Mars as a result of the TCM. Starship is designed to remove 99 % of its kinetic energy when approaching Mars purely with aerobraking and in this way reduce its orbital altitude. This is possible when Starship enters the atmosphere at a velocity of $7.5\,\mathrm{km\,s^{-1}}$ or less with respect to Mars [19]. It must be ensured that the periapse of the hyperbola is acceptably low to allow Starship to safely perform the aerobraking maneuver. Lu suggests that the periapse

should be below 129 km over the surface [20]. One could follow two different approaches in order to comply with the two restrictions. Either one demands a propulsive maneuver shortly before or at the periapse to lower the velocity to the required $7.5\,\mathrm{km\,s^{-1}}$, or one allows only trajectories that do not exceed this velocity by default without any maneuver. Since Starship has only one propulsion system that is used for the TOI, the landing and also for the potential MOI as well as for all maneuvers on the flight back to Earth, it may therefore be preferable to reduce the number of firings of the engines as this would lower the risk of a failure. I will describe and analyze both of these approaches in the later parts of my work. For convenience, I will call the first approach *Type A* and the second *Type B*.
It is not described by SpaceX over which time span or number of revolutions around Mars the aerobraking-process takes place. But after the aerobraking, the remaining speed is removed with a retro-propulsive maneuver.

3.1.4 Landing at Mars

For this maneuver, different numbers are given by SpaceX for the required Δv. In an animation of the landing on their website [19], the retro-propulsive maneuver starts at an altitude of 2.5 km and a Mach number of 2.4. The Mach number can be converted in a standard velocity with the following relation:

$$v = Ma \cdot u_S$$

Where Ma is the Mach number and u_S is the speed of sound in Mars' lower atmosphere. With the numbers from 2.2, the velocity equivalent to Mach 2.4 is to be computed as follows:

$$v_{eq} = 2.4 \cdot 240\,\frac{\mathrm{m}}{\mathrm{s}} = 576\,\frac{\mathrm{m}}{\mathrm{s}}$$

This value is then equivalent to the required Δv for landing, Δv_l. The animation does not mention any influencing parameter for this value. The presentation that SpaceX gave at the *International Aeronautic Congress* in 2016 [21], features a slide (37) which implies that the Δv is indeed dependant on the payload mass. The respective graphic can be seen in figure 8. Of particular interest for this consideration is the light grey area 'RESERVED FOR MARS LANDING'. The height of this area gives the Δv that is required for the landing of Starship on Mars. It can be seen that with an increasing payload mass, the needed Δv increases as well. I retrieved the values of the Δv for different payload masses graphically. Due to my method, it should be assumed that the uncertainty of the measured values is as large as $\pm 31\,\mathrm{m\,s^{-1}}$. The values are shown in table 4 below.

Table 4: Δv required for landing on Mars depending on the payload mass

Payload [t]	Δv_l [$\mathrm{m\,s^{-1}}$]
200	813
300	975
400	1163
500	1438
600	1625

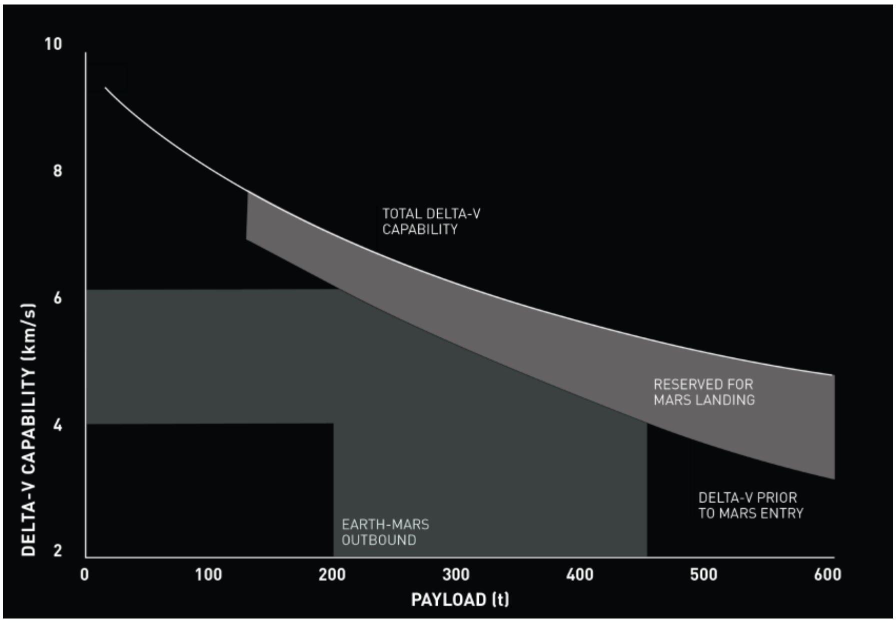

Figure 8: Δv-budget of a Starship mission according to SpaceX. (Source: [21], slide 37)

These values together with the uncertainty of the measurement are graphically presented in figure 9. Then a linear regression was performed in Excel to obtain a regression line that best fits the values.

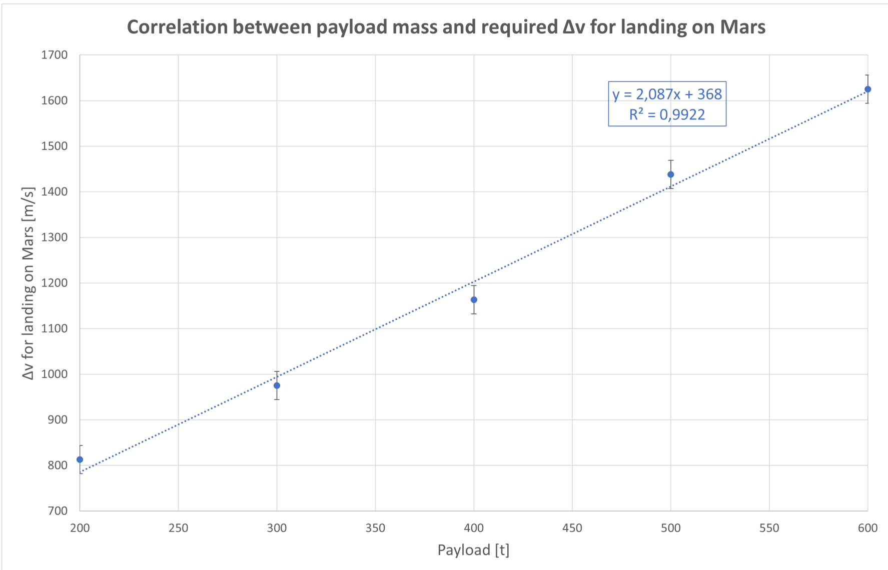

Figure 9: Δv required for landing on Mars depending on the payload mass. The dotted line represents a linear regression line to best fit the values. In the box, the linear equation for the regression line is given together with the determination coefficient.

The determination coefficient of 0.9922 indicates that the linear regression line fits the values good. After transferring the linear equation into my system with units, it will look as follows.

$$\Delta v_l = 2.087\,\frac{\mathrm{m}}{\mathrm{s}\cdot\mathrm{t}}\cdot m_{P/L} + 368\,\frac{\mathrm{m}}{\mathrm{s}}$$

Where $m_{P/L}$ is the payload mass and must be given in tons to fit the units. If one now adds the value of $576\,\mathrm{m\,s^{-1}}$ from the animation [19] to the values, the shape of the regression line changes only slightly. It is not directly stated that by SpaceX to which payload this value corresponds, but as their standard payload is 100 t, I assume that this is the corresponding payload.

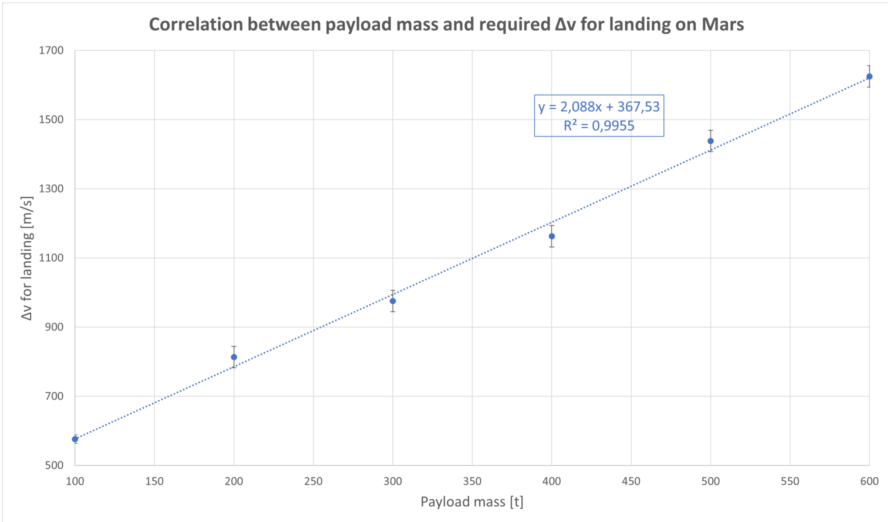

Figure 10: The concept is same as in figure 9, but this time includes the value from the animation [19].

After adding this data point, the determination coefficient increases slightly to 0.9955, which indicates that this linear regression is even more accurate. This approach yields the following equation for the value of Δv_l, which I will use for my simulation to obtain the values for the Δv required to land on Mars.

$$\Delta v_l = 2.088\,\frac{\mathrm{m}}{\mathrm{s}\cdot\mathrm{t}}\cdot m_{P/L} + 367.53\,\frac{\mathrm{m}}{\mathrm{s}} \tag{2}$$

It should be noted that the animation [19] and the presentation [21] assume a different entrance velocity into the martian atmosphere. But as the retro-propulsive maneuver would take place at the same velocity over ground in every landing, it is still acceptable to merge these two data.

3.2 Refuelling on Mars

From a mission analysis point of view, the stay on the martian surface is not of great interest. But since a key aspect of SpaceX' mission plans is to refuel Starship on Mars, and without this refuelling, there is no way to get back to Earth, I think it is a good idea to quickly discuss, how SpaceX plans to refuel the Starship on Mars. Key aspects during this stage of the mission are in situ resource utilization (ISRU) and the fuel production.

3.2.1 In situ resource utilization

ISRU describes the collection, processing, storing and utilization of materials found on another celestial body than Earth in order to replace materials that otherwise would have to be brought from Earth. In terms of Mars, the abundant chemical substances of particular interest are carbon dioxide (CO_2) and water ice (H_2O). As described in 2.2, Mars' atmosphere mainly consists of carbon dioxide and there are large sources of water ice beneath the surface. In order to use these resources, systems need to be developed and installed on Mars that can a) extract CO_2 from the atmosphere and b) drill into the ground to mine water ice and later melt it. With regard to the need of having such systems available in the next 10 - 20 years, concepts and prototypes have been developed for both the CO_2-extractor [22] as well as the water mining system [23].
These two resources can - and are planned to - be used by SpaceX for fuel production to use as propellant for Starship.

3.2.2 Fuel production

Starship uses liquid oxygen as oxidizer and methane as fuel for its propellant system. Oxidizer and fuel can be mined from carbon dioxide and water (ice) in the so called *Sabatier-Process*, which can be described with the following chemical equation [24].

$$CO_2 + 2\,H_2O \longrightarrow CH_4 + 2\,O_2$$

It is therefore possible to refuel Starship only with resources found and processed on Mars. This has two implications for the mission analysis. First, it is not necessary to save any propellant for the return flight, i.e. the 1200 t of propellant may be used for the flight to Mars only. In return, if there would be an excess in propellant after landing on Mars, it may be used for the return flight and would decrease the amount of propellant that must be produced on Mars. Second, it can be assumed that for the return flight, Starship can always be fully fueled up and therefore also utilize 1200 t of propellant.

3.3 Return to Earth

The last part of the mission is the return from Mars to Earth. The structure of this chapter is equivalent to the one of 3.1 and I am going to discuss the same aspects as in the latter. First, the start from Mars will be discussed, followed by the TCM and finally the arrival and landing at Earth.

3.3.1 Start from Mars

Different to the departure from Earth, Starship is not carried into orbit by the Super Heavy first stage. Therefore, Starship has to reach a low-altitude orbit first, from which it can then depart on a hyperbolic trajectory with respect to Mars. A circular Mars orbit with an altitude of 250 km has a corresponding orbital velocity of $3430\,\mathrm{m\,s^{-1}}$. If not for gravitational and frictional losses during the ascent, this would be the Δv to reach a low-mars-orbit (LMO). Since there is yet a spacecraft to start from Mars, no observation or measurement data is available for the mentioned losses. Some simulations for significantly smaller Mars Ascent Vehicles (MAV) have been carried out in the past. One that features a propulsion system similar to the one of Starship was proposed by Polsgrove et al. [25]. Their concept has a wet mass of 47.1 t, a LOX/CH_4 propulsion system that produces a thrust of 100 kN and therefore a thrust-to-weight ratio (TWR) of 1.75. It is a two-stage ascent vehicle and its first stage places it in an elliptical 100 km by 250 km orbit. The upper stage circularizes the orbit then to get into a circular 250 km altitude orbit. To reach its

final orbit, it requires a total Δv of $5274\,\mathrm{m\,s^{-1}}$. This means that in their case, the losses during the ascent sum up to $1844\,\mathrm{m\,s^{-1}}$.
The key performance parameter that influences the losses is the TWR, which is 3.04 in the case of Starship at Mars, when fully fueled with 1200 t of propellant. Due to the higher TWR, it is able to ascent faster than the MAV by Polsgrove et al., and the losses due to gravitational drag are smaller. On Earth, the gravity losses of a launch vehicle with a TWR of 1.75 are 2.5 to 3 times as high as for one with a TWR of 3 [26]. If one applies this proportionality factor to the value of $1844\,\mathrm{m\,s^{-1}}$, the losses would be in the range from $615\,\mathrm{m\,s^{-1}}$ to $738\,\mathrm{m\,s^{-1}}$. Vice versa, the atmospheric frictional losses are larger for launch vehicles with a high TWR, as they reach higher velocities inside the atmosphere. This value is even harder to estimate, as it also depends heavily on the aerodynamic profile and the launch trajectory. Considering the early stage of analysis of this study and the comparably thin atmosphere of Mars, I will neglect the atmospheric losses during ascent. Considering all of this, I will use a value of $700\,\mathrm{m\,s^{-1}}$ for the losses during ascent of a Starship flight. Therefore, the value to reach a LMO including losses, abbreviated with Δ_{LMO}, is $4130\,\mathrm{m\,s^{-1}}$.

3.3.2 Trajectory Correction Maneuver

Similar to the values of the losses during ascent in the previous section, also for the TCM of a return flight from Mars to Earth, no data is available. Therefore, I decided to use the same value as in 3.1.2, $200\,\mathrm{m\,s^{-1}}$, which is suitable, since in both cases the demanded landing accuracy is similar.

3.3.3 Arrival & landing at Earth

Similar to the arrival at Mars, Starship is proposed to remove almost all of its kinetic energy with aerobraking when entering Earth's atmosphere, as well. When approaching Earth, Starship is able to decelerate from perigee velocities of up to $12.5\,\mathrm{km\,s^{-1}}$ [21] with aerobraking only. Assuming that Earth's atmosphere ranges up to 500 km above ground, I will model the arrival hyperbola to have a perigee altitude of 500 km, where the process of aerobraking begins. This Δv that is achieved by aerobraking must not be considered in the calculations later. Only a comparably small velocity difference has to be overcome by the propulsion system and to be considered in the Δv-calculations. Based on figure 11, it seems plausible to assume that at Mach 0.25 in Earth's atmosphere, Starship begins to remove the remaining kinetic energy by retro-propulsion. The equivalent velocity to this Mach number is approximately:

$$v_{eq} = 85\,\frac{\mathrm{m}}{\mathrm{s}}$$

According to this NASA tool[1]. Taking into account some safety margin due to the inaccuracy of the graphic, I will use a fixed value of $100\,\mathrm{m\,s^{-1}}$ for the landing $\Delta v_{l,2}$ for all possible trajectories.

[1] https://www.grc.nasa.gov/www/k-12/rocket/machu.html

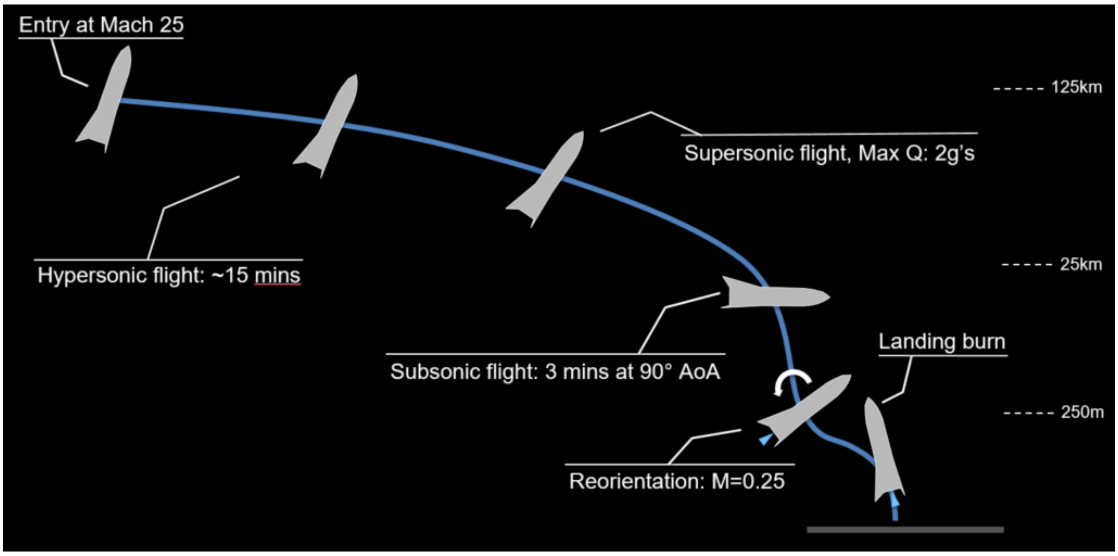

Figure 11: Schematic of Starship's reentry into Earth's atmosphere and landing. (Source: [4], Fig. 2-3)

3.4 Scheduling of flights

Since the mission plans of SpaceX are planning to built up a lasting human presence on Mars, there has to be a regular supply with materials, consumables and more. This means that there have to be regular launches of Starships over the first years until a working self-supporting infrastructure is installed on Mars.

3.4.1 SpaceX plans

This section is going to give a short overview over the desired time line by SpaceX for their first Mars flights. In figure 12, the mission plans by SpaceX back from 2017 can be seen. The time line presented there is no longer up-to-date, since flights to the Mars in 2022 are not possible. As stated by Elon Musk [28] and SpaceX COO Gwynne Shotwell [29], they now aim to land humans on Mars in 2029. This means that the above indicted crew & cargo missions for 2024 are now scheduled for 2029. Hence, the first cargo missions should be scheduled for 2027.

3.4.2 Launch opportunities

The feasibility to send a spacecraft from Earth to Mars is highly dependant on the alignment of the two planets. During certain periods, the planets are positioned relative to each other in a way that energy-efficient trajectories with an acceptable time of flight become possible. Outside of these periods, trajectories are only possible with high energy efforts, and hence a high Δv, what makes them practically infeasible. These periods are called *launch opportunities*, occur every 26 months between Earth and Mars [30] and span over the duration of a couple of months. It must be noted that these launch opportunities are not equivalent in terms of energy efficiency. The most energy efficient launch opportunity repeats every 15 years [30], the same accounts for the other opportunities. This means that there are seven different, repeating launch opportunities that can be ranked in terms of energy efficiency for possible trajectories.

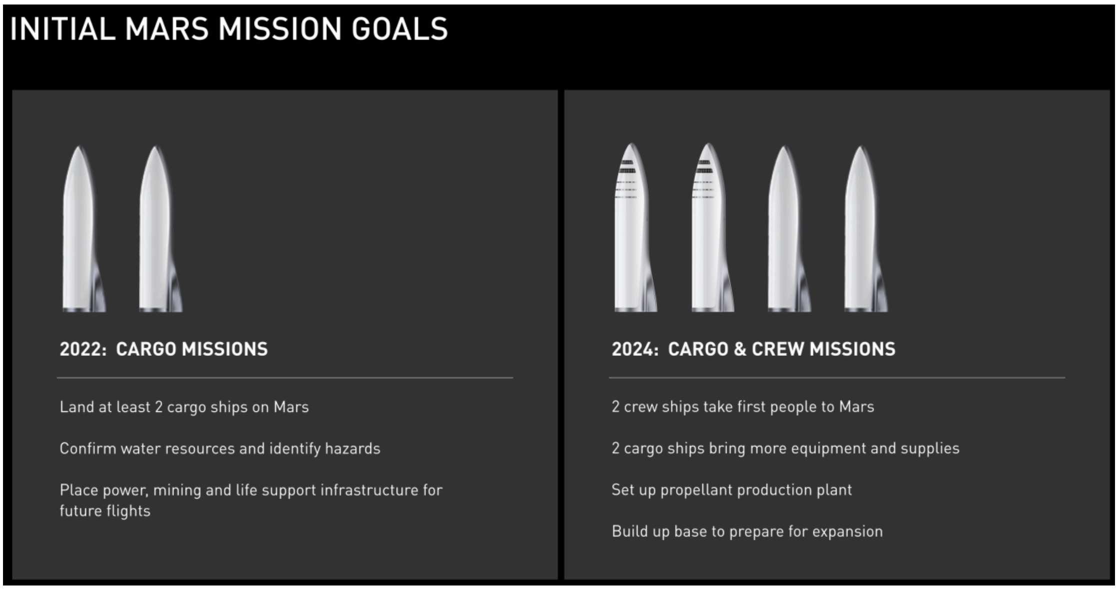

Figure 12: Mission plans of SpaceX. (Source: [27], Slide 31)

4 Model development and methodology for the trajectory analysis

Impulsive interplanetary transfers can be described with the so-called *Lambert's problem*, named after Johann Heinrich Lambert, where the departure and target positions as well as the time of flight between them is know. What is not known, is the orbit between the two positions [31]. Applying this information to this particular problem, the departure and target positions are the heliocentric vectors of Earth and Mars respectively. It should be noted, that the position vector of Earth must be obtained at the departure date, while the one of Mars must be obtained at the desired arrival date, i.e. the departure date plus the desired time of flight.
If one would simply aim to reach Mars from Earth, without applying any boundary constraints, an infinite number of possible trajectories exists. The two position vectors of Earth and Mars are then connected by ellipses with different semi-major axes or even hyperbolas. It should be noted that even though it is possible to travel between Earth and Mars on a hyperbola, this option is of no practical relevance because of the large propellant masses required for these transfers. Therefore, this study will be limited to elliptic transfers between Earth and Mars, only. The general principle of this problem can be seen schematically in figure 13, where multiple transfer paths connect two positions. But they all differ in the required time of flight between the two positions as well as the required Δv to insert the spacecraft in these orbits.

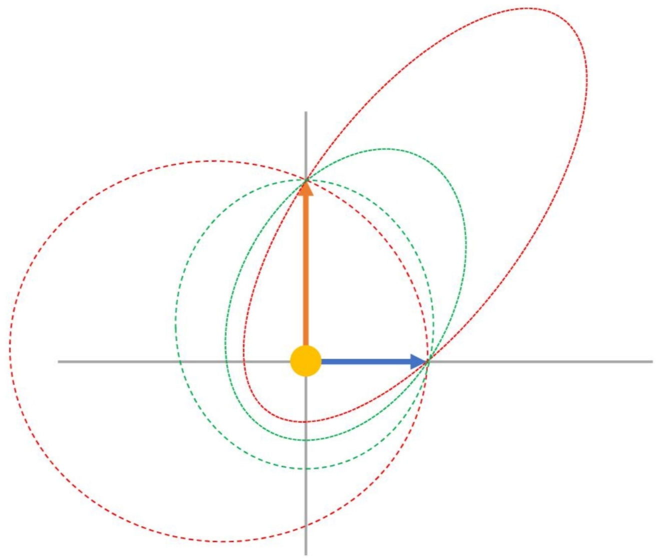

Figure 13: Different trajectories between two positions. The blue vector is at a position of $\begin{pmatrix}4\,\mathrm{LU} & 0 & 0\end{pmatrix}^\top$ and the orange vector is at $\begin{pmatrix}0 & 6\,\mathrm{LU} & 0\end{pmatrix}^\top$ (LU indicates an arbitrary length unit). The green trajectory-ellipses have a semi-major axis of 4.5 LU and the red ones have one of 8 LU.

Therefore, if a desired time of flight is set, the trajectory can be uniquely identified. This is the core idea of Lambert's problem and also of the different algorithms aiming to solve it. Once the transfer trajectory is obtained, one can also calculate the velocity changes needed to be applied according to fundamental orbital mechanics. The outline to solve this problem is to first obtain the position vectors, then solve the Lambert's problem using them as inputs and finally computing the required Δv for the transfer.

4.1 Modelling of the planets' movement

There are multiple ways to approach the positioning of the planets. In general it is always a trade-off between accuracy of the results and the required computation time. The highest accuracy would be obtained when using ephemeris data which are available in Matlab via the aerospace toolbox[2]. The accuracy comes at cost of the computational time, which is high compared to the alternatives discussed later. If one wants to examine a large number of possible trajectories, as I wanted to do, this is not feasible simply because of the time required. The ephemeris data is suitable to refine the values of an already identified trajectory.
Another option to implement elliptic planetary orbits is to use so-called mean orbital elements. These are time-dependant, linear functions that describe the run of the six keplerian elements over a long time interval so that the errors with respect to the ephemeris data stay acceptable low. The astronomical almanac by Seidelmann [37] gives the values for the mean values as well as for the rates of change over the interval from 1800 to 2050, which is suitable for my analysis. As pointed out by Seidelmann, the errors are neglectable small, in the magnitude of 0.0001 % in the case of Mars, relative to the mean value. Furthermore, since it is only a linear formula, it can be computed very fast also for a large amount of dates.
The last, and most simple and inaccurate option would be to model the planets' paths as circles with the radius being their semi-major axis. In terms of computational efficiency, this method offers no advance as the change of the position would still be modeled as a linear polynomial. The only advance would be that the position is only dependant on the time and the semi-major axis and the remaining keplerian elements would not be needed.

Table 5: Comparison of the different methods for modelling the planets' movement

Method	**Ephemeris**	**Mean elements**	**Circles**
Accuracy	very high	high	low
Computational effort	very high	low	very low

I decided to use the mean orbital elements because of the low computation time and the accuracy. Seidelmann provides the keplerian elements as a 6-tupel with the following elements

$$(a, e, i, \Omega, \varpi, L)$$

Where $\varpi = \Omega - \omega$ is the longitude of the periapsis, $L = M + \varpi$ is the mean longitude and these allow us to compute the conventional elements ω and M. To obtain the heliocentric coordinates that are required as input for the Lambert solver, one first needs to calculate the eccentric anomaly from Kepler's equation.

$$M = E - e \sin E$$

The eccentric anomaly can be derived from the mean anomaly with multiple methods, for example Newton's method or Halley's method. All methods try to find a root of the equation in the following format.

$$f(E) \equiv E - e \sin E - M = 0$$

[2] https://de.mathworks.com/matlabcentral/fileexchange/46671-ephemeris-data-for-aerospace-toolbox

Halley's method is more robust than Newton's method and also has cubic convergence, why I decided to use this approach[3]. It is an iterative method with the following equation

$$x_{i+1} = \frac{2f(x_i)f'(x_i)}{2(f'(x_i))^2 - f(x_i)f''(x_i)}$$

Which is repeated until the value of $x_{i+1} \approx x_i$. To solve Kepler's equation, the first two derivatives must be used.

$$\begin{aligned} f(E) &= E - e\sin E - M \\ f'(E) &= 1 - e\cos E \\ f''(E) &= e\sin E \end{aligned}$$

To decide when the above mentioned condition $x_{i+1} \approx x_i$ is met, is best done when the difference between the two undercuts a certain ϵ, in this case I used $\epsilon = 10^{-12}$. Afterwards, the value for E is retrieved. With the use of the eccentric anomaly, one can now obtain the true anomaly according to the following equation.

$$\varphi = 2\arctan\left(\sqrt{\frac{1+e}{1-e}} \cdot \tan\left(\frac{E}{2}\right)\right)$$

Using the true anomaly, we can now express the distance to the center of gravitation at any arbitrary point in time.

$$r = \frac{a \cdot (1-e^2)}{1 + e \cdot \cos(\varphi)}$$

To covert the distance into an euclidean position vector, we need rotate the ellipse to fit it into the solar ecliptic coordinate system. The vector can be computed as follows.

$$\overrightarrow{R} = \mathrm{Rot}_z(\Omega) \cdot \mathrm{Rot}_x(i) \cdot \mathrm{Rot}_z(\varphi + \omega) \cdot \begin{pmatrix} r \\ 0 \\ 0 \end{pmatrix}$$

The indices denote the axis in the aforementioned coordinate system around which the rotation is performed. These calculations have to be performed twice, once for the departure planet at departure date and once for the arrival planet at the day of arrival. When calculating the Δv later, it is also important to know the velocity at which the planet is moving. I modeled the velocity according to classical mechanics as follows:

$$\overrightarrow{V} = \lim_{dt \to 0} \frac{\overrightarrow{R}(t+dt) - \overrightarrow{R}(t)}{dt}$$

In the computation, the key question is how small dt must be to ensure sufficient accuracy. When assessing this problem for Earth and Mars, I decided to use $dt = 60\,\mathrm{s}$, because on an astrological scale this is so short that the velocity can be assumed as linear in this time frame. This allows to use the aforementioned approach. As for the position vector, this has also to be done for both planets.

[3] The Matlab-code for the implementation of Halley's method can be found in appendix A1 near the end of this document.

4.2 Lambert's problem

The difference in mean anomalies of the two positions can be described with the following formula, according to Kepler's third law. It should be noted that in the following equations, the index 2 marks properties of the target and the index 1 marks the properties of the departure.

$$M_2 - M_1 = \sqrt{\frac{\mu}{a^3}} \cdot (t_2 - t_1)$$

In this formula, a is the semi-major axis of the transfer ellipse and μ is the gravitational parameter of the dominating gravitating body, i.e. for an Earth-Mars-Transfer the Sun. M marks the mean anomaly and t the time since periapsis of the respective bodies. Using Kepler's equation, one can express the equation above also in the following way [32].

$$(t_2 - t_1) = \sqrt{\frac{a^3}{\mu}} \left(E_2 - E_1 - e\left(\sin E_2 - \sin E_1\right)\right) \tag{3}$$

Where E marks the eccentric anomaly and e the eccentricity of the transfer ellipse. To further simplify, I introduce the following four auxiliary variables according to cite1 cite2.

$$\begin{aligned} \sin\frac{\alpha_0}{2} &= \sqrt{\frac{s}{2a}} \\ \sin\frac{\beta_0}{2} &= \sqrt{\frac{s-c}{2a}} \\ A &= \frac{E_2 - E_1}{2} \\ B &= \frac{E_2 + E_1}{2} \end{aligned} \tag{4}$$

In this equation, c marks the chord of a triangle with the two position vectors as sides and s is the so-called *semiperimeter*, which is half the sum of the sides of the above mentioned triangle. For the parameters c and s, we can also use the following expressions, compare to the geometry in figure 14.

$$\begin{aligned} c &= \left\| \overrightarrow{R_2} - \overrightarrow{R_1} \right\| \\ s &= \frac{1}{2}\left(\left\|\overrightarrow{R_1}\right\| + \left\|\overrightarrow{R_2}\right\| + c \right) \end{aligned}$$

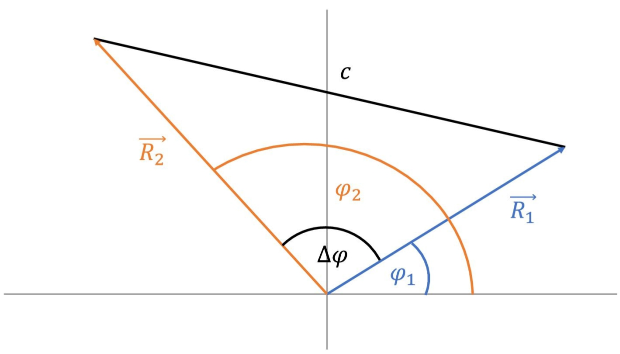

Figure 14: Geometry of the Lambert's Problem

From trigonometric considerations, one can also write:

$$\sin\frac{\alpha_0}{2} = \sin\left(\frac{A+B}{2}\right)$$
$$\sin\frac{\beta_0}{2} = \sin\left(\frac{B-A}{2}\right)$$

With all aforementioned expressions, we can reformulate equation (3) to obtain an equation that is called general time of flight or *Lagrange time equation*.

$$\Delta t = \sqrt{\frac{a^3}{\mu}}\left(\alpha - \beta + (\sin\beta - \sin\alpha)\right) \tag{5}$$

The trigonometric expressions in equation (4) are not unique and therefore α and β need to be adapted depending on the problem's actual properties as described by Prussing & Conway [32]:

$$\beta = \begin{cases} \beta_0 & \text{for} \quad \Delta\varphi \leq \pi \\ -\beta_0 & \text{for} \quad \Delta\varphi > \pi \end{cases}$$
$$\alpha = \begin{cases} \alpha_0 & \text{for} \quad \Delta t \leq t_m \\ 2\pi - \alpha_0 & \text{for} \quad \Delta t > t_m \end{cases}$$

Where $\Delta\varphi = \varphi_2 - \varphi_1$ is the difference in true anomaly of target and departure planet (compare figure 14) and t_m is the time of flight on the minimum energy arc, which can be computed as follows [33]:

$$t_m = \sqrt{\frac{2}{9\mu}}\left(s^{\frac{3}{2}} - (s-c)^{\frac{3}{2}}\right)$$

As α and β are both functions dependent only on a and the two position vectors, equation (5) allows to directly link the desired time of flight Δt and the transfer trajectory. This is the general formulation of the Lambert's Problem and there are multiple ways to solve it. Vallado [34] shows different solution strategies by Gauss, Thorne, Battin and with universal variables. As discussed before, the algorithms aim to find the fitting value of a for a given time of flight. On the basis of a, the velocities at departure and arrival can be calculated afterwards.
While Gauss' method is based on geometric considerations only, Thorne's method is based on a power series development of Lambert's equation and Battin's method is based on continued fractions. It may depend on the exact problem if one of the methods should be used preferably, but in my case, none of the methods offered any advantages. I decided to use Battin's method for the calculations and the results presented in the next chapters.
I implemented the Battin algorithm in a Matlab function, just as described by Vallado [35]. I will not discuss the algorithm in great detail, for this refer to the sources [35] [36]. Still, I will now discuss the critical parts of the algorithm and how they are implemented in my Matlab function[4].
In the loop-section of the code as provided by Vallado, the stopping condition is defined as "Until x stops changing". I decided to implement this condition in a while-loop in Matlab that stops when two consecutive values of x differ less then 10^{-12}. Inside of the loop, two continued fractions are evaluated, where I decided to use c_η up until $n = 6$ and c_U up until $n = 11$.
The rest of my code is implemented just as described by Vallado and returns in the end two velocity vectors $\overrightarrow{v_{T,1}}$ and $\overrightarrow{v_{T,2}}$. These describe the velocity at the intersection of the planet's

[4]The Matlab-code for the implementation of Battin's algorithm can be found in appendix A2 near the end of this document.

orbit with the interplanetary trajectory needed to be inserted in the transfer orbit. Therefore, the spacecraft has apply velocity changes equal to the following expressions:

$$\begin{aligned} \overrightarrow{\Delta v_1} &= \overrightarrow{v_{T,1}} - \overrightarrow{v_1} \\ \overrightarrow{\Delta v_2} &= \overrightarrow{v_2} - \overrightarrow{v_{T,2}} \end{aligned} \tag{6}$$

For a mission analysis the magnitude of the velocity changes are more important than the vectorial description, this is why I write:

$$\begin{aligned} \Delta v_1 &= \left\| \overrightarrow{\Delta v_1} \right\| \\ \Delta v_2 &= \left\| \overrightarrow{\Delta v_2} \right\| \end{aligned} \tag{7}$$

As this approach until now does not consider the influence of the planets on the trajectory, I refined the results using the patched conics approach.

4.3 Patched conics

The idea of the patched conics approach is to split up the trajectory in multiple, in this case three parts. The first is the departure from Earth, where the latter is the dominating gravitational body. The second is the travel from Earth to Mars, during which the Sun is the dominating body, and the last one is the arrival at Mars, where Mars is the dominating body.
The obvious question here is, when to switch between the two parts. The boundary of the influence of a planet is called *sphere of influence* (SOI), which in the case of the Earth at a distance of 925 000 km and for Mars at 578 000 km. Compared to Earth or Mars, the SOI can be considered infinitely far away [38]. As written before, the spacecraft will travel on an elliptic trajectory between Earth and Mars. The $v_{\infty,E}$ in the heliocentric frame must be equal to the heliocentric velocity at the beginning of the transfer ellipse. This means that it must leave Earth on a hyperbolic trajectory with a hyperbolic excess velocity $v_{\infty,E}$ just equal to the calculated Δv_1 in 4.2. This is the literal meaning of "patched conics" as the two conics, the hyperbola relative to Earth and the ellipse relative to the Sun, are patched together at the SOI of Earth. This yields the following equation for the velocity at the perigee of the departure hyperbola.

$$v_{p,E} = \sqrt{\frac{2\mu_E}{r_{p,E}} + v_{\infty,E}^2}$$

As the Starship is refuelled in a circular low-earth orbit, it has the following velocity.

$$v_{c,E} = \sqrt{\frac{\mu_E}{r_{p,E}}}$$

Therefore, the difference in these two velocities,

$$\Delta v_E = v_{p,E} - v_{c,E} = \sqrt{\frac{2\mu_E}{r_{p,E}} + v_{\infty,E}^2} - \sqrt{\frac{\mu_E}{r_{p,E}}} \tag{8}$$

Must be achieved by thrust ignition of the spacecraft. This boost is basically identical to the *transfer orbit injection* (TOI) maneuver as described in 2.3. After the ignition, it travels on the heliocentric ellipse and performs the *trajectory correction maneuvers* (TCM). Accordingly to the departure from Earth, the arrival at Mars is modeled. The spacecraft reaches Mars' SOI on a

hyperbolic orbit.
The arrival hyperbola is defined through the hyperbolic excess velocity $v_{\infty,M}$, which is equal to Δv_2 from equation (7). Therefore, it holds that the velocity at the perigee of the hyperbola is:

$$v_{p,M} = \sqrt{\frac{2\mu_M}{r_{p,M}} + v_{\infty,M}^2} \tag{9}$$

As Starship is designed to remove almost all of its kinetic energy with aerobraking, no thrust maneuver must be performed at arrival in some cases. Only if the velocity at the periapse of the hyperbola is larger than $7.5\,\mathrm{km\,s^{-1}}$, the velocity difference must be removed by a propulsive maneuver (Type A trajectory). As shown in 3.1.3, this velocity is the maximum at which the deceleration can be done with aerobraking only. This leads to the following formulation of the required Δv at Mars.

$$\Delta v_M = \begin{cases} 0 & \text{for} \quad v_{p,M} \leq 7.5\,\frac{\mathrm{km}}{\mathrm{s}} \\ v_{p,M} - 7.5\,\frac{\mathrm{km}}{\mathrm{s}} & \text{for} \quad v_{p,M} > 7.5\,\frac{\mathrm{km}}{\mathrm{s}} \end{cases} \tag{10}$$

This boost is carried out during the MOI maneuver as shown in 2.3.

4.4 Total Delta-v

Additional to the orbit insertion maneuver at departure, Δv_E, and the potential braking maneuver at arrival at Mars, Δv_M, it is also necessary to take into account the Δv for the TCM, Δv_c, and for landing, Δv_l, as described in 3.1.2, 3.1.3 and 3.1.4. The total Δv from the LEO to the Mars surface may therefore be described with the following equation.

$$\Delta v_{E\to M} = \Delta v_E + \Delta v_M + \Delta v_l + \Delta v_c$$

Additionally, I did also apply margins to the derived Δv values according to the ESA margin philosophy [39]. It suggests a margin of 5 % for accurately calculated maneuvers and a margin of 100 % for not analytically derived maneuvers. According to my understanding, the values of Δv_E, Δv_M and Δv_l fall under the first case, while the value of Δv_c falls under the second. This leads then to the final equation for $\Delta v_{E\to M}$, in case of a Type A trajectory, that I will use in the simulation.

$$\Delta v_{E\to M} = 1.05\Delta v_E + 1.05\Delta v_M + 1.05\Delta v_l + 2\Delta v_c \tag{11}$$

As described in 3.1.3, one type (Type B) of mission design allows only trajectories which have a periapse velocity at Mars that is low enough to forgo any Δv_M. This trajectory type would then be described with the following equation.

$$\Delta v_{E\to M} = 1.05\Delta v_E + 1.05\Delta v_l + 2\Delta v_c \tag{12}$$

Both trajectory types will be considered and evaluated later[5].

4.5 Maximum payload mass

In order to built up a permanent base on Mars for humans, it may be desirable to bring as much payload as possible to Mars with every flight. Looking at equation (1), it is evident that a higher payload always results in a smaller available Δv for the transfer. Vice versa, as most possible

[5]The Matlab-code for the evaluation of the needed Δv as described in 4.3 and 4.4 can be found in appendix A3 near the end of this document.

trajectories within a launch opportunity do not fully consume the available Δv, it is possible to bring a higher payload mass to the martian surface with these trajectories. The maximum payload that can be brought to Mars is always the $m_{P/L}$ that satisfies this equation.

$$\begin{aligned} I_{sp} \cdot g_0 \cdot \ln\left(\frac{m_p + m_s + m_{P/L}}{m_s + m_{P/L}}\right) &= 1.05\Delta v_E + 1.05\Delta v_M \\ + 2\Delta v_c + 1.05\left(2.088\,\frac{\mathrm{m}}{\mathrm{s}\cdot\mathrm{t}} \cdot m_{p/L} + 367.53\,\frac{\mathrm{m}}{\mathrm{s}}\right) \end{aligned} \tag{13}$$

The left-hand side of the equation is the maximum Δv available for a given payload mass. The right-hand side is just the equation for the total Δv for a trip from LEO to Mars surface. As the expression of the maximum Δv is a transcendental equation, equation (13) can not be solved analytically. I therefore decided to increase $m_{P/L}$ in steps of 0.001 t until the difference between the two sides of the equation is less than $1\,\mathrm{m\,s^{-1}}$. This is performed for every possible trajectory in every launch opportunity.

4.6 Free-return trajectories

As discussed in 2.3, to exploit the advantages of a free-return trajectory, the Starship must travel on a heliocentric, elliptic orbit with a period of almost exactly two Earth years. If the period does not exactly match this time, it could be possible to perform propulsive maneuvers that alter the period in such way that it still is possible to encounter Earth. So, the key parameter to evaluate the ability of a trajectory to serve as a free-return trajectory is the difference in orbital periods of the transfer ellipse and Earth.

$$\Delta P = P_T - 2P_E$$

With the orbital period of the Earth being just over 365 days, I decided to use a fixed value in the equation.

$$\Delta P = P_T - 730\,\mathrm{d}$$

The orbital period of the Starship may be described according to Kepler's third law as follows.

$$P_T = 2\pi\sqrt{\frac{a_T^3}{\mu_S}}$$

Where μ_S is the gravitational parameter of the Sun and a_T is the semi-major axis of the respective transfer trajectory and a result of the solution of the Lambert's problem as in 4.2. One may therefore express the equation for ΔP as follows.

$$\Delta P = 2\pi\sqrt{\frac{a_T^3}{\mu_S}} - 730\,\mathrm{d} \tag{14}$$

This equation now allows to examine every possible trajectory that is obtained from the solution of Lambert's problem on its ability to serve as a free-return trajectory. This will be carried out in the chapter 5.

4.7 Return flight

The return flight can be described with the same model developed for the flight from Earth to Mars. The solution of the Lambert Problem is obtained with switching the departure and arrival position vectors. So this yields the two hyperbolic excess velocities, which describe the departure hyperbola from Mars and the arrival hyperbola at Earth.
The departure from Mars is different as from the Earth earlier, because Starship starts from ground and not from an orbit. As discussed in 3.3.1, a Δv_{LMO} of approximately $4130\,\mathrm{m\,s^{-1}}$ is needed to reach a low-Mars orbit of 250 km altitude. From there on, the departure hyperbola can be computed just as in 4.3 to yield the required $\Delta v_{M,2}$. The required Δv_c for the TCM is the same as for the flight to Mars, and hence a value of $200\,\mathrm{m\,s^{-1}}$. Upon arrival at Earth, the paradigm is the same as prior when arriving at Mars. Below a certain perigee velocity, no propulsive maneuver is required. For the aerobraking at Earth this threshold is $12.5\,\mathrm{km\,s^{-1}}$ at an altitude of 125 km, according to the details in 3.3.3. So for the $\Delta v_{E,2}$ it holds:

$$\Delta v_{E,2} = \begin{cases} 0 & \text{for} \quad v_{p,E,2} \leq 12.5\,\frac{\mathrm{km}}{\mathrm{s}} \\ v_{p,E,2} - 12.5\,\frac{\mathrm{km}}{\mathrm{s}} & \text{for} \quad v_{p,E,2} > 12.5\,\frac{\mathrm{km}}{\mathrm{s}} \end{cases} \tag{15}$$

Additionally, a landing maneuver has to be performed. At Earth, the landing burn requires a $\Delta v_{l,2}$ of $100\,\mathrm{m\,s^{-1}}$ as described in 3.3.3. Hence, we can express the total Δv for the return flight as follows:

$$\Delta v_{M\to E} = \Delta v_{LMO} + \Delta v_{M,2} + \Delta v_{E,2} + \Delta v_{l,2} + \Delta v_c$$

When now applying the safety margins from [39] as discussed in 4.4, I obtain the following equation.

$$\Delta v_{M\to E} = 1.05\Delta v_{LMO} + 1.05\Delta v_{M,2} + 1.05\Delta v_{E,2} + 1.05\Delta v_{l,2} + 2\Delta v_c \tag{16}$$

For a Type B trajectory, i.e. without a propulsive maneuver to break down at the arrival hyperbola, the equation looks like the following.

$$\Delta v_{M\to E} = 1.05\Delta v_{LMO} + 1.05\Delta v_{M,2} + 1.05\Delta v_{l,2} + 2\Delta v_c \tag{17}$$

5 Evaluation and analysis of results

The presented model can be evaluated with respect to certain performance parameters. The most obvious parameters, which importance arise from the formulation of the Lambert's problem directly, are the total Δv for the transfer and the time of flight. Other aspects that I will evaluate in the following are the maximum payload mass that can be brought to Mars for a certain trajectories and the possibility of free-return trajectories. First, important restrictions for the simulation are described and afterwards, the aforementioned performance parameters are obtained for multiple launch opportunities.

5.1 Restrictions

5.1.1 Technical restrictions

The allowable flight paths as a solution of the Lambert's problem are subject to two boundary conditions. The technical design of Starship influences the maximum Δv that it is able to apply. As described by the Tsiolkowski-equation (1) and according to the data from 2.1.2 & 2.1.3, in the case of no payload that is brought to Mars, the maximum obtainable Δv is:

$$\Delta v_{max} = 378\,\mathrm{s} \cdot 9.806\,65\,\frac{\mathrm{m}}{\mathrm{s}^2} \cdot \ln\left(\frac{100\,\mathrm{t} + 1200\,\mathrm{t} + 0\,\mathrm{t}}{100\,\mathrm{t} + 0\,\mathrm{t}}\right) = 9508\,\frac{\mathrm{m}}{\mathrm{s}}$$

This poses an exceptional case which will not happen, because it is desired to bring a payload of at least 100 t to Mars. In this case, the maximum Δv will be as follows:

$$\Delta v_{max} = 378\,\mathrm{s} \cdot 9.806\,65\,\frac{\mathrm{m}}{\mathrm{s}^2} \cdot \ln\left(\frac{100\,\mathrm{t} + 1200\,\mathrm{t} + 100\,\mathrm{t}}{100\,\mathrm{t} + 100\,\mathrm{t}}\right) = 7213\,\frac{\mathrm{m}}{\mathrm{s}}$$

This allows us to reduce the Lambert's problem to only trajectories which total Δv is less than this number. As I will study the trajectories for different $m_{P/L}$ in later chapter, it is suitable to give an indication of how large the Δv_{max} is for different payload masses. This relation can be obtained from figure 15. Apart from that, the allowable trajectories are mainly constrained by the desired flight time to reach Mars. SpaceX uses different numbers and descriptions for the maximum flight time. On their website [11], they state that it takes six months to get to Mars. It is not quite evident whether that is the actual desired flight time or a maximum value. At the IAC 2016, Elon Musk gave a presentation [21] in which he provided an overview over the so-called trip times to get to Mars in the different launch opportunities. These values can be seen in table 6.

Table 6: Trip times for an Earth-Mars transfer proposed by SpaceX

Year	**Trip Time [d]**
2020	90
2022	120
2024	140
2027	150
2029	140
2031	110
2033	90
2035	80
2037	100
Average	**115**

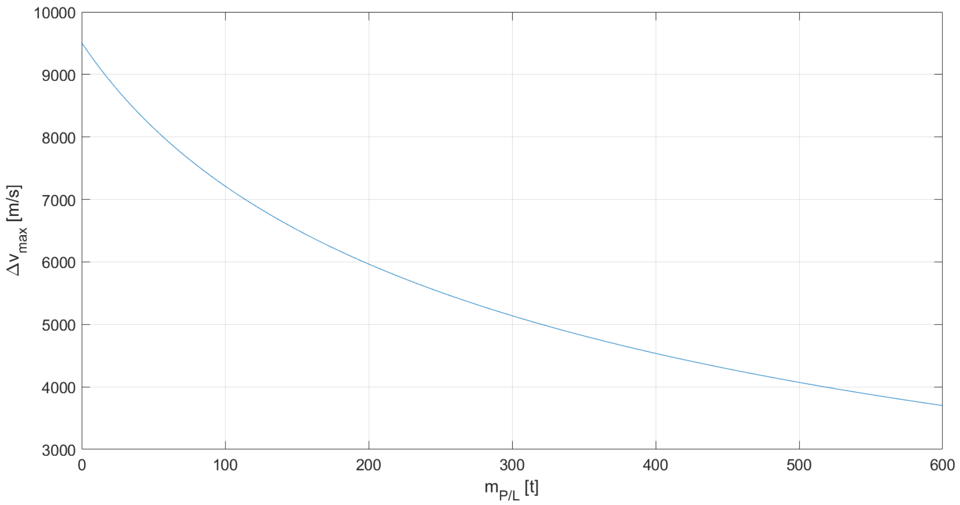

Figure 15: Maximum Δv that can be applied by Starship, depending on the payload mass.

These numbers seem to indicate the lowest possible number of days to reach Mars and they roughly follow the 15-year cycle described in 3.4.2. It must also be considered that the plans presented in 2016 got delayed and as they now aim to land humans on Mars just before the end of the decade [29] [28], the departures prior to 2029 are no more relevant for the scope of this study. I will start the analysis with the 2029 launch opportunity as in 2027, there will be only un-manned flights to Mars and it is not clear whether the mentioned flight times are also valid for these flights. Furthermore, Musk also stated that he "[...] expects [...] Mars transit times of as little as 30 days in the more distant future [...]" ([40], 43:30). I decided to use the six months, or 180 days, as the maximum allowable flight time and I will assess the possibility of (a) achieving the trip times from table 6 and (b) the feasibility of flight times of 30 days.

5.1.2 Computational restrictions

Furthermore, my program demands the span of departure dates as well as the possible times of flight to be quantized. I would like to stress that the following explanation may be easier to understand after reading 5.2.1 first.
To estimate the errors for different stepsizes, I decided to do a Richardson extrapolation for both quantities. When looking at the results of the simulation as f.e. in figure 18 and described in 5.2.1, it becomes evident that the minimum Δv always occurs for a flight time of 180 days. It is therefore not sensitive towards the stepsize of the time of flight. I decided to retrieve the value of the minimum Δv for a Type A trajectory in the 2028/2029 launch opportunity for varying values of the stepsize for the departure date. The stepsize of the time of flight was fixed to 1 h. The results can be seen in the following figure.

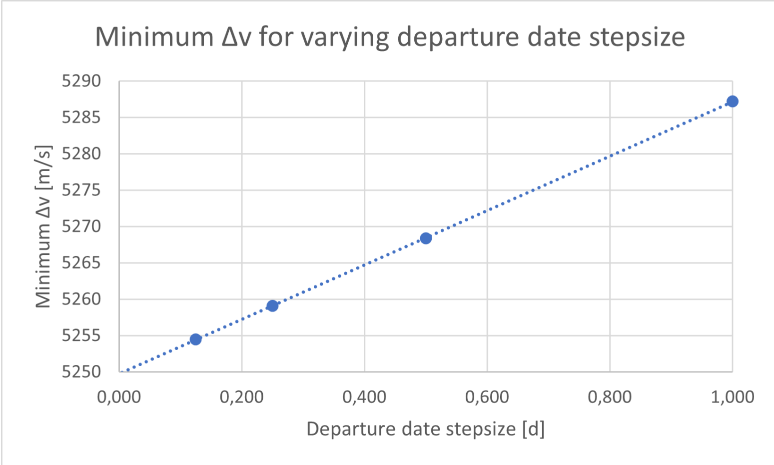

Figure 16: Minimum Δv for different departure date stepsizes. Richardson extrapolation used to determine suitable stepsize.

In this plot, as usual for a Richardson extrapolation, the stepsize of 0 d represents the so-called infinity-grid. This is because then, the function describing the values for the minimum Δv would be continuous and not quantized anymore. In this case, as the function described by the four retrieved values is linear, one can assume that the intersection of the line with the y-axis is the 'correct' value without quantization errors. Now, one can calculate the relative errors for the different stepsizes. For a stepsize of 0.5 d, the relative error would be smaller than 0.4 %.
For the stepsize of the time of flight, it is relevant to state that it is not sensitive towards the stepsize of the departure date. This was the result of my simulations. I therefore decided to do the same procedure as before, but this time for the minimum possible flight time in the 2028/2029 launch opportunity as in 5.2.1. The departure date stepsize was fixed to 0.25 d.

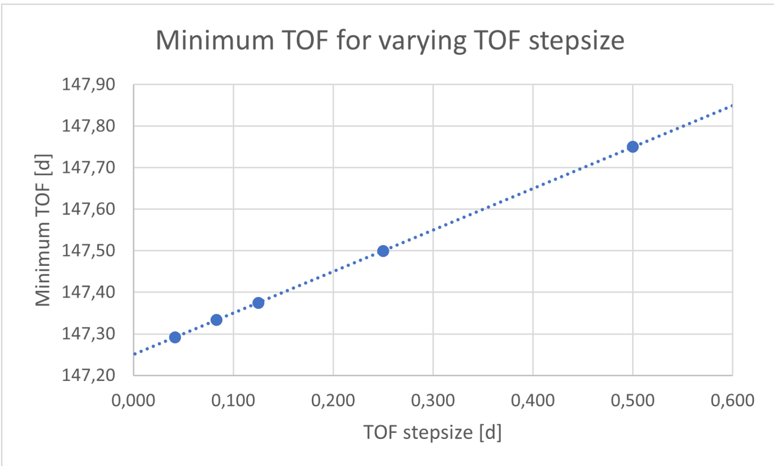

Figure 17: Minimum time of flight for different time of flight stepsizes. Richardson extrapolation used to determine suitable stepsize.

Also for the time of flight stepsize, the relative error can be calculated. For a stepsize of 0.5 d, the relative error would be around 0.3 %.
I therefore decided in both cases to use a step size of 0.5 d or 12 h, as this provides a good accuracy of results and for smaller step sizes, the colors in the plots would not be distinguishable anymore. The computation time was also acceptable for these stepsizes. Furthermore, the early stage of mission analysis does not require a better accuracy.

5.1.3 Fixed parameters

As the aforementioned equations consist of a broad number of different performance parameters, it is reasonable to fix them to ensure the comparability of the obtained results. Therefore, all trajectories analyzed in chapter 5 feature the same performance parameters. These are shown in the following table.

Table 7: Overview over the parameters for the flight from Earth to Mars

Parameter	**Variable**	**Value**	**Unit**	**Remarks**
Gravitational parameter of the Sun	μ_S	$1.327 \cdot 10^{11}$	$km^3\,s^{-2}$	-
Gravitational parameter of the Earth	μ_E	$3.986 \cdot 10^{5}$	$km^3\,s^{-2}$	-
Gravitational parameter of Mars	μ_M	$4.283 \cdot 10^{4}$	$km^3\,s^{-2}$	-
Radius of circular orbit around Earth	$r_{p,E}$	6563	km	Planet radius of 6378 km + orbital altitude of 185 km
Radius of periapse of Mars arrival hyperbola	$r_{p,M}$	3519	km	Planet radius of 3390 km + orbital altitude of 129 km
Gravitational acceleration at Earth	g_0	9.80665	$m\,s^{-2}$	-
Payload mass	$m_{P/L}$	100	t	-
Specific impulse	I_{sp}	378	s	-
Structural mass of Starship	m_s	100	t	-
Propellant mass onboard Starship at departure	m_p	1200	t	-

5.2 2028/2029 launch opportunity

5.2.1 Minimum Delta-v and time of flight

It is common practice to visualize the results of the Lambert's problem as a three-dimensional plot. As said before, one varies the values for the departure date and the time of flight to obtain the values for the total Δv for the transfer. This type of graphical representation is called *porkchop plot.*
The first launch opportunity that I will examine is the one indicated by table 6 as '2029'. The respective Δv for different tuple of departure date and time of flight can be seen in figures 18 (Type A trajectory), 19 (Type B trajectory) and 20 (comparison of both types). The color scheme indicates the value of $\Delta v_{E \to M}$, ranging from low values (blue) to high values at the boundary dictated by technical constraints (yellow).

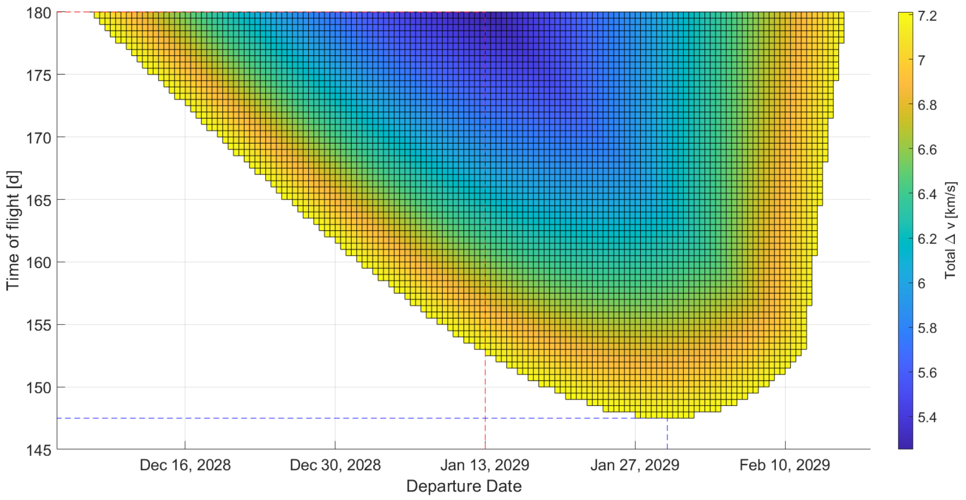

Figure 18: Porkchop plot for a Mars transfer in the 2028/2029 launch opportunity (Type A trajectory). The red, dashed line indicates the minimum Δv trajectory, the blue, dashed line the minimum possible time of flight trajectory.

In the case of a type A trajectory, the window during which an Earth-Mars transfer considering the given boundary conditions is possible, opens up on 06.12.2028 and closes on 15.02.2029, summing up to a total of 72 days. The transfer with the smallest amount of Δv to be applied would be a departure from Earth on 13.01.2029 and a time of flight to Mars of 180 days. It is marked in the figure above with the red, dashed line. The $\Delta v_{E \to M}$, as evaluated in equation (11), for this transfer would be $5252\,\mathrm{m\,s^{-1}}$. The split over the different maneuvers can be seen in the table below.

Table 8: Δv values for the different maneuvers (Minimum Δv in 2029, Type A)

Maneuver	**Value**
TOI	$4245\,\mathrm{m\,s^{-1}}$
TCM	$400\,\mathrm{m\,s^{-1}}$
MOI	$2\,\mathrm{m\,s^{-1}}$
Landing	$605\,\mathrm{m\,s^{-1}}$
Total	$5252\,\mathrm{m\,s^{-1}}$

As described before, the values for the TCM and the landing are constant, in case of the landing at least for a given payload. The major part of the total Δv is applied at the TOI, when leaving the circular low-Earth orbit. It can also be seen that the Δv at the MOI is so small that it is almost neglectable and probably, also in this case a trajectory without a boost at the MOI would be feasible.

The minimum flight time that can be achieved in this window is 147.5 days, when departing between 26.01.2029 and 01.02.2029. During that span, Starship can reach Mars with a $\Delta v_{E \to M}$ of as little as $7195\,\mathrm{m\,s^{-1}}$ for a departure on 29.01.2029. This trajectory is indicated by the blue, dashed line in figure 18. Again, the values of Δv for the respective maneuvers can be found in tabular form below.

Table 9: Δv values for the different maneuvers (Minimum TOF in 2029, Type A)

Maneuver	**Value**
TOI	$5215\,\mathrm{m\,s^{-1}}$
TCM	$400\,\mathrm{m\,s^{-1}}$
MOI	$975\,\mathrm{m\,s^{-1}}$
Landing	$605\,\mathrm{m\,s^{-1}}$
Total	$7195\,\mathrm{m\,s^{-1}}$

For this transfer, the applied Δv during the TOI is almost $1000\,\mathrm{m\,s^{-1}}$ higher than for the minimum Δv transfer. Additionally, also the MOI this time requires significantly more Δv. It becomes evident that it is not possible to achieve the flight time of 140 days as proposed by SpaceX in table 6 with Type A trajectories. Furthermore, this trajectory indicates that the MOI can become large and therefor it is logical that the mission design which would opt for Type B trajectories, constraints the number of possible trajectories. This can be seen in the following.

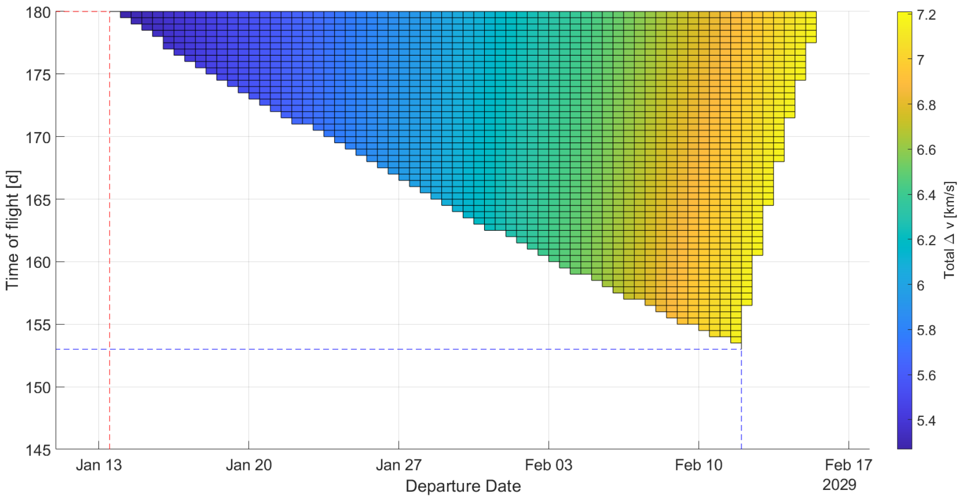

Figure 19: Porkchop plot for a Mars transfer in the 2028/2029 launch opportunity (Type B trajectory). The red, dashed line indicates the minimum Δv trajectory, the blue, dashed line the minimum possible time of flight trajectory.

In figure 19, the porkchop plot for an Earth-Mars transfer in this launch window is displayed for the use of Type B trajectories. The window for this type of trajectories opens up on 13.01.2029 and closes on 15.02.2029, as well. This is a span of 34 days and therefore less than half the time span of the Type A trajectories. In this case, the minimum achievable $\Delta v_{E \to M}$, considering the constraints, is $5259\,\mathrm{m\,s^{-1}}$ and hence slightly higher than for the Type A trajectories. This trajectory can accomplished when departing a little later, compared to Type A, on 13.01.2029 at 06:00 UTC and travelling for 180 days. The split over the different maneuvers is shown below.

Table 10: Δv values for the different maneuvers (Minimum Δv in 2029, Type B)

Maneuver	Value
TOI	$4254\,\mathrm{m\,s^{-1}}$
TCM	$400\,\mathrm{m\,s^{-1}}$
Landing	$605\,\mathrm{m\,s^{-1}}$
Total	$5259\,\mathrm{m\,s^{-1}}$

The slightly higher Δv applied during the TOI ensures that Starship reaches the Mars with a suitable low velocity, compared to the Type A trajectory. But in general, the two trajectories for the minimum Δv are almost similar. They are not, however, when it comes to comparing the minimum possible time of flight. The minimum achievable flight time for Type B trajectories is 153 days, accomplishable with a departure on 11.02.2029. This transfer requires a total Δv of $7182\,\mathrm{m\,s^{-1}}$, compare with the table below.

Table 11: Δv values for the different maneuvers (Minimum TOF in 2029, Type B)

Maneuver	Value
TOI	$6177\,\mathrm{m\,s^{-1}}$
TCM	$400\,\mathrm{m\,s^{-1}}$
Landing	$605\,\mathrm{m\,s^{-1}}$
Total	$7182\,\mathrm{m\,s^{-1}}$

Once again the TOI is larger than for the Type A trajectory, this time the difference is larger than $1900\,\mathrm{m\,s^{-1}}$. Neither in the case of a Type B trajectory, it is possible to reach Mars within 140 days as proposed by SpaceX, this time it is not even possible to undercut flight times of 150 days. In figure 20, the two trajectory types are compared in an identical frame to better indicate the differences. It became evident that the Type B trajectory is way more restrictive than the Type A trajectory. This condenses in the smaller window during which a transfer is possible and in the higher minimum possible time of flight. The values for the minimum achievable Δv are almost identical and in general, the transition from Type B trajectories to Type A trajectories is smooth for tuples of departure date and time of flight close to the border in between them.

5.2.2 Maximum allowable payload mass to Mars

As described in 4.5, it may be an important mission objective to deliver as much payload as possible to Mars with every flight. The presented equation (13) is evaluated for all possible trajectories within the 2028/2029 launch opportunity. The result of this simulation is presented in figure 21 as a porkchop plot.

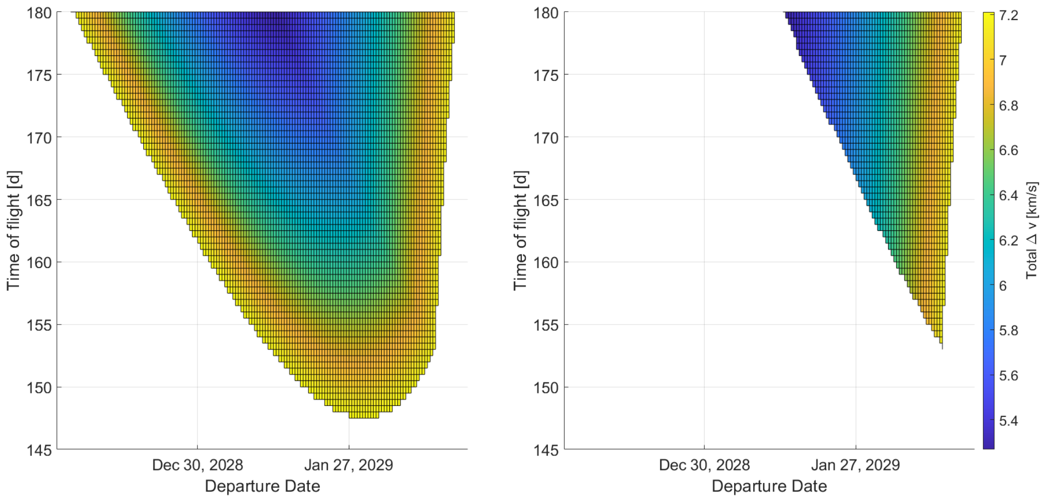

Figure 20: Comparison of trajectory types for a Mars transfer in the 2028/2029 launch opportunity in terms of needed Δv .

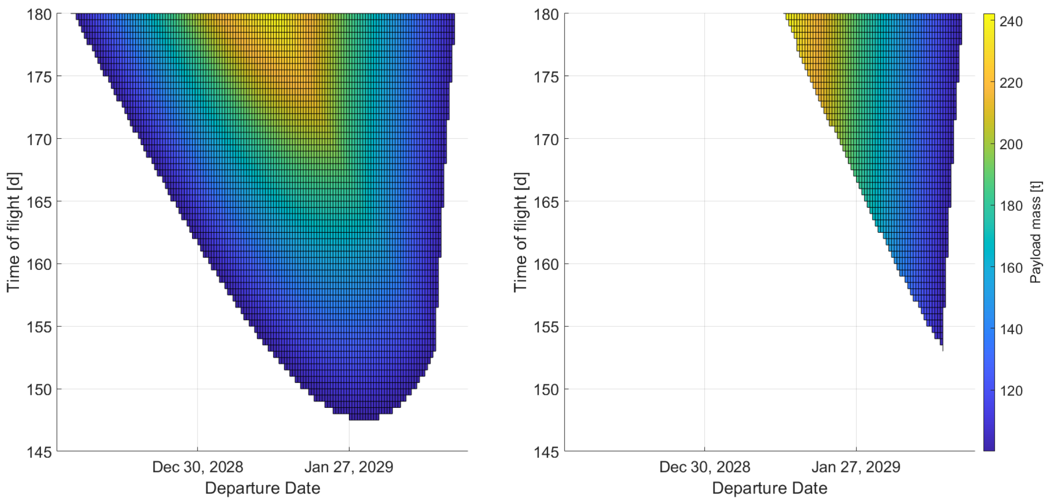

Figure 21: Porkchop plot indicating the maximum payload masses that can be brought to Mars for a transfer in the 2028/2029 launch opportunity.

The result is that it is possible to bring a payload mass of up to 243.732 t to Mars when travelling on the trajectory with the lowest Δv consumption. This is again a departure on 13.01.2029 00:00 UTC and a flight time of 180 days.

5.2.3 Free-return trajectories

As described in 4.6, by comparing the orbital period of the heliocentric transfer ellipse on which Starship travels with the orbital period of Earth, one can estimate whether its possible to use the advantages of a free-return trajectory with the respective trajectory. The code I use allows to obtain the value of the semi-major axis for every trajectory, which then makes it possible to evaluate equation (14) and retrieve a value for ΔP. I decided to divide the values of $|\Delta P|$ in five groups, depending on its value. The first group contains all values greater than 50 days, the second comprises all values between 20 and 50 days, the third all between 10 and 20 days, the fourth all values between 5 and 10 days, and the last group entails all values of under 5 days. These values are then graphically refined in a porkchop-like plot as in figure 22.

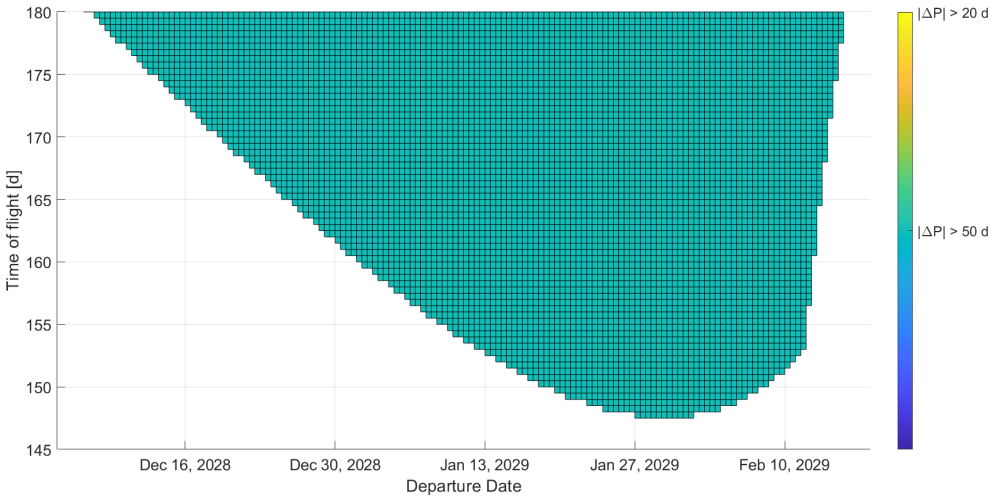

Figure 22: Porkchop plot displaying the values of ΔP from equation (14). Indicates the possibilities of performing a free-return trajectory for all possible Earth-Mars trajectories in the 2028/2029 launch opportunity.

In the case of the 2028/2029 launch opportunity, all trajectories have a difference of 50 days or more to the double orbital period of the Earth. Even though it is not easy to estimate the Δv required to alter the trajectory in order to 'fix' the orbital period to that of Earth, it can be said for sure that compared with other launch opportunities, the general situation of free-return trajectories is subpar in the 2028/2029 launch opportunity.

5.3 2031 launch opportunity

The next launch opportunity that I will examine is in 2031. SpaceX states that they are aiming for a minimum flight time of 110 days, as shown in table 6. I will now go through the results for the minimum Δv and the maximum payload mass for Type A and Type B trajectories as well as the safe return trajectories.

5.3.1 Minimum Delta-v and time of flight

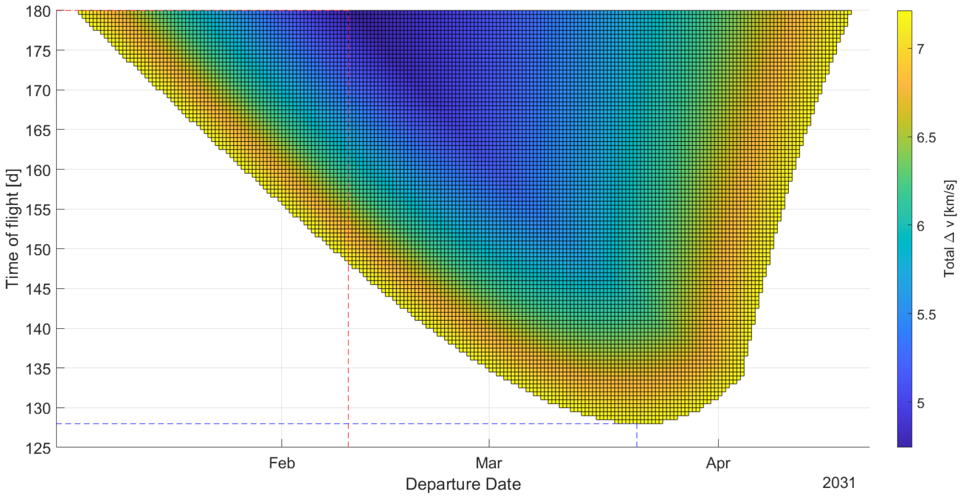

Figure 23: Porkchop plot for a Mars transfer in the 2031 launch opportunity (Type A trajectory). The red, dashed line indicates the minimum Δv trajectory, the blue, dashed line the minimum possible time of flight trajectory.

When looking at the Type A trajectories in figure 23, one can see that the windows, during which a departure is possible, opens up on 04.01.2031 and closes on 19.04.2031, spanning over 106 days. The transfer with the minimum Δv to be applied requires a departure on 10.02.2031 and a flight time of 180 days. It is indicated in figure 23 by the red dashed line. The total $\Delta v_{E \to M}$ for this transfer sums up to $4744\,\mathrm{m\,s^{-1}}$ and is split over the different maneuvers as shown in the following table.

Table 12: Δv values for the different maneuvers (Minimum Δv in 2031, Type A)

Maneuver	**Value**
TOI	$3735\,\mathrm{m\,s^{-1}}$
TCM	$400\,\mathrm{m\,s^{-1}}$
MOI	$4\,\mathrm{m\,s^{-1}}$
Landing	$605\,\mathrm{m\,s^{-1}}$
Total	$4744\,\mathrm{m\,s^{-1}}$

Compared with the values for the minimum Δv in the previous launch opportunity, it strikes that the TOI requires significantly less Δv. This results in a 9.7 % lower total minimum Δv in the 2031 launch opportunity compared with the 2029 launch opportunity and indicates the multi-year cycle as described in 3.4.2.
As stated before, the envisaged minimum flight time of SpaceX during this opportunity are 110 days. Upon comparison with figure 23, it becomes evident that the actual achievable minimum flight time is 128 days. This flight time becomes possible when departing on 21.03.2031 and requires a total $\Delta v_{E \to M}$ of $7189\,\mathrm{m\,s^{-1}}$, compare the blue, dashed line in figure 23.

Table 13: Δv values for the different maneuvers (Minimum TOF in 2031, Type A)

Maneuver	**Value**
TOI	$5277\,\mathrm{m\,s^{-1}}$
TCM	$400\,\mathrm{m\,s^{-1}}$
MOI	$907\,\mathrm{m\,s^{-1}}$
Landing	$605\,\mathrm{m\,s^{-1}}$
Total	$7189\,\mathrm{m\,s^{-1}}$

In the table above, the split of Δv over the different maneuvers is shown for a minimum time of flight transfer in the 2031 launch opportunity. Compared with the previous launch opportunity, the Δv for the TOI is larger, whereas the Δv for MOI is smaller. Inevitably, the total value is almost identical.

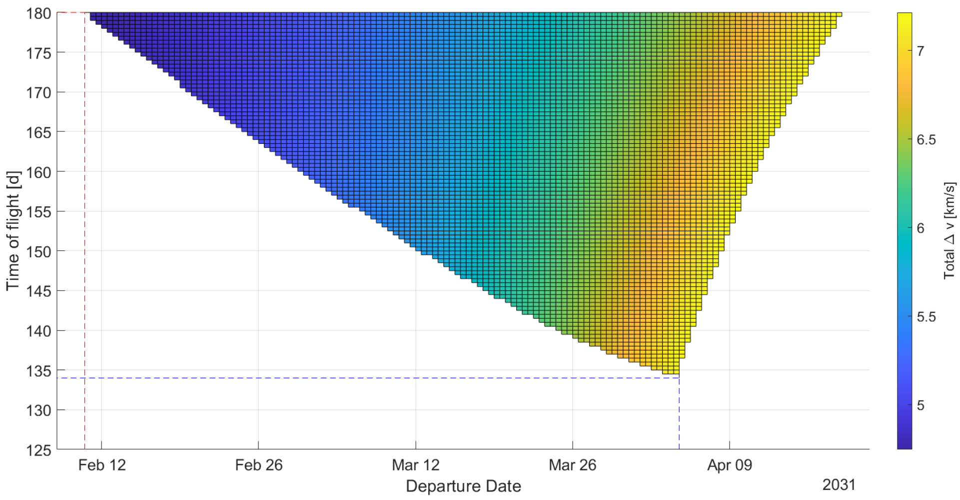

Figure 24: Porkchop plot for a Mars transfer in the 2031 launch opportunity (Type B trajectory). The red, dashed line indicates the minimum Δv trajectory, the blue, dashed line the minimum possible time of flight trajectory.

In figure 24, the porkchop plot for a Type B trajectory in the 2031 launch opportunity is shown. In this case, the window opens on 10.02.2031 and closes on 19.04.2031, spanning over a duration of 69 days. A minimum Δv transfer becomes possible when departing on 10.02.2031 with a flight time of 180 days, just as for a Type A trajectory. The values for the different maneuvers are also similar as shown in the table below.

Table 14: Δv values for the different maneuvers (Minimum Δv in 2031, Type B)

Maneuver	Value
TOI	$3741\,\mathrm{m\,s^{-1}}$
TCM	$400\,\mathrm{m\,s^{-1}}$
Landing	$605\,\mathrm{m\,s^{-1}}$
Total	$4746\,\mathrm{m\,s^{-1}}$

Once again, the values for minimum Δv are almost identical between Type A and Type B trajectories. When it comes to the minimum time of flight, the differences are larger. The minimum flight time that can be achieved on a Type B trajectory is 134 days, and hence 6 days longer as for a Type A trajectory. The trajectory is marked in figure 24 with the blue, dashed line. This becomes possible for a departure on 04.04.2031, with the total Δv split over the different maneuvers as indicated in the table below.

Table 15: Δv values for the different maneuvers (Minimum TOF in 2031, Type B)

Maneuver	Value
TOI	$6207\,\mathrm{m\,s^{-1}}$
TCM	$400\,\mathrm{m\,s^{-1}}$
Landing	$605\,\mathrm{m\,s^{-1}}$
Total	$7212\,\mathrm{m\,s^{-1}}$

This trajectory uses virtual all of the available Δv and hence consumes all available propellant. A comparison between the two trajectory types can be seen in figure 25. When comparing the minimum possible time of flight with the previous launch opportunity, a 12.4 % shorter minimum time of flight is possible. Also, the constraining character of Type B trajectories is smaller as in the last launch opportunity, at least when comparing the number of possible trajectories in the figures 20 and 25.

5.3.2 Maximum allowable payload mass to Mars

The next performance parameter that will be examined is the maximum payload that can be brought to Mars. It coincides with the trajectory for minimum total Δv on the 10.02.2031. On this trajectory it is possible to bring a payload mass of up to 295.230 t to Mars with a transfer time of 180 days. The maximum payload masses for different trajectories can be deduced from figure 26.

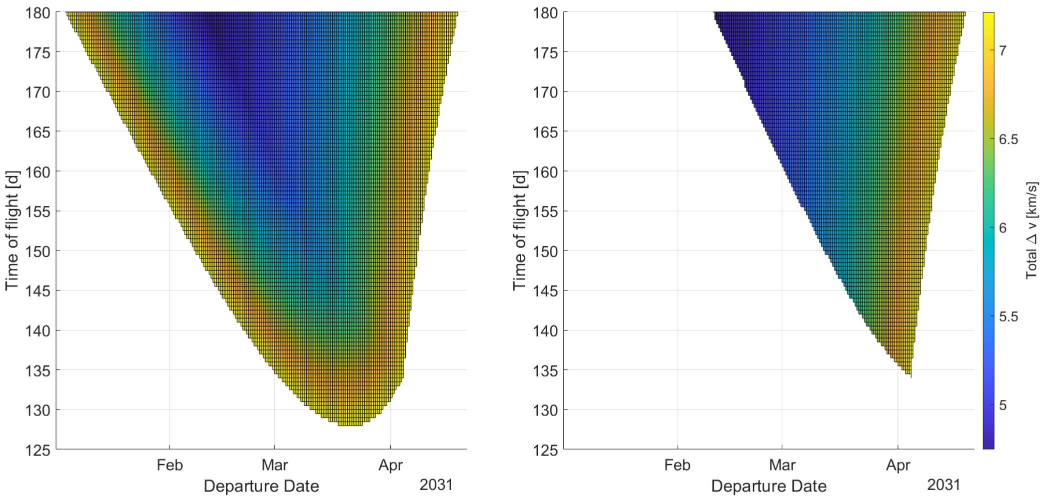

Figure 25: Comparison of trajectory types for a Mars transfer in the 2031 launch opportunity. The left figure displays the values for a Type A trajectory, the right figure for a Type B trajectory.

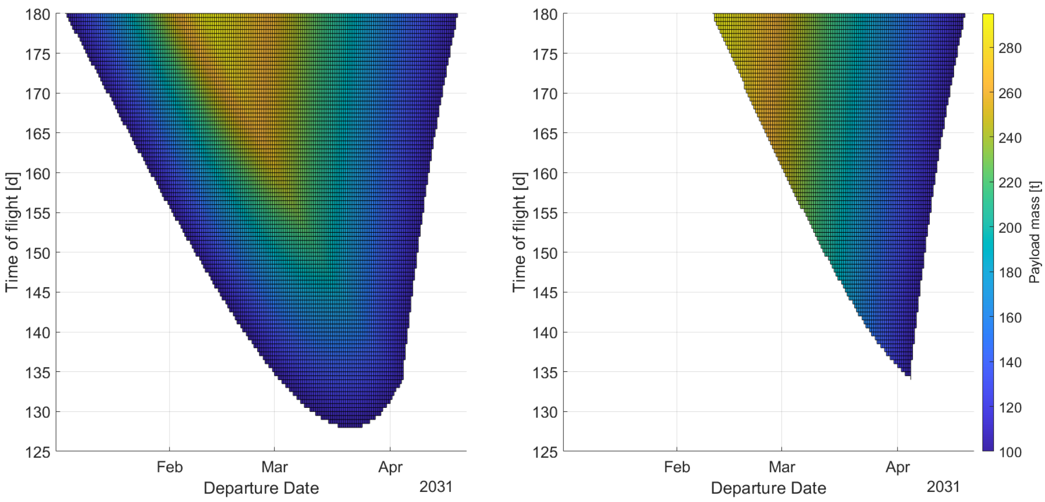

Figure 26: Porkchop plot indicating the maximum payload masses that can be brought to Mars for a transfer in the 2031 launch opportunity. The left figure displays the values for a Type A trajectory, the right figure for a Type B trajectory.

The maximum payload mass that can be brought to Mars in the 2031 launch opportunity depicts an increase of 21.1 % when compared with the previous opportunity.

5.3.3 Free-return trajectories

The last objective I will examine for the 2031 launch opportunity is the possibility for free-return trajectories. The observance made when looking at figure 27 is more or less identical to what described in 5.2.3. Also during this launch opportunity, no trajectory provides a ΔP of below 50 days.

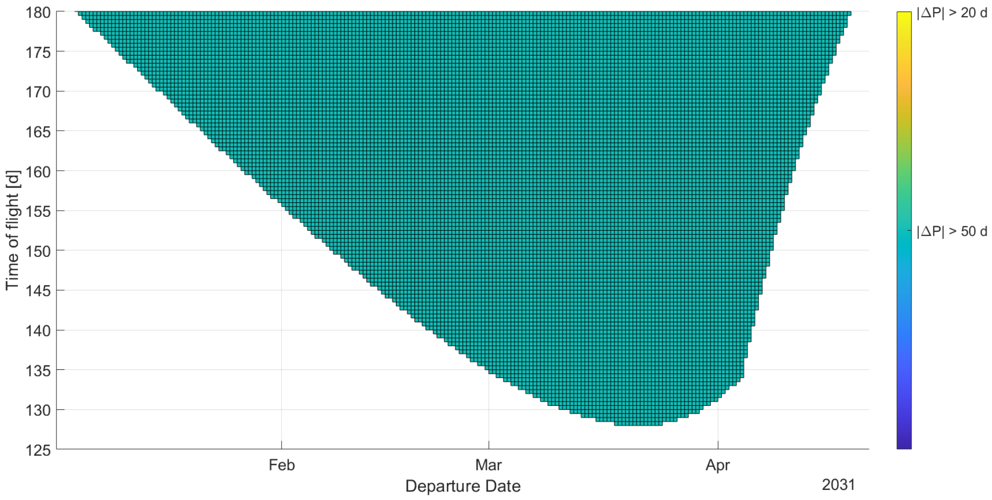

Figure 27: Porkchop plot displaying the values of ΔP from equation (14). Indicates the possibilities of performing a free-return trajectory for all possible Earth-Mars trajectories in the 2031 launch opportunity.

5.4 2033 launch opportunity

Next up is the 2033 launch opportunity, in which SpaceX - for the first time - are aiming to reach Mars in under 100 days, 90 days to be exactly. As for the previous launch opportunities, I will describe the Δv results, the maximum payload masses and give a brief look at free-return trajectories in the following sections.

5.4.1 Minimum Delta-v and time of flight

The launch opportunity in 2033 opens up on 08.02.2033 and closes on 08.07.2033, hence spanning over a duration of 151 days. This is an increase of 42.5 % in duration, compared with the 2031 launch opportunity. The minimum Δv with which a flight time of 180 days can still be achieved is $4650\,\mathrm{m\,s^{-1}}$, being achievable when departing on 04.04.2033. The split across the different stages of the transfer is presented in table 16. In figure 28, the porkchop plot for a Type A trajectory can be seen.

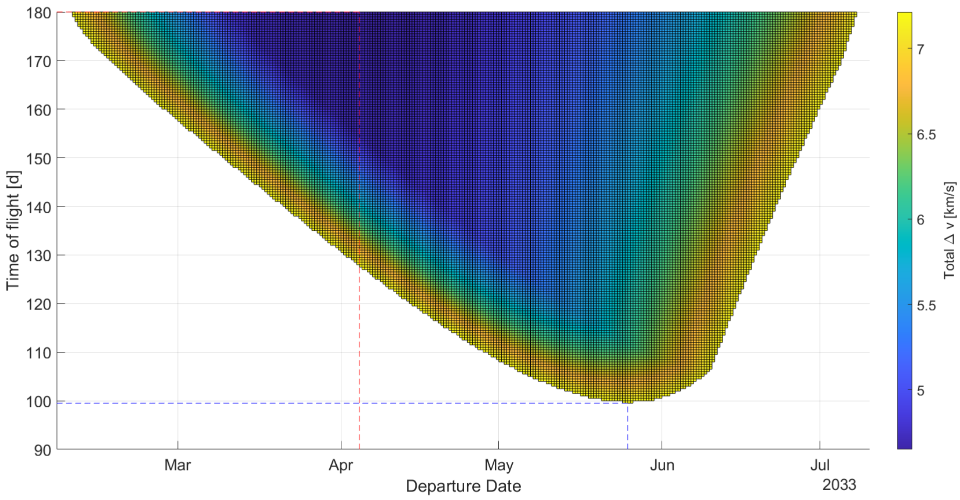

Figure 28: Porkchop plot for a Mars transfer in the 2033 launch opportunity (Type A trajectory). The red, dashed line indicates the minimum Δv trajectory, the blue, dashed line the minimum possible time of flight trajectory.

Table 16: Δv values for the different maneuvers (Minimum Δv in 2033, Type A)

Maneuver	**Value**
TOI	$3645\,\mathrm{m\,s^{-1}}$
TCM	$400\,\mathrm{m\,s^{-1}}$
MOI	$0\,\mathrm{m\,s^{-1}}$
Landing	$605\,\mathrm{m\,s^{-1}}$
Total	$4650\,\mathrm{m\,s^{-1}}$

Different to previous launch opportunities, this time the minimum Δv transfer does not require a propulsive maneuver at Mars and does therefore also fulfill the stricter constraints of a Type B trajectory. Compared with the minimum Δv during the 2031 opportunity, the minimum Δv is reduced by 2.0 %. The trajectory is again indicated by the red, dashed line in figure 28. The minimum achievable flight time during this opportunity is 99 days and therefore the first possibility in the considered timespan of this study to reach Mars in under 100 days. The corresponding trajectory features a departure on 25.05.2033 and a split of Δv across the maneuvers as follows.

Table 17: Δv values for the different maneuvers (Minimum TOF in 2033, Type A)

Maneuver	**Value**
TOI	$5344\,\mathrm{m\,s^{-1}}$
TCM	$400\,\mathrm{m\,s^{-1}}$
MOI	$861\,\mathrm{m\,s^{-1}}$
Landing	$605\,\mathrm{m\,s^{-1}}$
Total	$7210\,\mathrm{m\,s^{-1}}$

The flight time of 99 days depicts an decrease of 22.7 % when compared to the values of 5.3.1. Now, the Type B trajectory is analyzed. Figure 29 displays the porkchop plot for Type B trajectories during the 2033 launch opportunity.

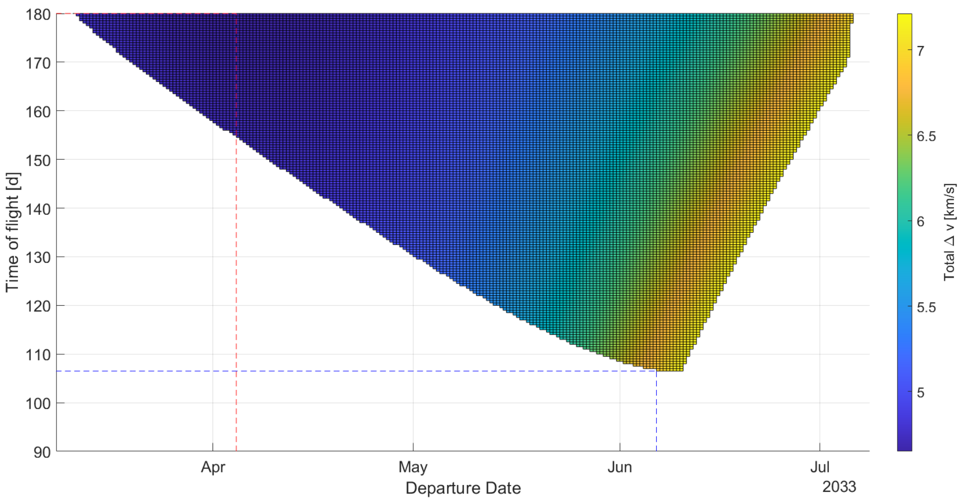

Figure 29: Porkchop plot for a Mars transfer in the 2033 launch opportunity (Type B trajectory). The red, dashed line indicates the minimum Δv trajectory, the blue, dashed line the minimum possible time of flight trajectory.

As described before, the minimum Δv trajectory is identical to the one for a Type A trajectory. But, different as in the previous opportunities, this time the minimum Δv is not at the boundary between Type A and Type B trajectories, but well within the Type B regime. Also, close to the end of the opportunity in July 2033, there are some trajectories that can be achieved with Type A trajectories only. Compare figures 28 and 29 on the top-right corner of the plot to visualize. This poses an effect that has not yet been observed in previous launch opportunities. When looking at the minimum achievable flight time, the effect is similar to the previous opportunities, i.e. that the flight for Type B is longer at 106 days. The Δv distribution among the maneuvers can be seen in the table below.

Table 18: Δv values for the different maneuvers (Minimum TOF in 2033, Type B)

Maneuver	Value
TOI	$6207\,\mathrm{m\,s^{-1}}$
TCM	$400\,\mathrm{m\,s^{-1}}$
Landing	$605\,\mathrm{m\,s^{-1}}$
Total	$7212\,\mathrm{m\,s^{-1}}$

The decrease in comparison to the Type B minimum flight time in 2031 is 20.9 % and hence slightly lower than for Type A trajectories. In figure 30, a comparison between the porkchop plots for Type A and Type B on identical scale is shown.

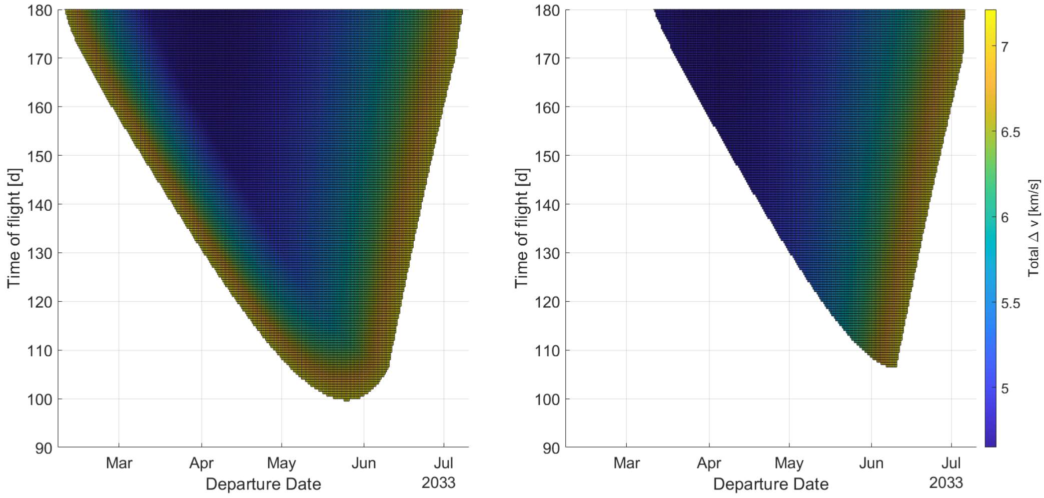

Figure 30: Comparison of trajectory types for a Mars transfer in the 2033 launch opportunity. The left figure displays the values for a Type A trajectory, the right figure for a Type B trajectory.

The trend that the Type B trajectories are getting less restricting can also be observed here, as the number of possible trajectories within the Type B trajectories is getting closer to the ones within Type A trajectories. Looking at the penalties for Type B trajectories, in this case there is none for the minimum Δv and the one for the minimum possible flight time is 7.1 %.

5.4.2 Maximum allowable payload mass to Mars

The maximum payload mass that can be brought to Mars is, necessarily when using the minimum Δv trajectory, 305.437 t. This is, compared with the previous launch opportunity, an increase of 3.5 %. In the figure below, more detailed information can be found.

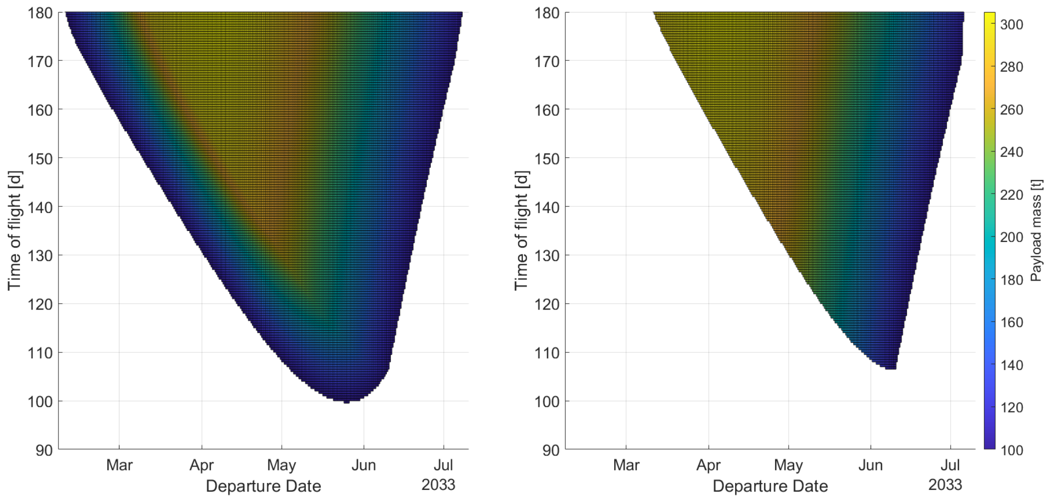

Figure 31: Porkchop plot indicating the maximum payload masses that can be brought to Mars for a transfer in the 2033 launch opportunity. The left figure displays the values for a Type A trajectory, the right figure for a Type B trajectory.

5.4.3 Free-return trajectories

The last objective I will examine for the 2033 launch opportunity is the possibility for free-return trajectories. The observance made when looking at figure 32 is more or less identical to what described in previous sections. Also during this launch opportunity, no trajectory provides a ΔP of below 50 days.

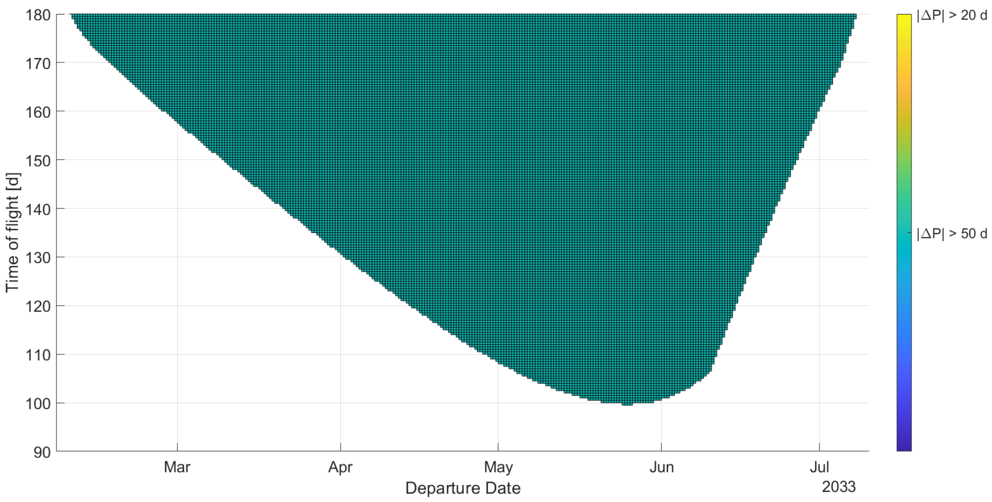

Figure 32: Porkchop plot displaying the values of ΔP from equation (14). Indicates the possibilities of performing a free-return trajectory for all possible Earth-Mars trajectories in the 2033 launch opportunity.

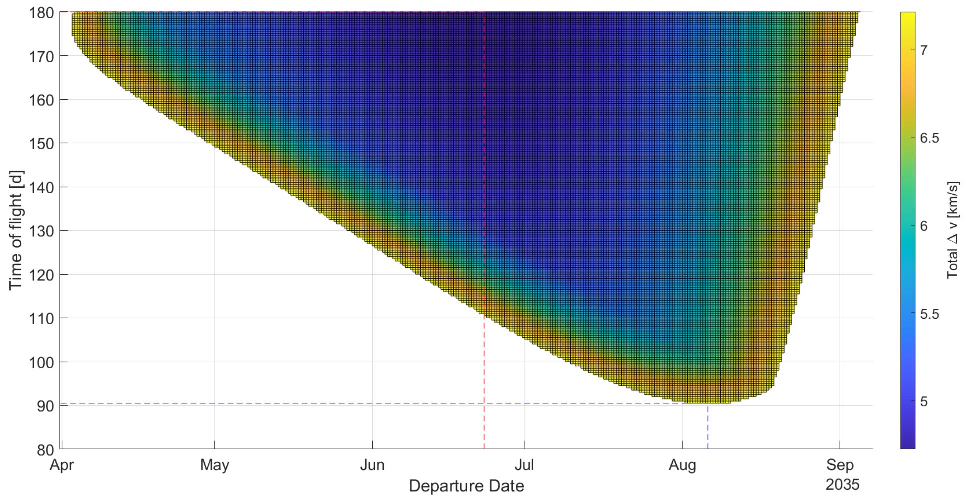

Figure 33: Porkchop plot for a Mars transfer in the 2035 launch opportunity (Type A trajectory). The red, dashed line indicates the minimum Δv trajectory, the blue, dashed line the minimum possible time of flight trajectory.

5.5 2035 launch opportunity

The next launch opportunity that is examined in this document, is the 2035 launch opportunity. SpaceX states that they want to reach Mars in 80 days during this time span, as of table 6. Just as in previous sections, I will go over the minimum Δv and time of flight trajectories, the related maximum payload masses as well as the possibility of free-return trajectories in the following section.

5.5.1 Minimum Delta-v and time of flight

For a Type A trajectory, the launch opportunity opens on 03.04.2035 and closes on 05.09.2035, therefore spanning over a duration of 156 days. Compared with the 2033 launch opportunity, this is an increase of 3.3 %, only. Also, an effect can be observed here that has not been present in previous launch windows. At the very beginning of the launch opportunity in early April, there are certain departure dates on which transfers with shorter times of flight are possible but not a time of flight of 180 days. This can be seen in figure 33. Again, the minimum Δv trajectory is marked with the red, dashed line and the minimum time of flight trajectory is marked with the blue, dashed line in figure 33. The minimum Δv can be achieved with a departure from Earth on 23.06.2035 and a flight time of 180 days, and requires a total $\Delta v_{E \rightarrow M}$ of $4724\,\mathrm{m\,s^{-1}}$. The split over the different maneuvers can be found in table 19.

Table 19: Δv values for the different maneuvers (Minimum Δv in 2035, Type A)

Maneuver	**Value**
TOI	$3719\,\mathrm{m\,s^{-1}}$
TCM	$400\,\mathrm{m\,s^{-1}}$
MOI	$0\,\mathrm{m\,s^{-1}}$
Landing	$605\,\mathrm{m\,s^{-1}}$
Total	$4724\,\mathrm{m\,s^{-1}}$

It can be seen that, just as in the last launch opportunity, the minimum Δv trajectory does not require a propulsive maneuver at Mars and hence also fulfils the stricter restrictions of a Type B trajectory. When comparing the Δv value with the one from 2033, it becomes evident that, for the first time in the observed time span, it increases. The increase of 1.6 % may not be considered large but it indicates that the global minimum of the 15-year cycle as described in 3.4.2 may have been surpassed.
When looking at the minimum flight time that is possible during this launch opportunity, it can be seen that it still decreases when compared with the previous opportunity. The minimum possible time of flight is 90.5 days, and therefore 8.6 % shorter as in 2033. Nevertheless, the proposed 80 days by SpaceX can not be achieved. The trajectory for the minimum flight time features a departure from Earth on 06.08.2035 and a split of Δv across the different maneuvers as shown in the table below.

Table 20: Δv values for the different maneuvers (Minimum TOF in 2035, Type A)

Maneuver	**Value**
TOI	$5403\,\mathrm{m\,s^{-1}}$
TCM	$400\,\mathrm{m\,s^{-1}}$
MOI	$751\,\mathrm{m\,s^{-1}}$
Landing	$605\,\mathrm{m\,s^{-1}}$
Total	$7159\,\mathrm{m\,s^{-1}}$

For Type B trajectories, the launch opportunity opens on 20.04.2035 and closes on 05.09.2035, hence spanning over a duration of 139 days. As described before, the minimum Δv trajectory for Type B is the same trajectory as for Type A, so it will not be discussed in more detail here. The porkchop plot for Type B is displayed in figure 34, the minimum time of flight trajectory is marked with the blue, dashed line.

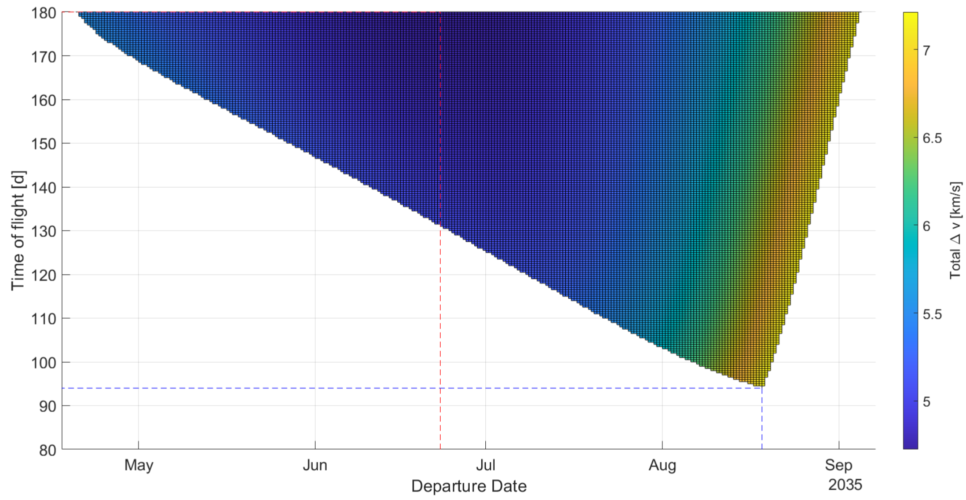

Figure 34: Porkchop plot for a Mars transfer in the 2035 launch opportunity (Type B trajectory). The red, dashed line indicates the minimum Δv trajectory, the blue, dashed line the minimum possible time of flight trajectory.

The minimum possible time of flight for Type B trajectories is 94 days, achievable with a departure on 18.08.2035. It requires a total Δv of $7180\,\mathrm{m\,s^{-1}}$, which is split across the different maneuvers as shown in the table below.

Table 21: Δv values for the different maneuvers (Minimum TOF in 2035, Type B)

Maneuver	**Value**
TOI	$6175\,\mathrm{m\,s^{-1}}$
TCM	$400\,\mathrm{m\,s^{-1}}$
Landing	$605\,\mathrm{m\,s^{-1}}$
Total	$7180\,\mathrm{m\,s^{-1}}$

Compared with the previous launch opportunity in 2033, the minimum possible time of flight for Type B is decreased by 11.3 %. When comparing Type A and Type B, as in figure 35, it becomes evident that they are getting closer and the restrictive character of Type B trajectories vanishes, at least in terms of number of possible trajectories.

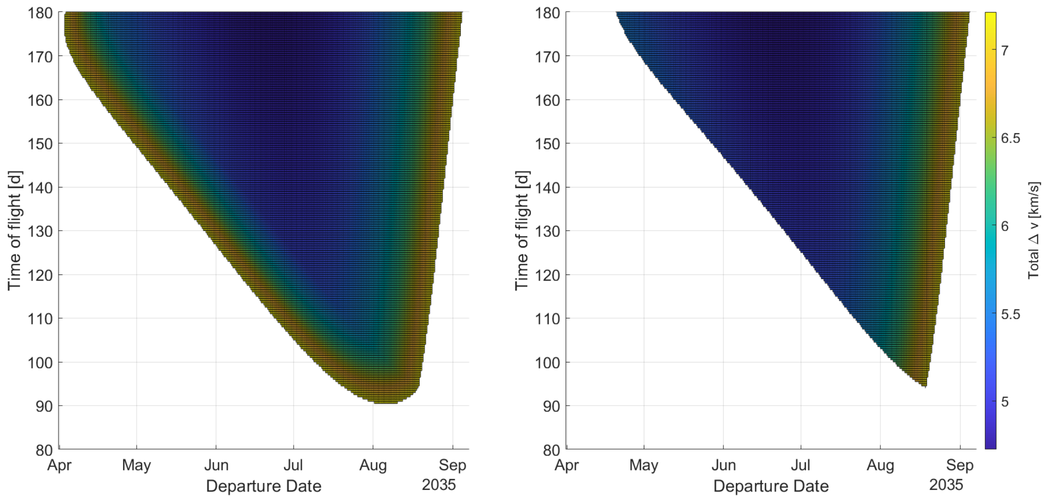

Figure 35: Comparison of trajectory types for a Mars transfer in the 2035 launch opportunity. The left figure displays the values for a Type A trajectory, the right figure for a Type B trajectory.

The penalty of the Type B trajectories for the minimum flight time is 3.9 % and hence smaller as in 2033, another indication that the two types converge more and more.

5.5.2 Maximum allowable payload mass to Mars

The maximum payload mass that can be brought to Mars is, again on the minimum Δv trajectory, 297.321 t. Compared with the previous launch opportunity in 2033, this is a decrease of 2.7 %. As for the minimum Δv, this is a turn in the trend and another indication that the minimum of the 15-year cycle is surpassed. The maximum payload mass for different trajectories is again presented as porkchop-like plot in figure 36.

5.5.3 Free-return trajectories

The last aspect that shall be discussed for this launch opportunity are the free-return trajectories. For the first time in the observed frame, some trajectories provide a better "quality" of free-return. This means that some trajectories with rather short times of flight in June and July only differ from the required orbital period by less than 20 days. A few trajectories also by less then 10 days. This is a significant improvement to previous launch opportunities. In figure 37, the results are displayed in a porkchop-like plot.

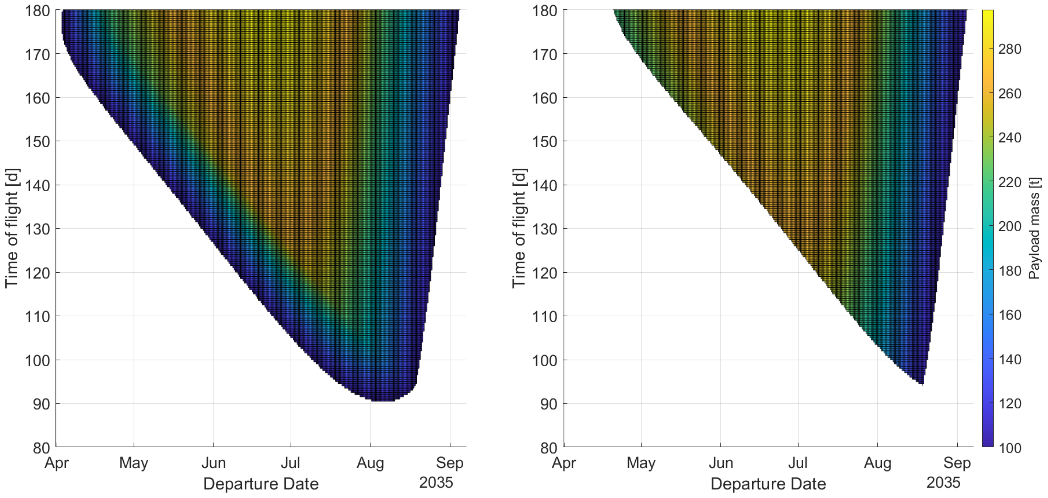

Figure 36: Porkchop plot indicating the maximum payload masses that can be brought to Mars for a transfer in the 2035 launch opportunity. The left figure displays the values for a Type A trajectory, the right figure for a Type B trajectory.

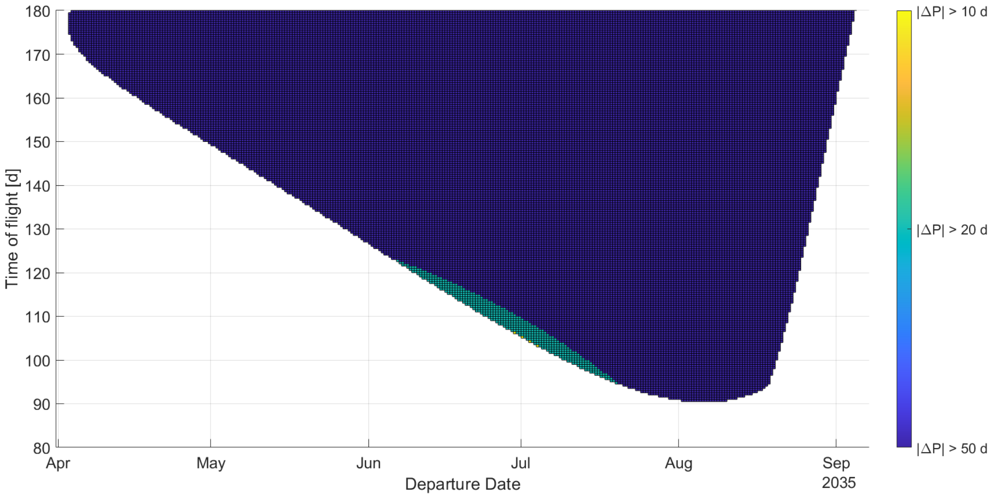

Figure 37: Porkchop plot displaying the values of ΔP from equation (14). Indicates the possibilities of performing a free-return trajectory for all possible Earth-Mars trajectories in the 2035 launch opportunity.

5.6 2037 launch opportunity

The next, and last launch opportunity that I will examine in this document is the one in 2037. It is the last for which SpaceX gives a target minimum time of flight. For this occasion it is 100 days, as presented in table 6.

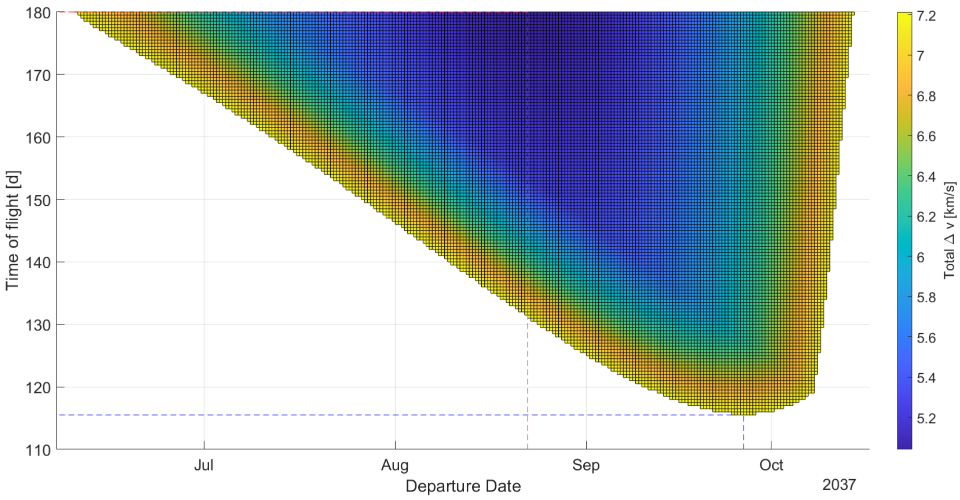

Figure 38: Porkchop plot for a Mars transfer in the 2037 launch opportunity (Type A trajectory). The red, dashed line indicates the minimum Δv trajectory, the blue, dashed line the minimum possible time of flight trajectory.

5.6.1 Minimum Delta-v and time of flight

The launch opportunity in 2037 opens on 10.06.2037 and remains open until 14.10.2037. Hence, it spans over a duration of 127 days, what corresponds to a decrease of 18.6 % in comparison to the previous launch window. The minimum Δv, with which Mars can be reached in 180 days in this launch opportunity, is $5041\,\mathrm{m\,s^{-1}}$ with a departure on 22.08.2037. It is indicated in figure 38 by the red, dashed line. Below, the values for the different propulsive maneuvers over the mission are shown.

Table 22: Δv values for the different maneuvers (Minimum Δv in 2037, Type A)

Maneuver	**Value**
TOI	$4036\,\mathrm{m\,s^{-1}}$
TCM	$400\,\mathrm{m\,s^{-1}}$
MOI	$0\,\mathrm{m\,s^{-1}}$
Landing	$605\,\mathrm{m\,s^{-1}}$
Total	$5041\,\mathrm{m\,s^{-1}}$

Similar to previous launch opportunities, also in this opportunity, no propulsive maneuver is required at MOI, hence the trajectory fulfills the restrictions of Type B trajectories. Upon comparison of the minimum Δv with the one from the 2035 launch opportunity, one observes another increase of 6.7 %. This substantiates the trend of increasing Δv after the 2033 launch opportunity. The same trend is observed for the minimum possible flight time, which is 115.5 days for a departure on 26.09.2037, an increase of 27.6 % in comparison to 2035. This trajectory is indicated by the blue, dashed line in figure 38 and its maneuvers are displayed below.

Table 23: Δv values for the different maneuvers (Minimum TOF in 2037, Type A)

Maneuver	Value
TOI	$5399\,\mathrm{m\,s^{-1}}$
TCM	$400\,\mathrm{m\,s^{-1}}$
MOI	$799\,\mathrm{m\,s^{-1}}$
Landing	$605\,\mathrm{m\,s^{-1}}$
Total	$7203\,\mathrm{m\,s^{-1}}$

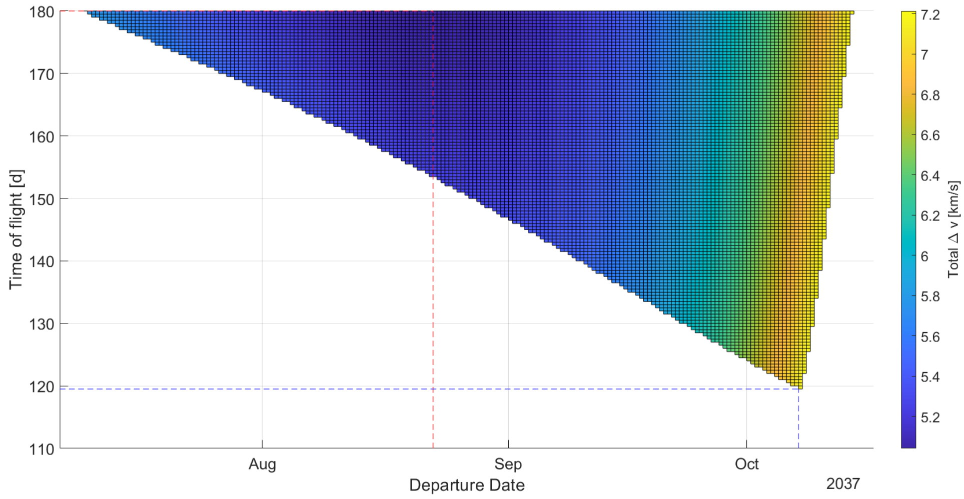

Figure 39: Porkchop plot for a Mars transfer in the 2037 launch opportunity (Type B trajectory). The red, dashed line indicates the minimum Δv trajectory, the blue, dashed line the minimum possible time of flight trajectory.

Looking at Type B trajectories, we can once more skip the minimum Δv and go directly to the minimum possible time of flight. For the 2037 launch opportunity, the minimum possible time of flight is 119.5 days for a departure from Earth on 07.10.2037. This is an increase of 27.1 %, compared with the previous launch opportunity. The Δv for the different maneuvers can be found in the table below.

Table 24: Δv values for the different maneuvers (Minimum TOF in 2037, Type B)

Maneuver	Value
TOI	$6145\,\mathrm{m\,s^{-1}}$
TCM	$400\,\mathrm{m\,s^{-1}}$
Landing	$605\,\mathrm{m\,s^{-1}}$
Total	$7150\,\mathrm{m\,s^{-1}}$

In figure 40, Type A and Type B trajectories are compared. It can be seen that the trend is continued that the difference between the two types is comparably small. Also, the penalty for the minimum possible flight time when using a Type B trajectory is comparably small at 4.4 %.

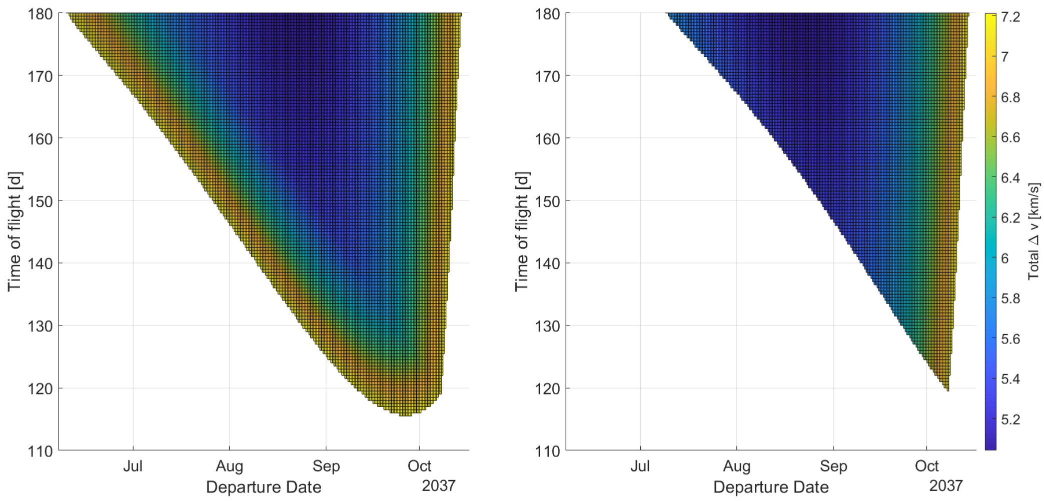

Figure 40: Comparison of trajectory types for a Mars transfer in the 2037 launch opportunity. The left figure displays the values for a Type A trajectory, the right figure for a Type B trajectory.

5.6.2 Maximum allowable payload mass to Mars

The next performance parameter to be considered is the maximum payload mass that can be brought to Mars. For a transfer in the 2037 launch opportunity, it is 264.323 t. As stated before, the trajectory on which this is possible, is always the minimum Δv trajectory. Compared with the previous launch opportunity in 2035, the number poses an decrease of 11.1 %, proving again the decreasing "quality" of launch opportunities. In figure 41, a detailed plot of the maximum payload mass capabilities for different trajectories is shown.

5.6.3 Free-return trajectories

The last aspect that shall be discussed for this launch opportunity are the free-return trajectories. This time, in figure 42, a clear gradation between the different categories can be seen. Compared with the previous launch opportunity, more trajectories have a deviation of less than 50 (light blue color), respectively 20 days (turquoise color). Furthermore, some trajectories differ by between 10 and 5 days (orange color) and less than 5 days (yellow color). This poses by far the best situation of potential free-return trajectories in the observed frame.

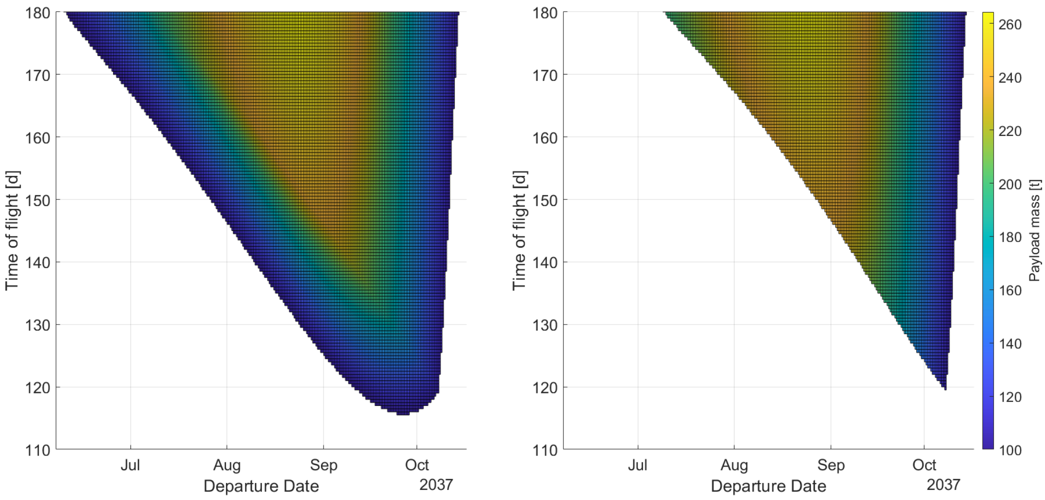

Figure 41: Porkchop plot indicating the maximum payload masses that can be brought to Mars for a transfer in the 2037 launch opportunity. The left figure displays the values for a Type A trajectory, the right figure for a Type B trajectory.

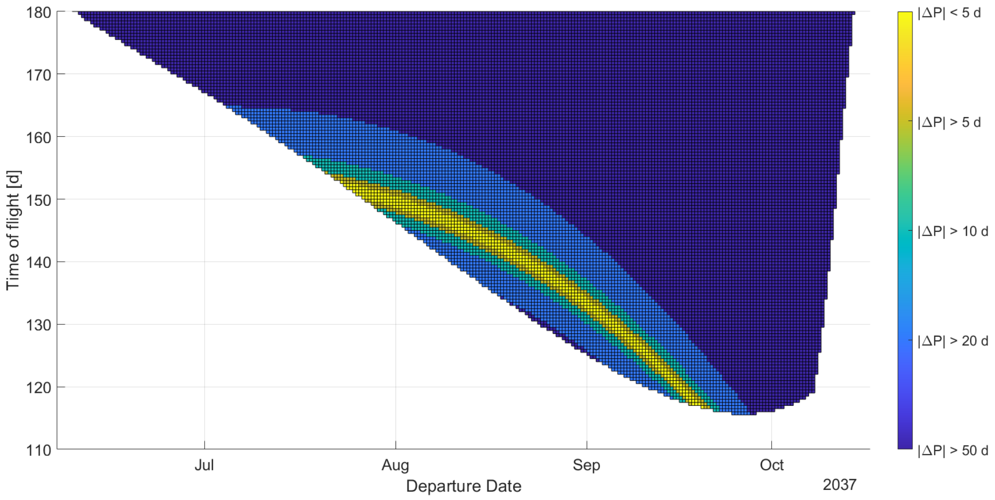

Figure 42: Porkchop plot displaying the values of ΔP from equation (14). Indicates the possibilities of performing a free-return trajectory for all possible Earth-Mars trajectories in the 2037 launch opportunity.

5.7 Summary

The five launch opportunities between 2029 and 2037 have been analyzed with respect to three key performance parameters: The minimum Δv, the minimum possible time of flight and the maximum payload mass. In table 25, these values are listed together with the penalties compared to the global minimum, respective maximum values.

Table 25: Overview over the performance parameters for the different launch opportunities

Launch Opportunity	Minimum Δv	Penalty to Minimum	Minimum TOF	Penalty to Minimum	Maximum Payload mass	Penalty to Maximum
2029	$5252\,\mathrm{m\,s^{-1}}$	12.9 %	147.5 d	63.0 %	243.732 t	18.9 %
2031	$4744\,\mathrm{m\,s^{-1}}$	2.0 %	128.0 d	41.4 %	295.320 t	3.3 %
2033	$4650\,\mathrm{m\,s^{-1}}$	-	99.0 d	9.4 %	305.437 t	-
2035	$4724\,\mathrm{m\,s^{-1}}$	1.6 %	90.5 d	-	297.321 t	2.7 %
2037	$5041\,\mathrm{m\,s^{-1}}$	8.4 %	115.5 d	27.6 %	264.323 t	13.5 %

As can be seen in the table, the launch opportunities in 2033 and 2035 are the best launch opportunities with regard to different performance parameters. The 2033 launch opportunity is the one with the global minimum Δv and hence the maximum global payload mass that can be brought to Mars. The 2035 launch opportunity provides the global minimum possible time of flight. In the other launch opportunities, the penalty compared to the global minimum or maximum become quite large, especially for the minimum time of flight. Additionally, the launch opportunities with the lower minimum Δv values and the shorter minimum times of flight span over a longer duration. Therefore, during these opportunities more flights at a reduced cost, in terms of needed propellant, become possible.
Compared with the targets by SpaceX as presented in table 6, the computed values for the minimum possible time of flight are always longer. The values differ between 7.5 and 18 days, while the mean deviation is 12.1 days. To achieve these flight times, a change in parameters as of table 7 is necessary. For example a lower payload mass could enable these flight times. These considerations will be dealt with in chapter 6.

5.8 Return flight from Mars to Earth

In this chapter I will evaluate the model for the return flight, presented in 4.7. It will be evaluated with respect to the minimum possible time of flight and the minimum possible Δv that is needed for the return.

5.8.1 Restrictions and fixed parameters

When looking at the restrictions, the maximum available Δv is again imposed by the technical design of Starship as of the Tsiolkowski's equation (1). I assume that the return flights will not bring any payload back to earth. According to the data from 2.1.2 and 2.1.3, the maximum available Δv for the return flight is:

$$\Delta v_{max} = 378\,\mathrm{s} \cdot 9.806\,65\,\frac{\mathrm{m}}{\mathrm{s}^2} \cdot \ln\left(\frac{1300\,\mathrm{t}}{100\,\mathrm{t}}\right) = 9508\,\frac{\mathrm{m}}{\mathrm{s}}$$

Again, the maximum time of flight is set to 180 d. This value has been picked arbitrarily since no information by SpaceX is available about how long the return flight shall take. Therefore, I opted to use the same value as for the flight to Mars. The decision by SpaceX would surely by influenced by the estimated time needed to refurbish Starship before the next flight to Mars. But for now, I will take 180 d as a maximum and evaluate the return flight from there on. The following table shows the fixed parameters for all return flights.

Table 26: Overview over the fixed parameters for the return flight

Parameter	Variable	Value	Unit	Remarks
Gravitational parameter of the Sun	μ_S	$1.327 \cdot 10^{11}$	$km^3 s^{-2}$	Rounded, see nomenclature for exact value
Gravitational parameter of the Earth	μ_E	$3.986 \cdot 10^5$	$km^3 s^{-2}$	Rounded, see nomenclature for exact value
Gravitational parameter of Mars	μ_M	$4.283 \cdot 10^4$	$km^3 s^{-2}$	Rounded, see nomenclature for exact value
Radius of circular orbit around Mars	$r_{p,M}$	3640	km	Planet radius of 3390 km + orbital altitude of 250 km
Radius of periapse of Earth arrival hyperbola	$r_{p,E}$	6503	km	Planet radius of 6378 km + orbital altitude of 125 km
Gravitational acceleration at Earth	g_0	9.80665	$m s^{-2}$	-
Payload mass	$m_{P/L}$	0	t	-
Specific impulse	I_{sp}	378	s	-
Structural mass of Starship	m_s	100	t	-
Propellant mass onboard Starship at departure	m_p	1200	t	-

In the following, I will now examine the earliest return possibilities for all presented launch opportunities. The analysis will be limited to Type B trajectories as it has been found out that none of the trajectories needs a propulsive maneuver at the periapse of the arrival hyperbola.

5.8.2 Return flight in 2030/2031

After the first Starship will have landed on Mars in late 2028 or early 2029, a return flight under the given Δv restrictions and in the desired time of flight does again become possible earliest in late 2030. In figure 43, the porkchop plot for this return is shown. The minimum Δv with which a transfer becomes possible is $7786 \, m \, s^{-1}$ for a departure from Mars on 05.01.2031, with a flight time of 180 days. The minimum possible time of flight is 141 days. If one recalls the results from 5.3, where a flight to Mars is possible from January to April, it becomes evident that Starships used in the 2029 launch opportunity can not be used in 2031. These Starships will not return to Earth before July 2031, and together with the needed maintenance time after the return flight, it is impossible to use them already again in the 2031 launch opportunity.

5.8.3 Return flight in 2033

The Starships that have landed on Mars in 2031 will aim for a return flight in 2033, as this is the earliest possible opportunity under the given restrictions. In figure 44, a porkchop plot for these return flights is shown. The minimum Δv for which a transfer becomes possible is $7258 \, m \, s^{-1}$ with a departure from Mars on 17.02.2033 and a flight duration of 180 days. The minimum possible time of flight are 110 days. The Starships will land again on Earth in July or August 2033, earliest. The launch opportunity in 2033 closes already in early July and therefore, it is impossible to use the Starships that have been launched in 2031 again for a Mars flight in 2033.

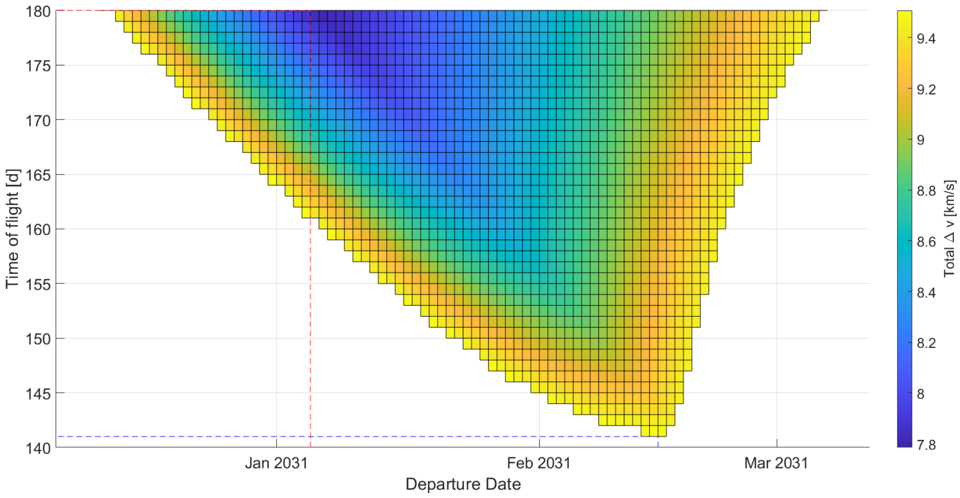

Figure 43: Porkchop plot for a return flight from Mars to Earth in 2030 and 2031. The red line marks the minimum Δv trajectory and the blue line marks the minimum time of flight trajectory.

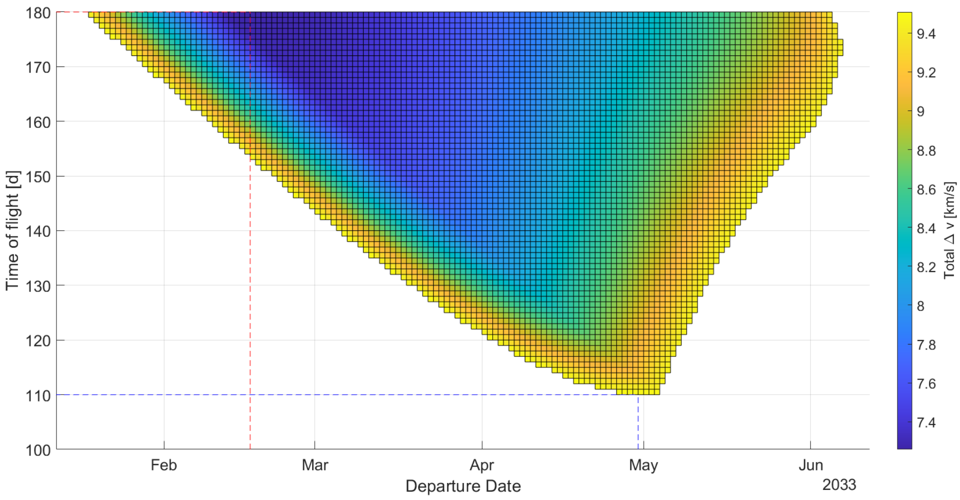

Figure 44: Porkchop plot for a return flight from Mars to Earth in 2033. The red line marks the minimum Δv trajectory and the blue line marks the minimum time of flight trajectory.

5.8.4 Return flight in 2035

The Starships that have been flown to Mars during the 2033 launch opportunity will return to Earth in 2035, which is the earliest opportunity possible due to the restrictions. In the figure 45, a porkchop plot displaying the return opportunities in 2035, is shown.

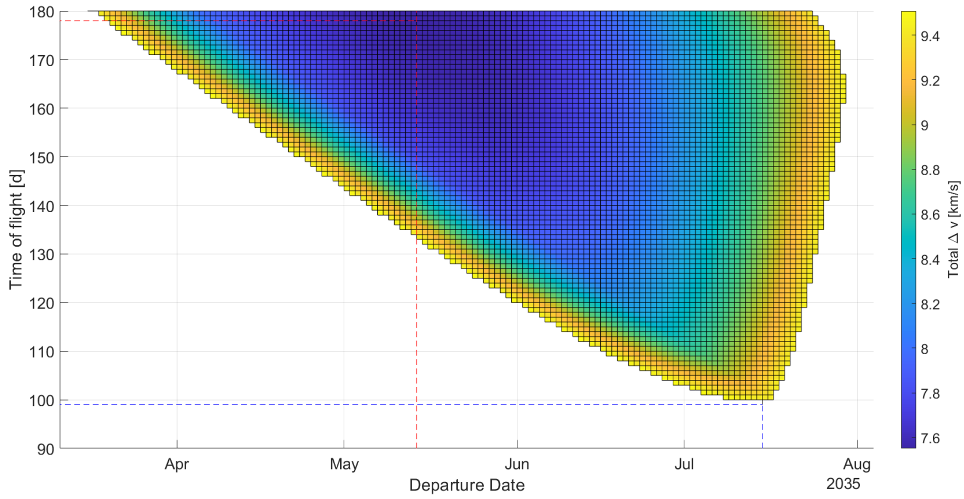

Figure 45: Porkchop plot for a return flight from Mars to Earth in 2035. The red line marks the minimum Δv trajectory and the blue line marks the minimum time of flight trajectory.

The minimum Δv for which a transfer becomes possible is $7552\,\mathrm{m\,s^{-1}}$ with a departure from Mars on 14.05.2035 and a flight duration of 178 days. The minimum possible time of flight are 99 days. This means that the Starships will not land on Earth earlier than in mid September 2035. According to the results from 5.5, the 2035 launch opportunity closes in early September. Therefore, the Starships used for a flight to Mars in 2033 can not be used for a flight to Mars in 2035.

5.8.5 Return flight in 2037

The Starships that have been flown to Mars during the 2035 launch opportunity will return to Earth in 2037, as this is the earliest opportunity possible due to the aforementioned restrictions. In figure 46, a porkchop plot displaying the return opportunities in 2037, is shown. The minimum Δv for which a transfer becomes possible is $8106\,\mathrm{m\,s^{-1}}$ with a departure from Mars on 14.07.2037 and a flight duration of 180 days. The minimum possible time of flight are 126 days. This means that the Starships will not land on Earth earlier than in December 2037. According to the results from 5.6, the 2037 launch opportunity closes in mid October. Therefore, the Starships used for a flight to Mars in 2035 can not be used for a flight to Mars in 2037.

5.8.6 Return flight in 2039

The Starships that have been flown to Mars during the 2037 launch opportunity will return to Earth in 2039, as this is the earliest opportunity possible due to the aforementioned restrictions. In figure 47, a porkchop plot displaying the return opportunities in 2039, is shown. The minimum

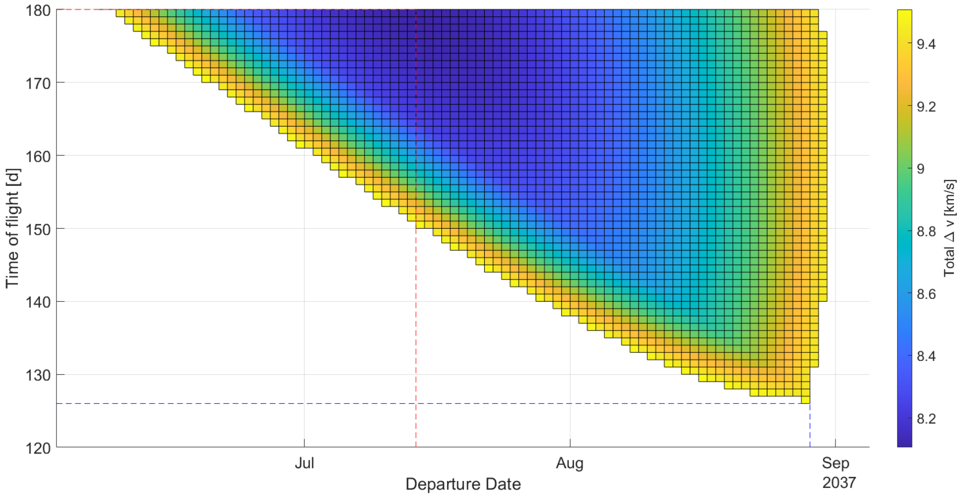

Figure 46: Porkchop plot for a return flight from Mars to Earth in 2037. The red line marks the minimum Δv trajectory and the blue line marks the minimum time of flight trajectory.

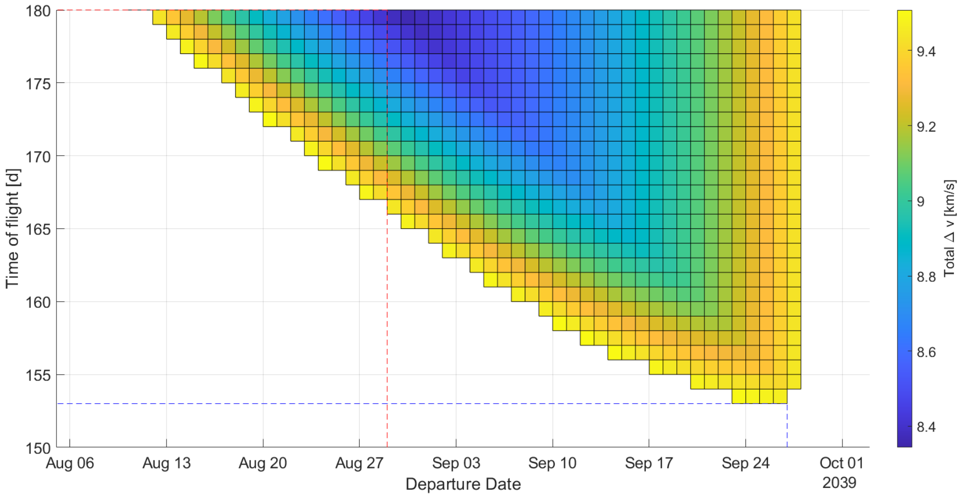

Figure 47: Porkchop plot for a return flight from Mars to Earth in 2039. The red line marks the minimum Δv trajectory and the blue line marks the minimum time of flight trajectory.

Δv for which a transfer becomes possible is $8344\,\mathrm{m\,s^{-1}}$ with a departure from Mars on 29.08.2039 and a flight duration of 180 days. The minimum possible time of flight are 153 days. This means that the Starships will not land on Earth earlier than in mid February 2040. I did not simulate an Earth to Mars transfer in 2039, but according to the observed pattern, it must be assumed that also in this case, the Starships launched to Mars in 2037 can not be used for a flight to Mars in 2039.

5.8.7 Summary

In the previous sections, the minimum possible Δv and flight times during a time span from 2031 to 2039 have been presented. Similar to the flights from Earth to Mars, the values of these two parameters depend strongly on the year in which Starship flies. The values for the minimum Δv range from $7258\,\mathrm{m\,s^{-1}}$ to $8344\,\mathrm{m\,s^{-1}}$, while the values for the minimum time of flight range from 99 to 153 days. In any case, the values are well below the restrictions imposed by the mission design. This means that every launch opportunity for a transfer from Earth to Mars is followed by an opportunity for a return flight about two years later. In between, no return flights are possible considering the restrictions. This has the effect that Starships used for a flight to Mars during a particular launch opportunity can not be used in the following launch opportunity. This means that between two flights to Mars of one Starship there is always a time span of about four years during which it can not be used for flights to Mars. It should be noted that even with a shorter refuelling time and hence an earlier departure, no significantly earlier arrival becomes possible. If one looks at the porkchop plots, it becomes evident that there is a linear relation between the earlier departure and the increased time of flight. Also, based on these results, I would advise against lowering the propellant mass in order to enable an earlier departure as this would only limit the number of possible trajectories without any advantage. Furthermore, if humans should be flown back to Earth, too long times of flight could again pose a risk to their health.
According to the mission plans of SpaceX, they plan to have at least four flights to Mars during every launch opportunity [21]. This means that they have to operate at least eight Starships in the near future - transforming the plans to the new schedule, in 2033 the latest.

5.9 Feasibility of flight times of 30 days

As written before, in his presentation at the IAC 2016, Elon Musk stated that he "[...] expects [...] Mars transit times of as little as 30 days in the more distant future [...]". As described in the previous sections, the current technical specifications of Starship do not allow flight times of under 90 days (compare with table 25). In this section, I will discuss which measures must be taken by SpaceX to lower the minimum flight time.
To be able to assess Musk's statement, it is necessary to first obtain a value for the minimum Δv_{30} that allows a flight time of 30 days, as this value can not be changed by SpaceX. Over the observed time span from 2028 to 2037, this minimum Δv_{30} is at a value of $28\,361\,\mathrm{m\,s^{-1}}$, achievable with a departure on 11.04.2036. For transfers outside of this frame, the values should be similar, because of the 15-year cycle described in 3.4.2. Taking a look at Tsiolkowski's equation (1), it becomes obvious that the technical design of Starship can change four parameters: The specific impulse I_{sp} of the Raptor engine, the propellant mass m_p, the sum structural mass m_s and the payload mass $m_{P/L}$. First, I will take a look, which values these parameters need to take if only one of them is changed at a time. For the parameters, which are not altered, I assume the "standard" values as follows: $I_{sp} = 378\,\mathrm{s}$, $m_p = 1200\,\mathrm{t}$, $m_s = 100\,\mathrm{t}$ and $m_{P/L} = 100\,\mathrm{t}$.
The first parameter that is examined, is the specific impulse of the raptor engine. Rewriting

Tsiolkowski's equation, it is evident that for the specific impulse it must hold that:

$$I_{sp} = \frac{\Delta v_{30}}{g_0 \cdot \ln\left(\frac{m_s + m_p + m_{P/L}}{m_s + m_{P/L}}\right)} = 1486\,\mathrm{s}$$

This value is 3.93 times as large as the current performance of the raptor engine. Also, compared with other liquid fueled rocket engines such as the RL10 of the Delta IV, which has one of the highest specific vacuum impulse among chemical propulsion systems of 465.5 s [41], this value is large. The value of 1486 s is more in the range of typical Ion thrusters, such as the NSTAR, flown onboard of the NASA Deep Space One mission. The NSTAR has a specific impulse between 1900 s and 3100 s [42].
Next, I will take a look at the propellant mass. Considering Tsiolkowski's equation, the required value of m_p is:

$$m_p = \left(m_s + m_{P/L}\right) e^{\frac{\Delta v_{30}}{I_{sp} \cdot g_0}} - \left(m_s + m_{P/L}\right) = 420\,282\,\mathrm{t}$$

Due to the exponential behavior, this value is 350 times higher as the standard value and current maximum propellant mass. Starship in it's standard configuration already has a large propellant mass, which would needed to be significantly increased in this scenario.
The next parameter is the structural mass m_s. It is evident that the smaller m_s gets, the larger the possible Δv gets. For a theoretical value of the structural mass of 0, the possible Δv is $9508\,\mathrm{m\,s^{-1}}$. Therefore, a change of the structural mass alone can not provide the required Δv of $28\,361\,\mathrm{m\,s^{-1}}$. The same accounts for the payload mass. Even for a flight without payload, the possible Δv is not high enough, as shown in figure 15. If the sum of structural and payload mass is small enough however, the achievement of a high enough Δv becomes possible, as indicated by the following equation.

$$m_s + m_{P/L} = \frac{m_p}{e^{\frac{\Delta v_{30}}{I_{sp} \cdot g_0}} - 1} = 571\,\mathrm{kg}$$

If no payload would be brought to Mars, a structural mass of 571 kg would enable the transfer to the determined conditions.
The previous calculations prove that the change of a single parameter is not suitable to enable a transfer time of 30 days. The required I_{sp} is well without reach for any kind of chemical propulsion system, the use of an ion propulsion system would require a re-design of the whole spacecraft. The required propellant mass would require a significantly higher structural mass as well. This would, again, result in a re-design of the whole system and an increase in dimensions. This may lead to difficulties in launching Starship into orbit because the Super Heavy first stage would also needed to be redesigned. The determined structural mass will not be sufficient to support the system when exposed to forces acting on it.
Another approach would be to alter multiple of the parameters simultaneously. The first step is to not bring any payloads to Mars, i.e. $m_{P/L} = 0$. Starting from the specific impulse of the RL10 of 465.5 s, I assumed a theoretical specific impulse of 500 s for this calculation. The structural mass remained at 100 t, which is in fact an improvement as the propellant mass will still be significantly higher and therefore requires bigger tanks. Staying at the same structural mass therefore indicates a better material used for the structure. Using these values, the required propellant mass is 32 407 t.
Even though this value is quite smaller than the one in case of changing only the propellant mass, it still is 27 times higher as the status quo. Also, the specific impulse of 500 s is most likely

only achievable with a LH2/LOX propulsion system, as in the RL10 engine, if achievable at all. This would then require a different approach for the propellant plant on Mars.
The calculations suggest that even in the case of major design changes, Starship is not capable of reaching Mars in 30 days. If SpaceX sticks to these plans, it is very likely necessary to develop a new spacecraft with either a LH2/LOX propulsion system and significantly improved structural materials or a spacecraft using ion thrusters. Then, the whole trajectory analysis in this study would be meaningless as it would use low-thrust trajectories, which require a different model.

6 Sensitivity analysis

As the analysis of the mission baseline has been conducted in chapter 5, I will now have a look at the influence of different parameters on the performance of the Starship system. The motivation for this sensitivity analysis lies in the fact that it is really important to assess the influence of non-nominal performance on the whole system.

6.1 Departure Date

The first parameter on which I will conduct a sensitivity analysis is the departure date. This means that it is to examine how the performance parameters are influenced by a delay in launching by for example five or ten days. Such a delay may not be necessarily caused by Starship itself, but more during the launch process of Super Heavy. As it must be assumed that the refuelling in orbit will always take the same time, a delay in launch will always delay the departure of Starship. Potential reasons for delaying the launch are the meteorological conditions, like storms or heavy winds which do not allow a safe ascent flight or technical difficulties with the fuelling process.

Under the assumption that SpaceX would use the minimum Δv trajectories during the launch opportunities as described in 5, I set the time of flight to 180 days and compared the values for the Δv for different delays with the local minimum value. This allows to directly estimate how sensitive the mission design is in terms of the aforementioned delays. Depending on the sensitivity of the system, I will recommend actions to counteract the sensitivities.

6.1.1 2029 launch opportunity

Calling back the results from 5.2.1, it was shown that the minimum possible Δv during this opportunity was $5252\,\mathrm{m\,s^{-1}}$ and the corresponding maximum possible payload mass that could be brought to Mars, was 243.7 t. Starting from these values, I will examine what influence a delay of 5, 10, 15 and 20 days would have on the nominal values. For a graphical representation, please refer to figure 18, as the delays do not influence the shape of the porkchop plot. The following table displays the values of the performance parameters for the aforementioned delays.

Table 27: Performance parameters for different delays in the 2029 launch opportunity

	Minimum Δv	**Penalty to Minimum**	**Maximum Payload mass**	**Penalty to Maximum**
Nominal launch on 13.01.2029	$5252\,\mathrm{m\,s^{-1}}$	-	243.7 t	-
Delay of 5 days	$5451\,\mathrm{m\,s^{-1}}$	3.8 %	225.5 t	−7.5 %
Delay of 10 days	$5686\,\mathrm{m\,s^{-1}}$	8.3 %	205.0 t	−15.9 %
Delay of 15 days	$5954\,\mathrm{m\,s^{-1}}$	13.4 %	183.3 t	−24.8 %
Delay of 20 days	$6251\,\mathrm{m\,s^{-1}}$	19.0 %	160.9 t	−34.0 %

It can be seen from table 27 that the penalties get quite significant for comparably large delays. This is due to the fact that the 2029 launch opportunity is comparably narrow, considering the time span during which a transfer is possible. Therefore, the boundaries are reached faster, and the Δv grows. But also for medium delays, the penalty influences the mission design. For example, a delay of 10 days results in a total reduction of the maximum possible payload mass of 38.7 t. Especially at the beginning of the flights of Starship, technical difficulties would be expected to occur at a higher rate. Considering this, SpaceX should account for the risks and not fully exhaust the maximum capability of Starship during the first launch opportunity. This could be done by e.g. implementing a payload buffer of 60 t during the 2029 launch opportunity. This would provide them a better flexibility and eliminate the need to re-load Starship with a lower payload mass, e.g. in the case of a problem during refuelling, which would again delay the launch. This buffer would cover against a delay of almost 15 days, allowing to resolve technical problems as mentioned above.

6.1.2 2031 launch opportunity

Remembering the results from 5.3.1, it was shown that the minimum possible Δv during this opportunity was $4744\,\mathrm{m\,s^{-1}}$ and the corresponding maximum possible payload mass that could be brought to Mars, was 295.2 t. Starting from these values, I will again examine the influence of delays, stepped as in the previous section, on the nominal values. For a graphical representation, please refer to figure 23. The following table displays the values of the performance parameters for the aforementioned delays.

Table 28: Performance parameters for different delays in the 2031 launch opportunity

	Minimum Δv	**Penalty to Minimum**	**Maximum Payload mass**	**Penalty to Maximum**
Nominal launch on 10.02.2031	$4744\,\mathrm{m\,s^{-1}}$	-	295.2 t	-
Delay of 5 days	$4808\,\mathrm{m\,s^{-1}}$	1.4 %	288.3 t	−2.3 %
Delay of 10 days	$4899\,\mathrm{m\,s^{-1}}$	3.3 %	278.8 t	−5.6 %
Delay of 15 days	$5010\,\mathrm{m\,s^{-1}}$	5.6 %	267.3 t	−9.5 %
Delay of 20 days	$5142\,\mathrm{m\,s^{-1}}$	8.4 %	254.3 t	−13.9 %

By comparing the values of table 28 with the values from 27, it becomes evident that the influence of a delay on the performance parameters in 2031 is not as strong as in 2029. The payload penalty for a delay of 20 days is −13.9 % and hence less than half as large as the value of −34.0 % from 2029. As mentioned before, this is due to the longer time span over which the launch opportunity remains open in 2031. Assuming a maturation of technology between 2029 and 2031, the payload mass safety buffer can be significantly reduced, also taking in consideration the general improved conditions during this launch opportunity. I propose a buffer of 20 t to cover against a delay of over 10 days, which could be interpreted as technical problems that can be resolved faster as in the 2029 launch opportunity.

6.1.3 2033 launch opportunity

Considering the results from 5.4.1, it was shown that the minimum possible Δv during this opportunity was $4650\,\mathrm{m\,s^{-1}}$ and the corresponding maximum possible payload mass that could be brought to Mars, was 305.4 t. Starting from these values, I will again examine the influence of delays, stepped as in the previous section, on the nominal values. For a graphical representation, please refer to figure 28. The following table displays the values of the performance parameters for the aforementioned delays.

Table 29: Performance parameters for different delays in the 2033 launch opportunity

	Minimum Δv	Penalty to Minimum	Maximum Payload mass	Penalty to Maximum
Nominal launch on 05.04.2033	$4650\,\mathrm{m\,s^{-1}}$	-	305.4 t	-
Delay of 5 days	$4656\,\mathrm{m\,s^{-1}}$	0.1 %	304.8 t	−0.2 %
Delay of 10 days	$4674\,\mathrm{m\,s^{-1}}$	0.5 %	302.8 t	−0.9 %
Delay of 15 days	$4704\,\mathrm{m\,s^{-1}}$	1.2 %	299.5 t	−1.9 %
Delay of 20 days	$4747\,\mathrm{m\,s^{-1}}$	2.1 %	294.9 t	−3.4 %

Once again, the observation is that the sensitivity of the trajectories with respect to the departure date is further reduced. The penalty for a delay of 20 days does not exceed −3.5 % in the 2033 launch opportunity. Compared with the previous launch opportunity in 2031, this is a reduction by almost three fourths. Considering that there will be a further development of the used technologies and that they will be less error-prone, I propose a payload mass buffer of 5 t. This will cover against a delay of more than 10 days, which I would consider sufficient under the assumption that technical problems occur less often and can be resolved in a shorter time.

6.1.4 2035 launch opportunity

Calling to mind the results from 5.5.1, it was shown that the minimum possible Δv during this opportunity was $4724\,\mathrm{m\,s^{-1}}$ and the corresponding maximum possible payload mass that could be brought to Mars, was 297.3 t, both marking a decline from the values in 2033. Starting from these values, I will again examine the influence of delays, stepped as in the previous section, on the nominal values. For a graphical representation, please refer to figure 33. The following table displays the values of the performance parameters for the aforementioned delays.

Table 30: Performance parameters for different delays in the 2035 launch opportunity

	Minimum Δv	Penalty to Minimum	Maximum Payload mass	Penalty to Maximum
Nominal launch on 23.06.2035	$4724\,\mathrm{m\,s^{-1}}$	-	297.3 t	-
Delay of 5 days	$4731\,\mathrm{m\,s^{-1}}$	0.2 %	296.6 t	−0.2 %
Delay of 10 days	$4754\,\mathrm{m\,s^{-1}}$	0.6 %	294.1 t	−1.1 %
Delay of 15 days	$4795\,\mathrm{m\,s^{-1}}$	1.5 %	289.8 t	−2.5 %
Delay of 20 days	$4854\,\mathrm{m\,s^{-1}}$	2.8 %	283.4 t	−4.7 %

Just as the absolute values, also the penalties mark a decline from the previous launch opportunity. The payload mass penalty for a delay of 20 days is growing by 38 % compared to 2033, but the absolute values are not significantly higher. Even under the assumption that a further maturation of technology will take place between 2033 and 2035, I would still propose a small payload mass buffer of 5 t. This allows to cover against a delay of over 10 days as potentially caused by bad weather conditions or minor technical problems. Furthermore, a buffer of 5 t will not affect the general mission design in a heavily negative manner.

6.1.5 2037 launch opportunity

The last opportunity that I will deal with is the 2037 one. Considering the results from 5.6.1, it was shown that the minimum possible Δv during this opportunity was $5041\,\mathrm{m\,s^{-1}}$ and the corresponding maximum possible payload mass that could be brought to Mars, was 264.3 t, once again indicating a clear decline. Starting from these values, I will again examine the influence of delays, stepped as in the previous section, on the nominal values. For a graphical representation, please refer to figure 38. The following table displays the values of the performance parameters for the aforementioned delays.

Table 31: Performance parameters for different delays in the 2037 launch opportunity

	Minimum Δv	**Penalty to Minimum**	**Maximum Payload mass**	**Penalty to Maximum**
Nominal launch on 22.08.2037	$5041\,\mathrm{m\,s^{-1}}$	-	264.3 t	-
Delay of 5 days	$5056\,\mathrm{m\,s^{-1}}$	0.3 %	262.8 t	−0.6 %
Delay of 10 days	$5103\,\mathrm{m\,s^{-1}}$	1.2 %	258.1 t	−2.4 %
Delay of 15 days	$5187\,\mathrm{m\,s^{-1}}$	2.9 %	250.0 t	−5.4 %
Delay of 20 days	$5308\,\mathrm{m\,s^{-1}}$	5.3 %	238.5 t	−9.8 %

This time, the penalty for the payload mass for a delay of 20 days has doubled since the last launch opportunity. Based on the aforementioned considerations, I propose again a payload buffer of 5 t. Even though this is not enough to cover against a delay of 10 days, the ongoing development of the technology in use justifies the smaller buffer.

6.1.6 Summary

It was shown that the sensitivity of the key performance parameters, in this case especially the maximum allowable payload, with respect to delays in the departure date is strongly dependant on the launch opportunity. The penalty of payload mass varies between −3.4 % and −34.0 % for a delay of 20 days, which is a factor of 10. The initially proposed payload mass buffer of 60 t for a transfer within the 2029 launch opportunity was reduced to 5 t from the 2033 launch opportunity forward. This is not only due to the effect of the launch opportunity itself, but also considering a maturation of the used technology over time, which reduces the risk of capital technical problems and allows to solve the problems faster.

6.2 Time of flight

The next parameter on which I will conduct a sensitivity analysis is the time of flight. I will examine how the performance parameters are influenced by a reduction of the flight time by steps of 10 days. In general, SpaceX has to perform a trade-off between the time of flight and the minimum Δv, hence the maximum payload. If the penalties for the latter are small, it might be preferred to reduce the time of flight. Also, it might be beneficial from a medical point of view, considering the health risks for the astronauts exposed to the radiation onboard Starship. For every of the five launch opportunities, I started with a time of flight of 180 days and reduced it in steps of 10 days as far as possible. For every time of flight, I obtained the minimum possible Δv for a transfer and the related maximum payload mass that can be brought to Mars. I then computed the penalties compared with the nominal values for a time of flight of 180 days.
I will also assess whether a reduction of the time of flight is reasonable. To assess that, I used the following guidelines:

- The penalty for the minimum Δv shall be below 10.0 %.
- The penalty for the maximum payload mass shall be below −20.0 %.
- The reduction must be 20 days or more, due to the early stage of analysis. A reduction by 10 days is not meaningful due to the given inaccuracies.

6.2.1 2029 Launch Opportunity

For the 2029 launch opportunity the nominal values are described in 5.2. Also, in figure 18, the porkchop plot for a nominal transfer is shown, also the minimum possible time of flight of 147.5 days can be seen. In table 32, the aforementioned values for different times of flight are displayed.

Table 32: Performance parameters for different time of flights during the 2029 launch opportunity

	Minimum Δv	**Penalty to minimum**	**Maximum payload mass**	**Penalty to maximum**
Nominal flight time of 180 days	$5252\,\mathrm{m\,s^{-1}}$	-	243.7 t	-
TOF 170 days	$5718\,\mathrm{m\,s^{-1}}$	8.9 %	202.3 t	−17.0 %
TOF 160 days	$6306\,\mathrm{m\,s^{-1}}$	20.1 %	157.0 t	−35.6 %
TOF 150 days	$7002\,\mathrm{m\,s^{-1}}$	33.3 %	112.0 t	−54.0 %

For this launch opportunity, already a small reduction of 10 days leads to penalties of 8.9 % for the Δv and −17.0 % for the payload mass. A medium reduction of 30 days leads to a 33.3 % penalty for the Δv, while the maximum payload mass is more than halved. Considering these numbers, a selection of a trajectory with a flight time of under 180 days does not seem reasonable.

6.2.2 2031 Launch Opportunity

For the 2031 launch opportunity the nominal values are described in 5.3. Also, in figure 23, the porkchop plot for a nominal transfer is shown, also the minimum possible time of flight of 128 days can be seen. In table 33, the aforementioned values for different times of flight are displayed.

Table 33: Performance parameters for different time of flights during the 2031 launch opportunity

	Minimum Δv	**Penalty to minimum**	**Maximum payload mass**	**Penalty to maximum**
Nominal flight time of 180 days	$4744\,\mathrm{m\,s^{-1}}$	-	295.2 t	-
TOF 170 days	$4911\,\mathrm{m\,s^{-1}}$	3.5 %	277.5 t	−6.0 %
TOF 160 days	$5193\,\mathrm{m\,s^{-1}}$	9.5 %	249.4 t	−15.5 %
TOF 150 days	$5628\,\mathrm{m\,s^{-1}}$	18.6 %	209.9 t	−28.9 %
TOF 140 days	$6252\,\mathrm{m\,s^{-1}}$	31.8 %	160.9 t	−45.5 %
TOF 130 days	$7016\,\mathrm{m\,s^{-1}}$	47.9 %	111.1 t	−62.4 %

It can be seen that compared with the 2029 launch opportunity, the penalties are significantly smaller. For a delay of 10 days, the penalty for the Δv is 3.5 %, hence less than half as large as in 2029, and the penalty for the maximum payload mass is −6.0 %, hence about one third of the 2029 penalty. Also a medium decrease of the time of flight to 150 days leads to, compared with 2029, low penalties. For the Δv, the penalty is at 18.6 %, hence about half as large as in 2029,the same accounts for the maximum payload mass at −28.9 %. For a transfer in 2031, a reduction of the time of flight by 20 days to 160 days is reasonable.

6.2.3 2033 Launch Opportunity

For the 2033 launch opportunity the nominal values are described in 5.4. Also, in figure 28, the porkchop plot for a nominal transfer is shown, also the minimum possible time of flight of 99 days can be seen. In table 34, the aforementioned values for different times of flight are displayed.

Table 34: Performance parameters for different time of flights during the 2033 launch opportunity

	Minimum Δv	**Penalty to minimum**	**Maximum payload mass**	**Penalty to maximum**
Nominal flight time of 180 days	$4650\,\mathrm{m\,s^{-1}}$	-	305.4 t	-
TOF 170 days	$4675\,\mathrm{m\,s^{-1}}$	0.5 %	302.7 t	−0.9 %
TOF 160 days	$4711\,\mathrm{m\,s^{-1}}$	1.3 %	298.7 t	−2.2 %
TOF 150 days	$4762\,\mathrm{m\,s^{-1}}$	2.4 %	293.3 t	−4.0 %
TOF 140 days	$4868\,\mathrm{m\,s^{-1}}$	4.7 %	281.9 t	−7.7 %
TOF 130 days	$5084\,\mathrm{m\,s^{-1}}$	9.3 %	260.0 t	−14.9 %
TOF 120 days	$5484\,\mathrm{m\,s^{-1}}$	17.9 %	222.5 t	−27.1 %
TOF 110 days	$6198\,\mathrm{m\,s^{-1}}$	33.3 %	164.8 t	−46.0 %
TOF 100 days	$7156\,\mathrm{m\,s^{-1}}$	53.9 %	103.1 t	−66.2 %

Again, one observes a further reduction of the penalties across all reductions steps compared to 2029 and 2031. For a launch in 2033, a reduction of the time of flight by 50 days to 130 days is reasonable, considering the small penalty of 9.3 % for the needed Δv and −14.9 % for the maximum payload mass. For reductions beyond this value, the penalties increase vastly and hence a reduction of the time of flight below 130 days should be avoided.

6.2.4 2035 Launch Opportunity

For the 2035 launch opportunity the nominal values are described in 5.5. Also, in figure 33, the porkchop plot for a nominal transfer is shown, also the minimum possible time of flight of 90.5 days can be seen. In table 35, the aforementioned values for different times of flight are displayed.

Table 35: Performance parameters for different time of flights during the 2035 launch opportunity

	Minimum Δv	**Penalty to minimum**	**Maximum payload mass**	**Penalty to maximum**
Nominal flight time of 180 days	$4724\,\mathrm{m\,s^{-1}}$	-	297.3 t	-
TOF 170 days	$4770\,\mathrm{m\,s^{-1}}$	1.0 %	292.4 t	−1.7 %
TOF 160 days	$4821\,\mathrm{m\,s^{-1}}$	2.1 %	287.0 t	−3.5 %
TOF 150 days	$4880\,\mathrm{m\,s^{-1}}$	3.3 %	280.7 t	−5.6 %
TOF 140 days	$4953\,\mathrm{m\,s^{-1}}$	4.9 %	273.1 t	−8.2 %
TOF 130 days	$5046\,\mathrm{m\,s^{-1}}$	6.8 %	263.8 t	−11.3 %
TOF 120 days	$5170\,\mathrm{m\,s^{-1}}$	9.4 %	251.6 t	−15.4 %
TOF 110 days	$5468\,\mathrm{m\,s^{-1}}$	15.8 %	223.9 t	−24.7 %
TOF 100 days	$6162\,\mathrm{m\,s^{-1}}$	30.4 %	167.4 t	−43.7 %

The observation that one makes when looking at the table is similar to the observation for the 2033 launch opportunity. For small reductions, the penalties are higher, but for bigger reductions, the penalties are smaller then in 2033. In this case, a reduction of the time of flight by 60 days to 120 days is reasonable considering the penalties which are similar to the values for a 50 days reduction in 2033. A further reduction would lead to comparably higher penalties and should therefore be avoided in order to ensure a good performance of the system.

6.2.5 2037 Launch Opportunity

For the 2037 launch opportunity the nominal values are described in 5.6. Also, in figure 38, the porkchop plot for a nominal transfer is shown, also the minimum possible time of flight of 115.5 days can be seen. In table 36, the aforementioned values for different times of flight are displayed.

Table 36: Performance parameters for different time of flights during the 2037 launch opportunity

	Minimum Δv	**Penalty to minimum**	**Maximum payload mass**	**Penalty to maximum**
Nominal flight time of 180 days	$5041\,\mathrm{m\,s^{-1}}$	-	264.3 t	-
TOF 170 days	$5106\,\mathrm{m\,s^{-1}}$	1.3 %	257.8 t	−2.5 %
TOF 160 days	$5187\,\mathrm{m\,s^{-1}}$	2.9 %	250.0 t	−5.4 %
TOF 150 days	$5286\,\mathrm{m\,s^{-1}}$	4.9 %	240.5 t	−9.0 %
TOF 140 days	$5492\,\mathrm{m\,s^{-1}}$	9.0 %	221.8 t	−16.1 %
TOF 130 days	$6006\,\mathrm{m\,s^{-1}}$	19.1 %	179.2 t	−32.2 %
TOF 120 days	$6792\,\mathrm{m\,s^{-1}}$	34.7 %	124.7 t	−52.8 %

Compared with the 2033 and 2035 launch opportunities, the penalties in 2037 are higher, but still smaller than in 2029 and 2031. Considering the values of the penalties, a reduction of the time of flight by 40 days to 140 days is reasonable.

6.2.6 Summary

It was again shown that the sensitivity of the performance parameters on the time of flight is strongly dependant on the launch opportunity.
For the 2029 launch opportunity, a reduction of the time of flight influences the performance parameters in such a manner that any reductions should be avoided. For a transfer in 2031, a small reduction of the time of flight by 20 days is reasonable and can be implemented in the mission design. The drawback from this reduction is acceptable, but the advantage of a flight time of 160 days is also small. For the 2033 and 2035 launch opportunities, large reductions of the time of flight become reasonable. In 2033, the numbers allow a reduction of the time of flight by 50 days to 130 days. In 2035 a reduction of 60 days is possible, hence only two thirds of the nominal time. The mission design should exploit these two opportunities considering the big savings that come at acceptable costs. For a transfer in 2037, a reduction of 40 days is possible according to the defined rules. Also in this case, this opportunity should be used.

6.3 Specific Impulse

Next, I will conduct a sensitivity analysis on the specific impulse of the Raptor engine. A reduction of the specific impulse could be caused by technical problems of the engine. So it is necessary to examine how the performance of the system would be influenced in the case of such a technical problem, in order to perform a risk assessment.
For every of the five examined launch opportunity, I analyzed the effect of a reduction of the specific impulse on the minimum possible time of flight and the maximum payload mass. The minimum Δv is not affected by the reduction. I reduced the specific impulse in steps to 370 s, 360 s, 350 s and 340 s, what is a reduction by 10 % from the nominal value of 378 s.

6.3.1 2029 Launch Opportunity

For the 2029 launch opportunity the nominal values for the minimum time of flight and the maximum payload mass are described in 5.2.1 and 5.2.2, respectively. Also, in figure 18, the porkchop plot for a nominal transfer is shown, the minimum possible time of flight can be seen. Figure 21 displays a porkchop plot for the payload mass. In table 37, the aforementioned values for different specific impulses are displayed.

Table 37: Performance parameters for different specific impulses in the 2029 launch opportunity

	Minimum TOF	**Penalty to minimum**	**Maximum payload mass**	**Penalty to maximum**
Nominal specific impulse of 378 s	147.5 d	-	243.7 t	-
Specific impulse 370 s	149.5 d	1.4 %	232.6 t	−4.6 %
Specific impulse 360 s	152.0 d	3.1 %	218.6 t	−10.3 %
Specific impulse 350 s	154.5 d	4.7 %	204.6 t	−16.0 %
Specific impulse 340 s	157.5 d	6.8 %	190.6 t	−21.8 %

The values show that the effect of the reduction of the specific impulse on the minimum time of flight is small. A reduction of the specific impulse by 10 % leads to an increase of the minimum time of flight by below 7 %. However, the influence of the maximum payload mass is bigger. The reduction of the specific impulse by 10 % causes a reduction of the maximum payload mass by 21.8 %. One also observes an almost linear correlation between the reduction of the specific impulse and the penalty for the maximum payload mass. An empiric formula for the relation is that for a reduction of the specific impulse, a penalty of about 5 % occurs for the maximum payload mass.

6.3.2 2031 Launch Opportunity

For the 2031 launch opportunity the nominal values for the minimum time of flight and the maximum payload mass are described in 5.3.1 and 5.3.2, respectively. Also, in figure 23, the porkchop plot for a nominal transfer is shown, the minimum possible time of flight can be seen.

Figure 26 displays a porkchop plot for the payload mass. In table 38, the aforementioned values for different specific impulses are displayed.

Table 38: Performance parameters for different specific impulses in the 2031 launch opportunity

	Minimum TOF	Penalty to minimum	Maximum payload mass	Penalty to maximum
Nominal specific impulse of 378 s	128.0 d	-	295.3 t	-
Specific impulse 370 s	129.5 d	1.2 %	283.4 t	−4.0 %
Specific impulse 360 s	132.0 d	3.1 %	268.5 t	−9.1 %
Specific impulse 350 s	134.5 d	5.1 %	253.5 t	−14.2 %
Specific impulse 340 s	137.0 d	7.0 %	238.5 t	−19.2 %

The analysis of the derived data shows almost identical numbers as the analysis of the numbers from 2029. The reduction of the specific impulse by 10 % causes a penalty of the minimum possible time of flight of 7 %. And the penalty for the maximum payload mass is about 20 % for this reduction, but slightly lower than in 2029.

6.3.3 2033 Launch Opportunity

For the 2033 launch opportunity the nominal values for the minimum time of flight and the maximum payload mass are described in 5.4.1 and 5.4.2, respectively. Also, in figure 28, the porkchop plot for a nominal transfer is shown, the minimum possible time of flight can be seen. Figure 31 displays a porkchop plot for the payload mass. In table 39, the aforementioned values for different specific impulses are displayed.

Table 39: Performance parameters for different specific impulses in the 2033 launch opportunity

	Minimum TOF	Penalty to minimum	Maximum payload mass	Penalty to maximum
Nominal specific impulse of 378 s	99.0 d	-	305.4 t	-
Specific impulse 370 s	101.0 d	2.0 %	293.5 t	−3.9 %
Specific impulse 360 s	103.0 d	4.0 %	278.4 t	−8.8 %
Specific impulse 350 s	105.0 d	6.1 %	263.3 t	−13.8 %
Specific impulse 340 s	107.0 d	8.1 %	248.1 t	−18.8 %

The analysis of the derived data shows similar numbers as the analysis of the numbers from previous launch opportunity. The reduction of the specific impulse by 10 % causes a penalty of the minimum possible time of flight of 8.1 % and hence slightly larger than in 2029 and 2031. The penalty for the maximum payload mass is at 18.8 % for this reduction, again slightly lower than in 2031.

6.3.4 2035 Launch Opportunity

For the 2035 launch opportunity the nominal values for the minimum time of flight and the maximum payload mass are described in 5.5.1 and 5.5.2, respectively. Also, in figure 33, the porkchop plot for a nominal transfer is shown, the minimum possible time of flight can be seen. Figure 36 displays a porkchop plot for the payload mass. In table 40, the aforementioned values for different specific impulses are displayed.

Table 40: Performance parameters for different specific impulses in the 2035 launch opportunity

	Minimum TOF	**Penalty to minimum**	**Maximum payload mass**	**Penalty to maximum**
Nominal specific impulse of 378 s	90.5 d	-	297.3 t	-
Specific impulse 370 s	91.5 d	1.1 %	285.4 t	−4.0 %
Specific impulse 360 s	93.5 d	3.3 %	270.5 t	−9.0 %
Specific impulse 350 s	95.0 d	5.0 %	255.5 t	−14.1 %
Specific impulse 340 s	97.0 d	7.2 %	240.4 t	−19.1 %

Also the numbers for 2035 strengthens the observations made for previous launch opportunities. The penalty for the minimum time of flight for a reduction of the specific impulse by 10 % is again at about 7 % and slightly lower than in 2033. The penalty for the maximum payload is 19.1 % and hence slightly higher than in 2033, but lower than in 2031 and 2029.

6.3.5 2037 Launch Opportunity

For the 2037 launch opportunity the nominal values for the minimum time of flight and the maximum payload mass are described in 5.6.1 and 5.6.2, respectively. Also, in figure 38, the porkchop plot for a nominal transfer is shown, the minimum possible time of flight can be seen. Figure 41 displays a porkchop plot for the payload mass. In table 41, the aforementioned values for different specific impulses are displayed.

Table 41: Performance parameters for different specific impulses in the 2037 launch opportunity

	Minimum TOF	**Penalty to minimum**	**Maximum payload mass**	**Penalty to maximum**
Nominal specific impulse of 378 s	115.5 d	-	264.3 t	-
Specific impulse 370 s	117.5 d	1.7 %	252.9 t	−4.3 %
Specific impulse 360 s	119.5 d	3.5 %	238.5 t	−9.8 %
Specific impulse 350 s	121.5 d	5.2 %	224.1 t	−15.2 %
Specific impulse 340 s	124.0 d	7.4 %	209.7 t	−20.7 %

Also in 2037, the penalties follow the observed pattern. In this case both penalties experience a slight increase compared with 2035.

6.3.6 Summary

Different to the results of the sensitivity analysis of other parameters, the penalties in this case are only affected by the different launch opportunities in a small manner. It was observed that a reduction of the specific impulse by 10 % causes an increase of about 7 % of the minimum time of flight. The reduction also causes a penalty of the maximum payload mass of about 20 %, slightly following the influence of the different launch opportunities. As an empiric formula for the penalty for the maximum payload mass, the following can be used:

$$\Psi_{m_{P/L}} = -5\,\frac{\%}{\mathrm{s}} \cdot \frac{(378\,\mathrm{s} - I_{sp})}{10} \tag{18}$$

This formula has a certain inaccuracy but still provides, at this early stage of analysis, a sufficient accuracy to estimate the penalty.

6.4 Maximum hyperbolic periapse velocity at Mars

The next parameter that I will perform a sensitivity analysis on is the hyperbolic periapse velocity at Mars $v_{p,M}$. As pointed out earlier, the maximum value for this velocity has been reduced from $8.5\,\mathrm{km\,s^{-1}}$ to $7.5\,\mathrm{km\,s^{-1}}$ in the past. As can be seen from looking at equation (9), a change in the acceptable values for $v_{p,M}$ always leads to a higher or lower acceptable hyperbolic excess velocity $v_{\infty,M}$. The hyperbolic excess velocity is a direct result of the propulsive maneuver performed when arriving at Mars as computed by the algorithm described in 4.2. Therefore, a change in the maximum acceptable value for $v_{p,M}$, influences the number of possible trajectories and potentially also the key performance parameters as indicated by equation (10).
Since there has been a reduction in the past, I will limit this analysis to a further reduction of the maximum value of $v_{p,M}$ to $7\,\mathrm{km\,s^{-1}}$ and $6.5\,\mathrm{km\,s^{-1}}$. Such a reduction would most likely be caused by problems with the heat flux on the heat shield. The higher $v_{p,M}$ is, the higher the heat flux onto the surface becomes. If the heat flux would surpass a critical value, it becomes necessary to lower the velocities in order to avoid failure of the system. I will once again go through the different launch opportunities and calculate the influence of the reduced $v_{p,M}$ on the performance parameters.

6.4.1 2029 launch opportunity

For a transfer in the 2029 launch opportunity, the nominal performance parameters are a minimum possible Δv of $5252\,\mathrm{m\,s^{-1}}$, a minimum possible time of flight of 147.5 days and a maximum payload mass of 247.7 t that can be brought to Mars, as described in 5.2. Below in figure 48, a porkchop plot for a hyperbolic periapse velocity of $7\,\mathrm{km\,s^{-1}}$ is shown. For comparison, refer to figure 18, where the porkchop plots for a nominal transfer is displayed.

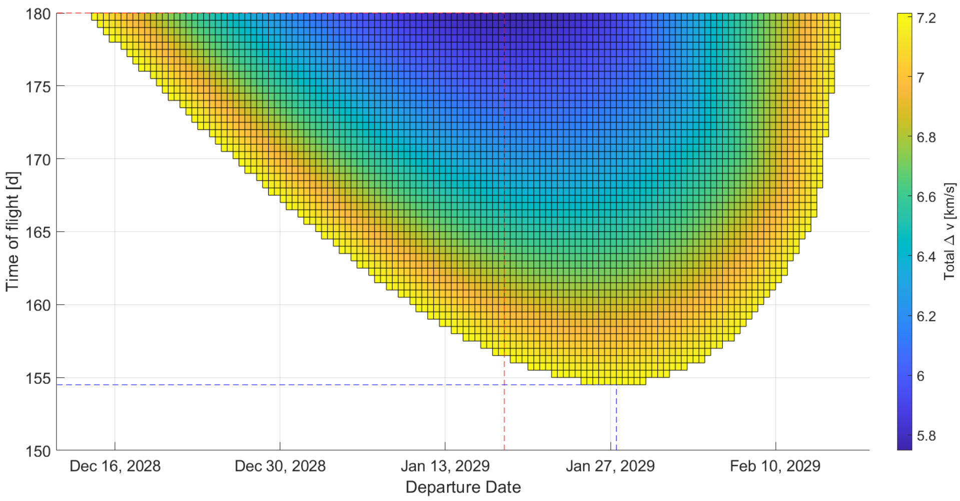

Figure 48: Porkchop plot displaying the values of Δv for a transfer in the 2029 launch opportunity. The maximum value for $v_{p,M}$ was set to $7\,\mathrm{km\,s^{-1}}$. The red, dashed line indicates the minimum Δv trajectory, the blue, dashed line the minimum possible time of flight trajectory.

By looking at the figure above, it becomes evident that the reduction of the hyperbolic periapse velocity has a major influence on the shape of the porkchop plot. It affects all three of the key performance parameters with an increase of the minimum possible time of flight, an increase of the minimum possible Δv and therefore a decrease of the maximum payload mass that can be brought to Mars. In the following table, the key performance parameters for the two velocities are compared and the penalties are displayed.

Table 42: Comparison of key performance parameter values for a maximum hyperbolic periapse velocity $v_{p,M,max} = 7\,\mathrm{km\,s^{-1}}$ with the nominal velocity for a transfer during the 2029 launch opportunity.

	$v_{p,M,max} = 7.5\,\mathrm{km\,s^{-1}}$	$v_{p,M,max} = 7\,\mathrm{km\,s^{-1}}$	Penalty
Minimum TOF	147.5 d	154.5 d	4.7 %
Minimum Δv	$5252\,\mathrm{m\,s^{-1}}$	$5748\,\mathrm{m\,s^{-1}}$	9.4 %
Maximum payload mass	247.7 t	199.8 t	−19.3 %

While the penalty for the minimum possible time of flight is modest, the penalties for the minimum Δv and the maximum payload mass are large. Considering that the reduction of the maximum hyperbolic periapse velocity from $7.5\,\mathrm{km\,s^{-1}}$ to $7\,\mathrm{km\,s^{-1}}$ is a decrease of 6.7 %, the penalties are more than double as large.
Now, I will analyse the results for a further reduced maximum hyperbolic periapse velocity of $6.5\,\mathrm{km\,s^{-1}}$. The reduction from the nominal velocity displays a decrease of 13.3 %. In figure 49, the porkchop plot for the reduced maximum hyperbolic periapse velocity is shown.

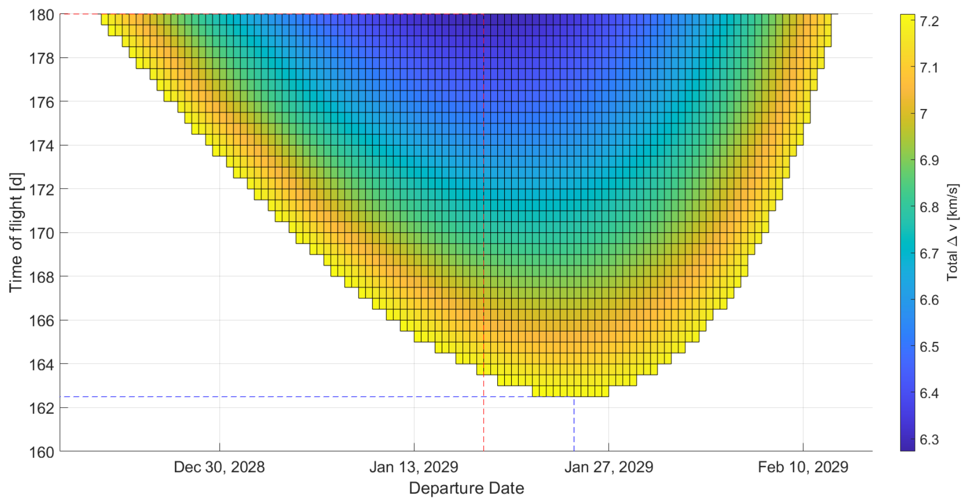

Figure 49: Porkchop plot displaying the values of Δv for a transfer in the 2029 launch opportunity. The maximum value for $v_{p,M}$ was set to $6.5\,\mathrm{km\,s^{-1}}$. The red, dashed line indicates the minimum Δv trajectory, the blue, dashed line the minimum possible time of flight trajectory.

The reduction of the maximum hyperbolic periapse velocity to $6.5\,\mathrm{km\,s^{-1}}$ further restricts the number of possible trajectories, which can be seen best by looking at the minimum possible time of flight. The detailed numbers for the key performance parameters are presented in the table below together with the respective penalties.

Table 43: Comparison of key performance parameter values for a maximum hyperbolic periapse velocity $v_{p,M,max} = 6.5\,\mathrm{km\,s^{-1}}$ with the nominal velocity for a transfer during the 2029 launch opportunity.

	$v_{p,M,max} = 7.5\,\mathrm{km\,s^{-1}}$	$v_{p,M,max} = 6.5\,\mathrm{km\,s^{-1}}$	Penalty
Minimum TOF	147.5 d	162.5 d	10.2 %
Minimum Δv	$5252\,\mathrm{m\,s^{-1}}$	$6273\,\mathrm{m\,s^{-1}}$	19.4 %
Maximum payload mass	247.7 t	159.4 t	−35.6 %

It can be seen that the penalties increase compared with a maximum hyperbolic periapse velocity of $7\,\mathrm{km\,s^{-1}}$. The penalty for the minimum time of flight is more than double as high, while the penalties for minimum Δv and maximum payload mass are less than double as high. Regardless of the exact numbers, it has become evident that a reduction of the maximum hyperbolic periapse velocity has a significant negative influence on the key performance parameters, when using a transfer in the 2029 launch opportunity. I will now go on to the next launch opportunity in 2031 to analyse whether transfers during this opportunity are as sensitive as in 2029.

6.4.2 2031 launch opportunity

In the 2031 launch opportunity, the nominal values for the three key performance parameters mark an improvement compared with 2029. The minimum time of flight is 128 days, the minimum Δv is $4744\,\mathrm{m\,s^{-1}}$ and the maximum payload is 295.3 t. In figure 48, the porkchop plot for a maximum hyperbolic periapse velocity of $7.0\,\mathrm{km\,s^{-1}}$ is displayed. For comparison, refer to figure 18, where the porkchop plot under nominal conditions is shown.

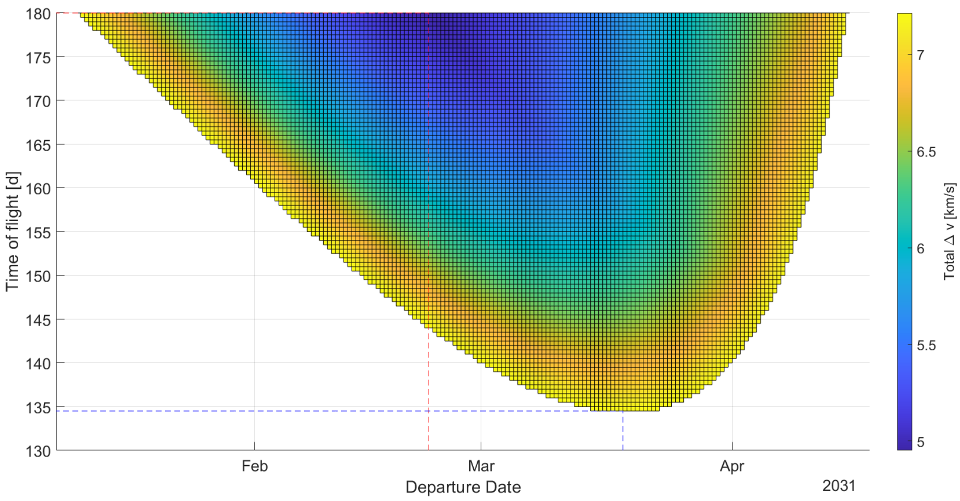

Figure 50: Porkchop plot displaying the values of Δv for a transfer in the 2031 launch opportunity. The maximum value for $v_{p,M}$ was set to $7\,\mathrm{km\,s^{-1}}$. The red, dashed line indicates the minimum Δv trajectory, the blue, dashed line the minimum possible time of flight trajectory.

As expected, the number of possible trajectories is reduced by the restrictions. Most notably,

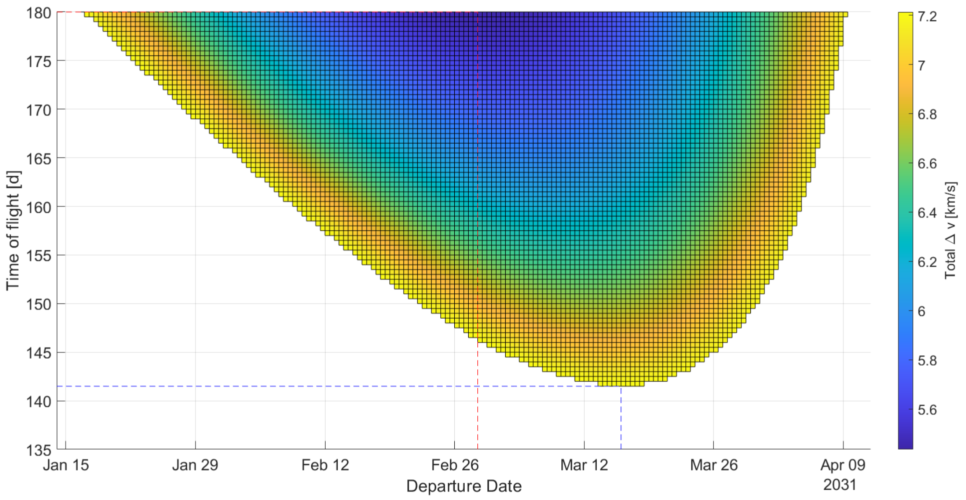

Figure 51: Porkchop plot displaying the values of Δv for a transfer in the 2031 launch opportunity. The maximum value for $v_{p,M}$ was set to $6.5\,\mathrm{km\,s^{-1}}$. The red, dashed line indicates the minimum Δv trajectory, the blue, dashed line the minimum possible time of flight trajectory.

the minimum time of flight is increased, what can be seen directly from comparing the figures. In the table below, the values for the key parameters and the penalties when compared with the nominal values are provided.

Table 44: Comparison of key performance parameter values for a maximum hyperbolic periapse velocity $v_{p,M,max} = 7\,\mathrm{km\,s^{-1}}$ with the nominal velocity for a transfer during the 2031 launch opportunity.

	$v_{p,M,max} = 7.5\,\mathrm{km\,s^{-1}}$	$v_{p,M,max} = 7\,\mathrm{km\,s^{-1}}$	Penalty
Minimum TOF	128 d	134.5 d	5.1 %
Minimum Δv	$4744\,\mathrm{m\,s^{-1}}$	$4952\,\mathrm{m\,s^{-1}}$	4.4 %
Maximum payload mass	295.3 t	273.3 t	−7.5 %

It can be seen that the penalty for the minimum time of flight is close to the value from 2029, displaying a small increase of 0.4 %. In contrast, the penalties for minimum Δv and maximum payload mass are lower, being more than halved. This is a clear indication of the lower sensitivity for the 2031 launch opportunity with respect to the maximum hyperbolic periapse velocity.
In figure 51, the porkchop plot for a maximum hyperbolic periapse velocity of $6.5\,\mathrm{km\,s^{-1}}$ is displayed. By direct comparison of figures 51 and 50, one can observe the restricting character of a lower maximum hyperbolic periapse velocity. The minimum time of flight is again increasing and the launch opportunity itself becomes narrower in terms of the time it remains open. In the table below, the key performance parameters and the penalties compared with the nominal values are displayed.

Table 45: Comparison of key performance parameter values for a maximum hyperbolic periapse velocity $v_{p,M,max} = 6.5\,\mathrm{km\,s^{-1}}$ with the nominal velocity for a transfer during the 2031 launch opportunity.

	$v_{p,M,max} = 7.5\,\mathrm{km\,s^{-1}}$	$v_{p,M,max} = 6.5\,\mathrm{km\,s^{-1}}$	Penalty
Minimum TOF	128 d	141.5 d	10.5 %
Minimum Δv	$4744\,\mathrm{m\,s^{-1}}$	$5435\,\mathrm{m\,s^{-1}}$	14.6 %
Maximum payload mass	295.7 t	226.8 t	−23.2 %

Compared with a maximum hyperbolic periapse velocity of $7\,\mathrm{km\,s^{-1}}$, the penalty for the minimum time of flight has more than doubled, while the penalties for minimum Δv and maximum payload mass have more than triplicated. Compared with the values of the key parameters for a maximum hyperbolic periapse velocity of $6.5\,\mathrm{km\,s^{-1}}$ in the 2029 launch opportunity, the penalties are lower, 5.0 % in case of the minimum Δv, and 12.4 % in the case of the maximum payload mass.

6.4.3 2033 launch opportunity

Next up is the sensitivity analysis for the 2033 launch opportunity. The nominal values of the key performance parameters during this launch opportunity are 99 days for the minimum time of flight, $4650\,\mathrm{m\,s^{-1}}$ for the minimum Δv and 305.4 t for the maximum payload mass, the latter two representing a global minimum and maximum. In figure 52, the porkchop plot for a maximum hyperbolic periapse velocity of $7\,\mathrm{km\,s^{-1}}$ for transfers in 2033 is displayed.

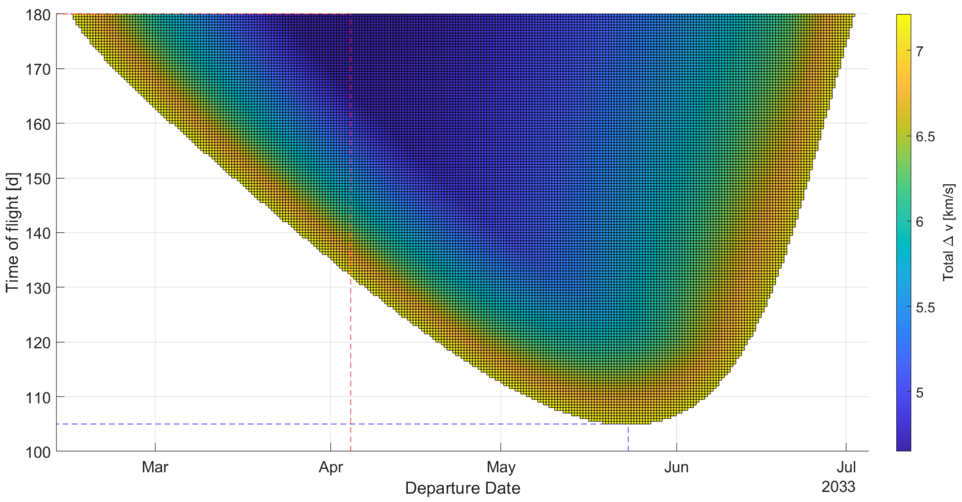

Figure 52: Porkchop plot displaying the values of Δv for a transfer in the 2033 launch opportunity. The maximum value for $v_{p,M}$ was set to $7\,\mathrm{km\,s^{-1}}$. The red, dashed line indicates the minimum Δv trajectory, the blue, dashed line the minimum possible time of flight trajectory.

Upon comparison with the nominal porkchop plot in figure 28, the expected result of an increasing minimum time of flight can be observed. In the table below, detailed results for the key performance parameter are displayed.

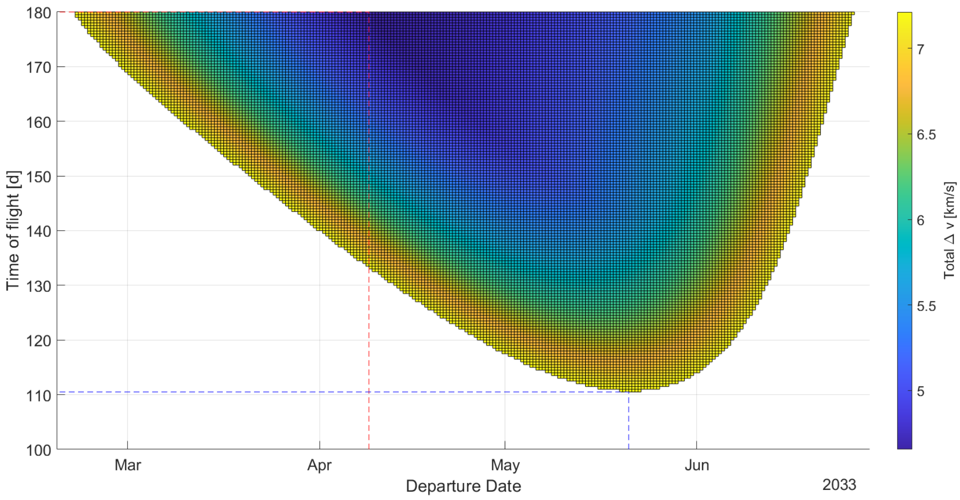

Figure 53: Porkchop plot displaying the values of Δv for a transfer in the 2033 launch opportunity. The maximum value for $v_{p,M}$ was set to $6.5\,\mathrm{km\,s^{-1}}$. The red, dashed line indicates the minimum Δv trajectory, the blue, dashed line the minimum possible time of flight trajectory.

Table 46: Comparison of key performance parameter values for a maximum hyperbolic periapse velocity $v_{p,M,max} = 7\,\mathrm{km\,s^{-1}}$ with the nominal velocity for a transfer during the 2033 launch opportunity.

	$v_{p,M,max} = 7.5\,\mathrm{km\,s^{-1}}$	$v_{p,M,max} = 7\,\mathrm{km\,s^{-1}}$	Penalty
Minimum TOF	99 d	105 d	6.1 %
Minimum Δv	$4650\,\mathrm{m\,s^{-1}}$	$4650\,\mathrm{m\,s^{-1}}$	-
Maximum payload mass	305.4 t	305.4 t	-

The minimum time of flight penalty again depicts a small increase to the 2031 launch opportunity at 6.1 %. In contrast, the penalties for the minimum Δv and the maximum payload mass vanish. This is an indication that a good performance in terms of Δv consumption and payload mass that can be brought to Mars is also possible on less demanding transfer trajectories. In figure 53, the porkchop plot for a maximum hyperbolic periapse velocity of $6.5\,\mathrm{km\,s^{-1}}$ is shown. It can be observed in the plot that the minimum time of flight is increasing compared with higher maximum hyperbolic periapse velocities. In the table below, the values of the key performance parameters are shown and compared with the nominal values.

Table 47: Comparison of key performance parameter values for a maximum hyperbolic periapse velocity $v_{p,M,max} = 6.5\,\mathrm{km\,s^{-1}}$ with the nominal velocity for a transfer during the 2033 launch opportunity. The red, dashed line indicates the minimum Δv trajectory, the blue, dashed line the minimum possible time of flight trajectory.

	$v_{p,M,max} = 7.5\,\mathrm{km\,s^{-1}}$	$v_{p,M,max} = 6.5\,\mathrm{km\,s^{-1}}$	Penalty
Minimum TOF	99 d	110.5 d	11.6 %
Minimum Δv	$4650\,\mathrm{m\,s^{-1}}$	$4655\,\mathrm{m\,s^{-1}}$	0.1 %
Maximum payload mass	305.4 t	304.9 t	−0.2 %

The obtained values follow the observed pattern that has been present for past launch opportunities. The penalty for the minimum time of flight is about double as large as for a maximum hyperbolic periapse velocity of $7\,\mathrm{km\,s^{-1}}$, and about 10 % when compared to the nominal values. The penalties for minimum Δv and maximum payload mass are low and approaching zero for transfers in the 2033 launch opportunity.

6.4.4 2035 launch opportunity

For a transfer in the 2035 launch opportunity, the nominal values for a transfer are as follows. The minimum time of flight is 90.5 days, indicating a global minimum, the minimum Δv is $4724\,\mathrm{m\,s^{-1}}$ and the maximum payload mass that can be brought to Mars is 297.3 t. In figure 54, a porkchop plot for a maximum hyperbolic periapse velocity of $7\,\mathrm{km\,s^{-1}}$ for transfers in the 2035 launch opportunity is shown.

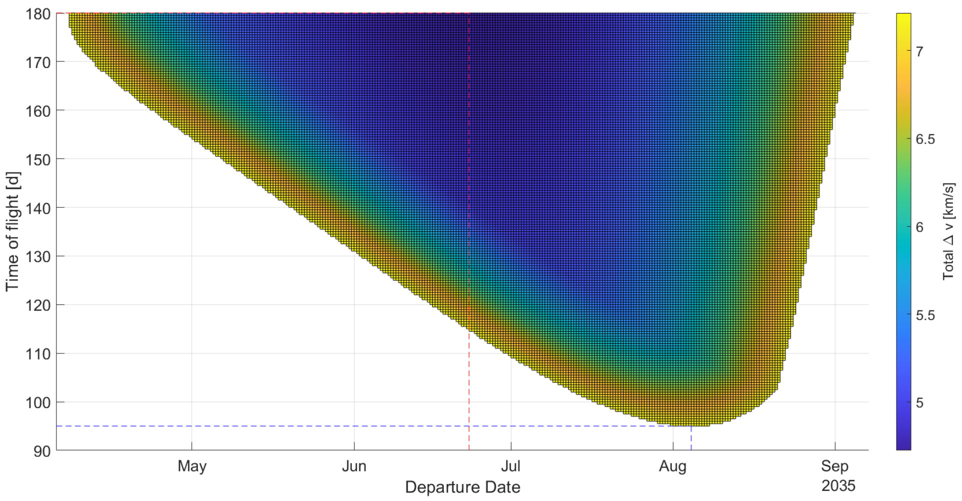

Figure 54: Porkchop plot displaying the values of Δv for a transfer in the 2035 launch opportunity. The maximum value for $v_{p,M}$ was set to $7\,\mathrm{km\,s^{-1}}$. The red, dashed line indicates the minimum Δv trajectory, the blue, dashed line the minimum possible time of flight trajectory.

Table 48: Comparison of key performance parameter values for a maximum hyperbolic periapse velocity $v_{p,M,max} = 7\,\mathrm{km\,s^{-1}}$ with the nominal velocity for a transfer during the 2035 launch opportunity.

	$v_{p,M,max} = 7.5\,\mathrm{km\,s^{-1}}$	$v_{p,M,max} = 7\,\mathrm{km\,s^{-1}}$	Penalty
Minimum TOF	90.5 d	95 d	5.0 %
Minimum Δv	$4724\,\mathrm{m\,s^{-1}}$	$4724\,\mathrm{m\,s^{-1}}$	-
Maximum payload mass	297.3 t	297.3 t	-

Looking at the values in table 48 and figure 54, it is evident that the observed pattern is the same as in 2033. Again, the penalty for the minimum time of flight is about 5 %, while there is no penalty for neither the minimum Δv nor the maximum payload mass. Figure 55 shows the porkchop plot for a maximum hyperbolic periapse velocity of 6.5 % for transfers in 2035, and table 49 displays the values for the key performance parameters and the penalties when compared with their nominal values.

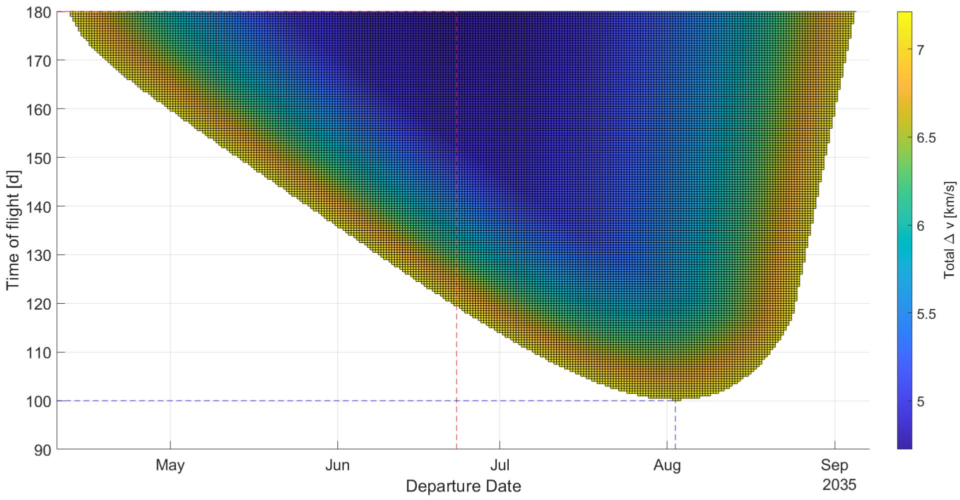

Figure 55: Porkchop plot displaying the values of Δv for a transfer in the 2035 launch opportunity. The maximum value for $v_{p,M}$ was set to $6.5\,\mathrm{km\,s^{-1}}$. The red, dashed line indicates the minimum Δv trajectory, the blue, dashed line the minimum possible time of flight trajectory.

Table 49: Comparison of key performance parameter values for a maximum hyperbolic periapse velocity $v_{p,M,max} = 6.5\,\mathrm{km\,s^{-1}}$ with the nominal velocity for a transfer during the 2035 launch opportunity.

	$v_{p,M,max} = 7.5\,\mathrm{km\,s^{-1}}$	$v_{p,M,max} = 6.5\,\mathrm{km\,s^{-1}}$	Penalty
Minimum TOF	90.5 d	100 d	10.5 %
Minimum Δv	$4724\,\mathrm{m\,s^{-1}}$	$4724\,\mathrm{m\,s^{-1}}$	-
Maximum payload mass	297.3 t	297.3 t	-

Now, also for a maximum hyperbolic periapse velocity of 6.5 %, there are no penalties for the minimum Δv and the maximum payload mass. The penalty for the minimum possible time of flight is at 10.5 % around double as large as for a maximum hyperbolic velocity of $7\,\mathrm{km\,s^{-1}}$, thus fortifying this pattern.

6.4.5 2037 launch opportunity

The last launch opportunity that I will go through is the 2037 one. The nominal value for the minimum time of flight is 115.5 days, for the minimum Δv it is $5041\,\mathrm{m\,s^{-1}}$ and for the maximum payload mass it is 264.3 t. In the figure and the table below, a graphical presentation together with the values of key performance parameters can be found.

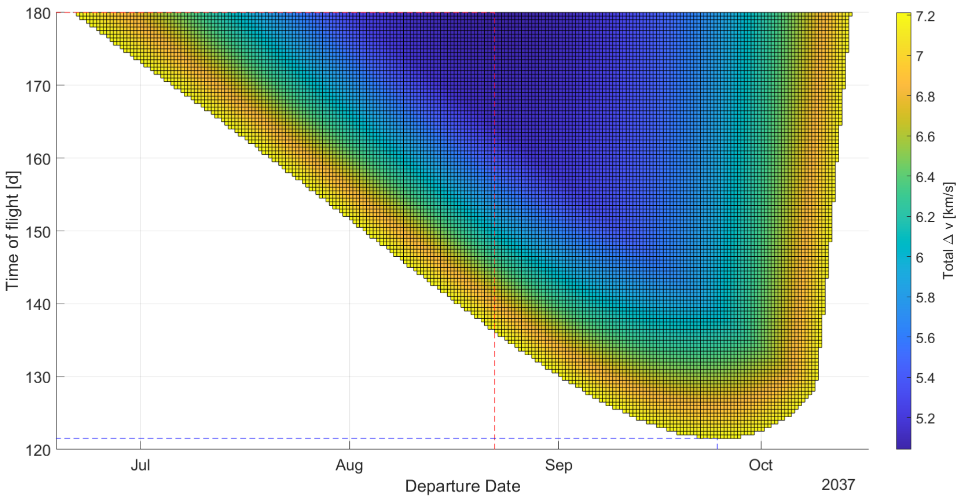

Figure 56: Porkchop plot displaying the values of Δv for a transfer in the 2037 launch opportunity. The maximum value for $v_{p,M}$ was set to $7\,\mathrm{km\,s^{-1}}$. The red, dashed line indicates the minimum Δv trajectory, the blue, dashed line the minimum possible time of flight trajectory.

Table 50: Comparison of key performance parameter values for a maximum hyperbolic periapse velocity $v_{p,M,max} = 7\,\mathrm{km\,s^{-1}}$ with the nominal velocity for a transfer during the 2037 launch opportunity.

	$v_{p,M,max} = 7.5\,\mathrm{km\,s^{-1}}$	$v_{p,M,max} = 7\,\mathrm{km\,s^{-1}}$	Penalty
Minimum TOF	115.5 d	121.5 d	5.2 %
Minimum Δv	$5041\,\mathrm{m\,s^{-1}}$	$5041\,\mathrm{m\,s^{-1}}$	-
Maximum payload mass	264.3 t	264.3 t	-

Just as in previous launch opportunity, the key performance parameters show the same sensitivity. The penalty for the minimum time of flight is about 5 %, while the values for minimum Δv and the maximum payload mass are not affected by the reduction of the maximum hyperbolic periapse velocity to $7\,\mathrm{km\,s^{-1}}$. Below, figure 57 shows a porkchop plot for a maximum hyperbolic periapse velocity of $6.5\,\mathrm{km\,s^{-1}}$.

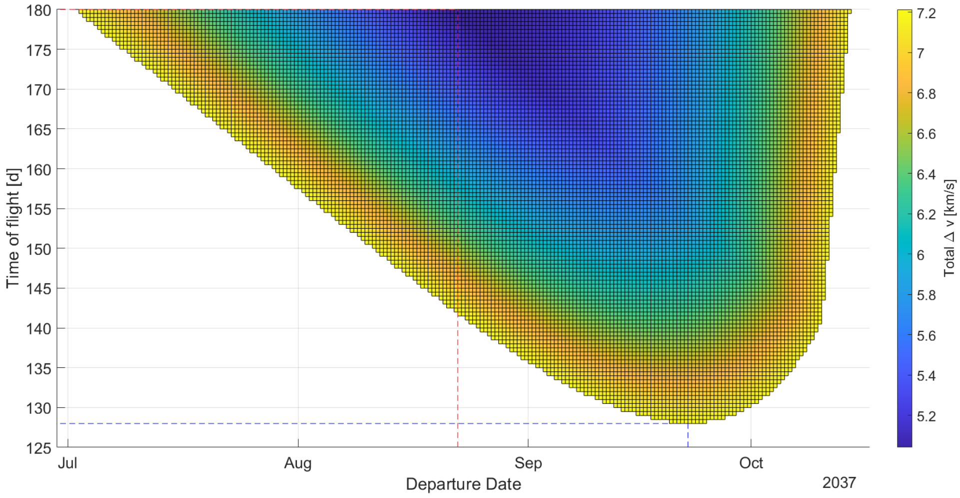

Figure 57: Porkchop plot displaying the values of Δv for a transfer in the 2037 launch opportunity. The maximum value for $v_{p,M}$ was set to $6.5\,\mathrm{km\,s^{-1}}$. The red, dashed line indicates the minimum Δv trajectory, the blue, dashed line the minimum possible time of flight trajectory.

Table 51: Comparison of key performance parameter values for a maximum hyperbolic periapse velocity $v_{p,M,max} = 6.5\,\mathrm{km\,s^{-1}}$ with the nominal velocity for a transfer during the 2037 launch opportunity.

	$v_{p,M,max} = 7.5\,\mathrm{km\,s^{-1}}$	$v_{p,M,max} = 6.5\,\mathrm{km\,s^{-1}}$	Penalty
Minimum TOF	115.5 d	128 d	10.8 %
Minimum Δv	$5041\,\mathrm{m\,s^{-1}}$	$5041\,\mathrm{m\,s^{-1}}$	-
Maximum payload mass	264.3 t	264.3 t	-

As shown in the table above, once again the sensitivity with respect to the maximum hyperbolic periapse velocity shows the same pattern. The penalty for the minimum time of flight is about 10 % when compared with the nominal value, and the penalties for the minimum Δv and the maximum payload mass vanishes.

6.4.6 Summary

It has been shown that the minimum time of flight has a sensitivity towards the maximum hyperbolic periapse velocity, regardless of the launch opportunity. Also, it is only slightly dependent on the launch opportunity. For a reduction of the maximum hyperbolic periapse velocity to $7\,\mathrm{km\,s^{-1}}$, the minimum time of flight shows penalties of 4.7 % to 6.1 % when compared with the nominal values. In absolute numbers this corresponds to penalties of 4.5 to 7 days. For a reduction to $6.5\,\mathrm{km\,s^{-1}}$ the penalties range from 10.2 % to 11.6 %, corresponding to absolute values of 9.5 to 15 days. The largest penalties percentaged do both occur in the 2033 launch opportunity, while the largest absolute penalties occur in the 2029 launch opportunity.
As shown before, the penalties for the minimum Δv and the maximum payload mass are closely related and with regard to their sensitivity with respect to the maximum hyperbolic periapse

velocity, their penalties are strongly dependent on the launch opportunity.
For a reduction to $7\,\mathrm{km\,s^{-1}}$, from the 2033 launch opportunity on, there are no penalties anymore for these two parameters. In the 2029 launch opportunity, the penalties are 9.4 % for the minimum Δv and −19.3 % for the maximum payload mass, corresponding to an absolute value of 47.9 t. For the 2031 launch opportunity, the penalties are lower at 4.4 % for the minimum Δv and at −7.5 % for the maximum payload mass, displaying an absolute value of 22.0 t.
For a reduction to $6.5\,\mathrm{km\,s^{-1}}$ there are no penalties for these two parameters from 2035 on. For 2029, the further reduction causes about double as large penalties with 19.4 % for the minimum Δv and −35.6 % for the maximum payload mass, displaying an absolute value of 88.3 t. For 2031, the penalties are smaller than in 2031, but the further reduction has caused a triplication. Now, the penalty for the minimum Δv is at 14.6 %, while the penalty for the maximum payload mass is at −23.2 %, displaying an absolute penalty of 68.9 t. For 2033, there are penalties for both parameters, but they are small at 0.1 % for the minimum Δv and at −0.2 % for the maximum payload mass.
While there is a constant penalty across all launch opportunities for the minimum time of flight, the penalties for the minimum Δv and the maximum payload mass are only present and relevant for transfers in 2029 and 2031. But within these two opportunities, the reduction of the maximum hyperbolic periapse velocity causes absolute penalties of up to 88.3 t, which will for sure negatively affect the mission design. For later launch opportunities, the reduction would have no effect on the mission design, apart from the longer minimum times of flight.

6.5 Propellant mass

The last parameter I will perform a sensitivity analysis on, is the propellant mass m_p. I will discuss the effects of a reduction of the propellant mass that is fuelled into Starship during the re-fuelling phase in LEO. As can be seen by looking at equations (1) and (13), a lower propellant mass will lead to a lower available Δv for the transfer and, hence, to a lower maximum payload mass that can be brought to Mars. Looking at the defined performance parameters, in this analysis, the values for the maximum payload and the minimum time of flight will change, while there will be no effect on the minimum Δv.
The motivation for this analysis is originated mainly in the technology that is used for storing the propellant in orbit. As the propellants are cryogenic, boil-off is a big problem, as the solar influx will cause vaporization of the propellant. Therefore, it is preferable to speed up the process to reduce the propellant mass that will be made unserviceable through vaporization. So, there might be the possibility that a trade-off between propellant mass and payload mass is reasonable. In the following, I will analyse the results for a reduction of the nominal propellant mass of 1200 t down to 800 t in steps of 100 t for all launch opportunities. The following figure shows the maximum possible Δv for a varying payload mass m_p as of equation (1).

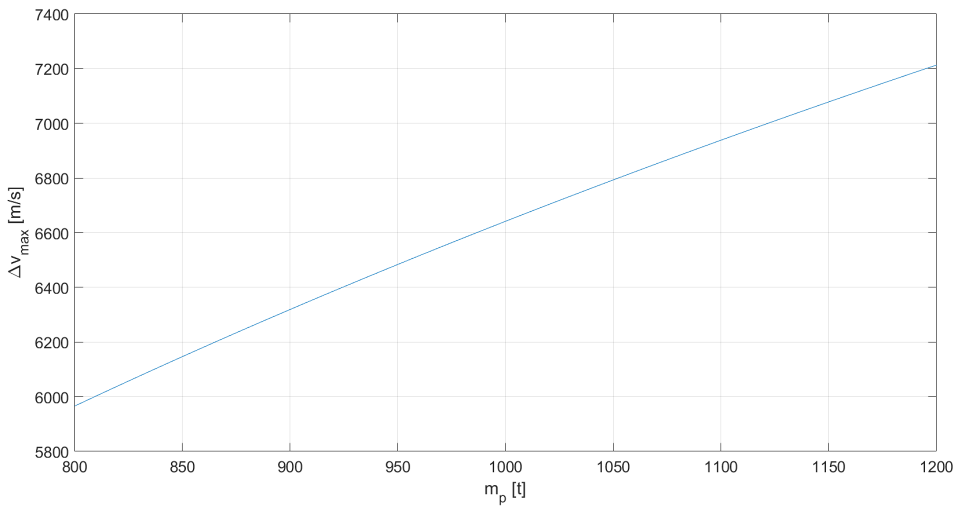

Figure 58: Maximum possible Δv_{max} that can be applied by Starship for a varying propellant mass m_p.

6.5.1 2029 launch opportunity

Starting with the 2029 launch opportunities, the nominal values for the minimum time of flight and the maximum payload mass are 147.5 d and 247.7 t. In figure 59, a porkchop plot for a reduced propellant mass of 1100 t is displayed. The minimum time of flight goes up to 151 d and the maximum payload mass is decreased to 220.7 t. Hence, the saving of 100 t reduces the maximum possible payload mass by 27.0 t, which is a penalty of −10.9 %. The minimum time of flight experiences a penalty of 2.4 %, caused by the reduced propellant mass.
In figure 60, the porkchop plot for a propellant mass of 1000 t is shown. For this reduction of the propellant mass, the minimum time of flight is increased to 155 d, and the maximum payload mass is decreased to 196.9 t. The reduction of the propellant mass by 200 t leads to a reduction of

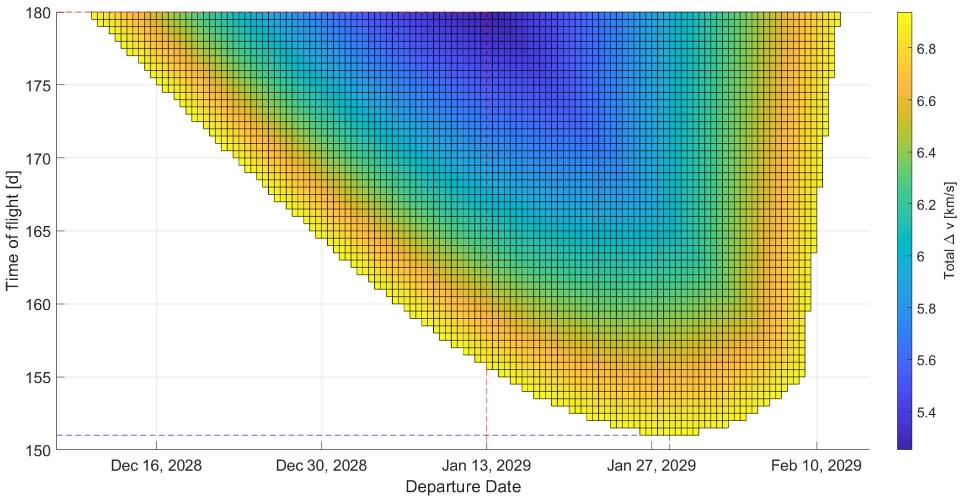

Figure 59: Porkchop plot displaying the values of Δv for a transfer in the 2029 launch opportunity. The value for m_p was set to 1100 t. The red, dashed line indicates the minimum Δv trajectory, the blue, dashed line the minimum possible time of flight trajectory.

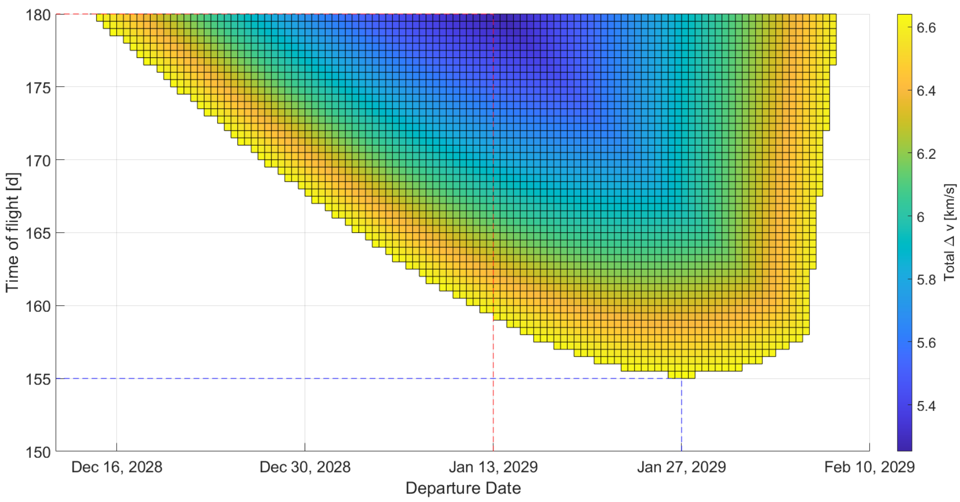

Figure 60: Porkchop plot displaying the values of Δv for a transfer in the 2029 launch opportunity. The value for m_p was set to 1000 t. The red, dashed line indicates the minimum Δv trajectory, the blue, dashed line the minimum possible time of flight trajectory.

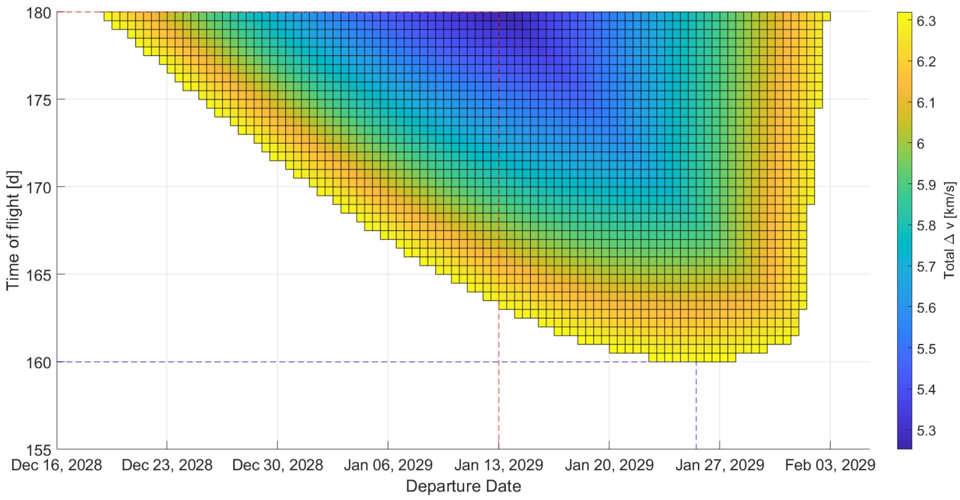

Figure 61: Porkchop plot displaying the values of Δv for a transfer in the 2029 launch opportunity. The value for m_p was set to 900 t. The red, dashed line indicates the minimum Δv trajectory, the blue, dashed line the minimum possible time of flight trajectory.

the maximum payload mass by 50.8 t, displaying a penalty of −20.5 %. This is slightly less than double as much as for a propellant mass reduction of 100 t. The penalty for the minimum time of flight is 5.1 %, hence slightly more than double as much as for the reduction of the propellant mass by 100 t.

In figure 61, the porkchop plot for a reduction of the propellant mass by 300 t, i.e. a propellant mass of 900 t, is shown. For this reduction, the minimum time of flight is raised to 160 d and the maximum payload mass is reduced to 172.3 t. Hence, the reduction of the propellant mass by 300 t causes a reduction of the maximum payload mass by 75.4 t, a penalty of −30.4 %. The minimum time of flight is increased by 12.5 d, a penalty of 8.5 %.

In figure 62, the porkchop plot for a propellant mass of 800 t, hence a reduction of 400 t, is displayed. It can be seen that the minimum time of flight is increased to 166 d, the maximum payload mass is decreased to 146.8 t. This is a reduction by 100.9 t, caused by the propellant mass reduction by 400 t. This is a penalty of −40.7 %, while the penalty for the minimum time of flight is at 12.5 %.

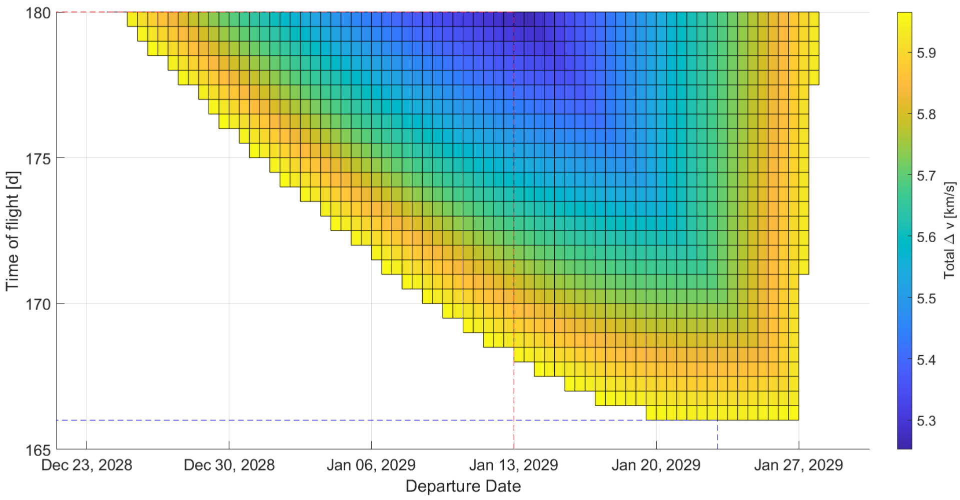

Figure 62: Porkchop plot displaying the values of Δv for a transfer in the 2029 launch opportunity. The value for m_p was set to 800 t. The red, dashed line indicates the minimum Δv trajectory, the blue, dashed line the minimum possible time of flight trajectory.

The penalty for the maximum payload mass shows an almost perfect linear relation to the propellant mass reduction. Per 100 t reduction of the propellant mass, the maximum payload mass experiences a penalty of about $-10\,\%$, or in absolute numbers, a reduction by about 25 t. The penalty for the minimum time of flight shows a more rapid than linear incline. Further analysis shows that the penalty follows a quadratic behavior, with the following equation:

$$\Psi_t = 4 \cdot 10^{-5}\,\frac{\mathrm{d}}{\mathrm{t}^2} \cdot m_p^2 - 0.1317\,\frac{\mathrm{d}}{\mathrm{t}} \cdot m_p + 96.4\,\mathrm{d}$$

I will now go on to the next launch opportunity in 2031 and analyse the sensitivity behavior.

6.5.2 2031 launch opportunity

For the 2031 launch opportunity, the nominal values for the minimum time of flight and the maximum payload mass are 128 d and 295.3 t, respectively. In figure 63, a porkchop plot for a reduced propellant mass of 1100 t, i.e. a reduction by 100 t, is displayed. For this reduction, the minimum time of flight is increased to 131 d, and the maximum payload mass is decreased to 269.7 t. Therefore, the saving of propellant mass by 100 t reduces the maximum payload mass by 25.6 t, a penalty of $-8.7\,\%$. The experienced penalty for the minimum time of flight, caused by the reduced propellant mass, is 2.3 %. In figure 64, a porkchop plot for a further reduction by 200 t, i.e. a propellant mass of 1000 t, is shown. This reduction leads to an increase of the minimum time of flight to 135 d, and the maximum payload mass is decreased to 243.2 t. This is a reduction by 52.1 t compared to the nominal value, a penalty of $-17.6\,\%$. The penalty for the minimum time of flight is 5.5 %, more than double the penalty for a reduction by 100 t. In figure 65, a porkchop plot for a reduction of the propellant mass to 900 t is displayed. The reduction of the propellant mass by 300 t causes an increase of the minimum time of flight to 139.5 d and a decrease of the maximum payload mass to 215.7 t. Hence, a reduction of the maximum payload mass by 79.6 t, i.e. a penalty of $-27.0\,\%$, is caused by the reduction. The penalty for the minimum time of flight is at 9.0 %.

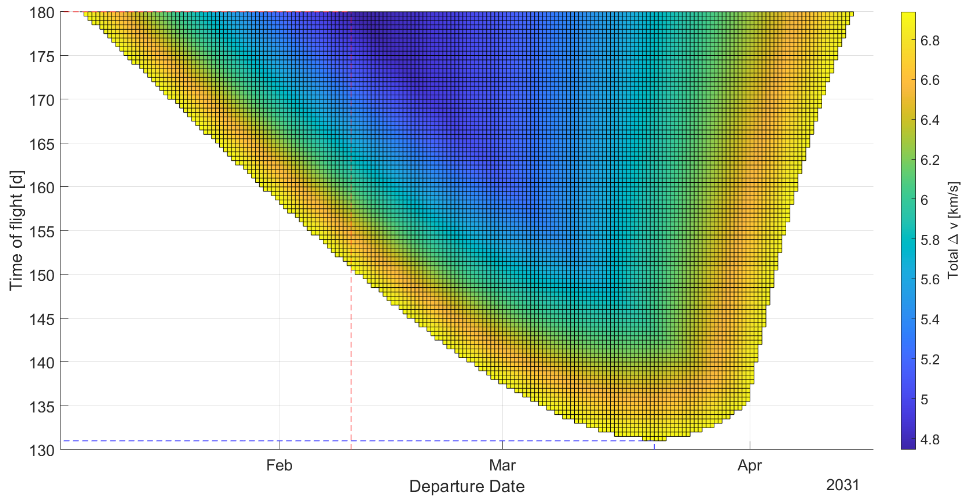

Figure 63: Porkchop plot displaying the values of Δv for a transfer in the 2031 launch opportunity. The value for m_p was set to 1100 t. The red, dashed line indicates the minimum Δv trajectory, the blue, dashed line the minimum possible time of flight trajectory.

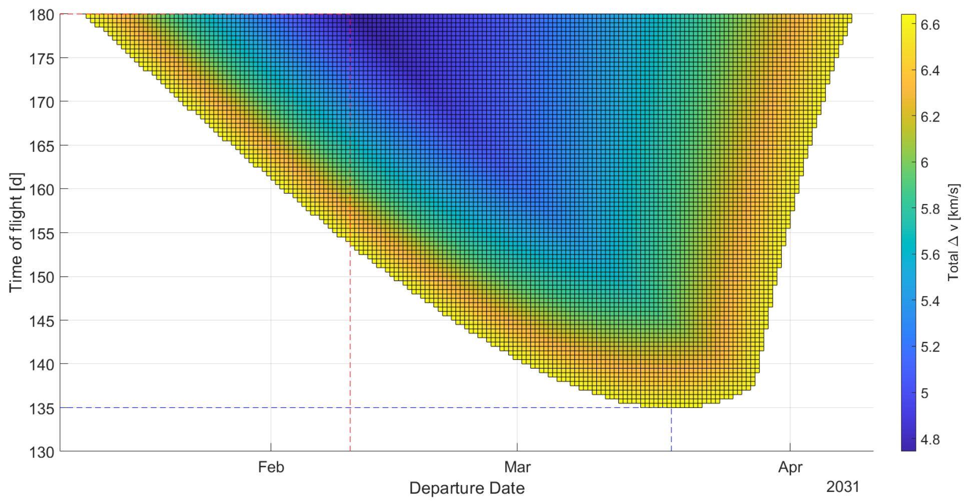

Figure 64: Porkchop plot displaying the values of Δv for a transfer in the 2031 launch opportunity. The value for m_p was set to 1000 t. The red, dashed line indicates the minimum Δv trajectory, the blue, dashed line the minimum possible time of flight trajectory.

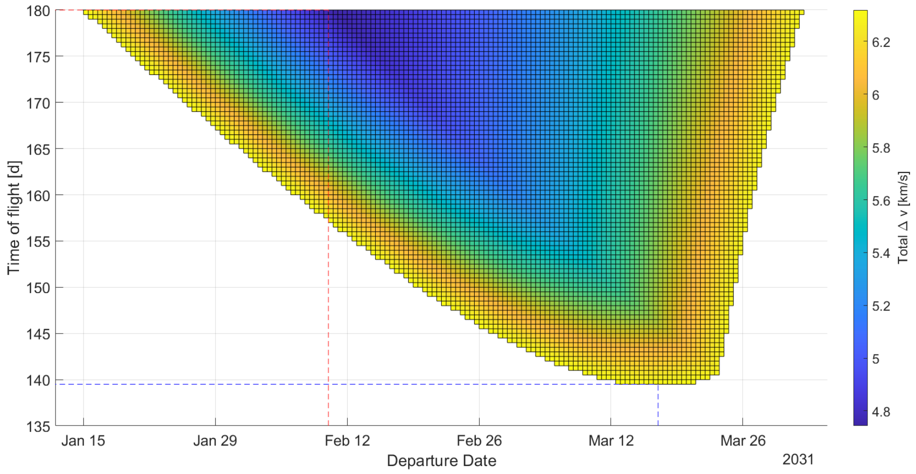

Figure 65: Porkchop plot displaying the values of Δv for a transfer in the 2031 launch opportunity. The value for m_p was set to 900 t. The red, dashed line indicates the minimum Δv trajectory, the blue, dashed line the minimum possible time of flight trajectory.

Now, I take a look at a reduction of the propellant mass by 400 t to 800 t. The plot for this can be seen in figure 66. The minimum time of flight was increased to 144.5 d, and the maximum payload mass was decreased to 187.1 t. Hence, the reduction of the propellant mass causes a penalty for the maximum payload mass of −36.6 %, corresponding to an absolute value of 108.2 t. The penalty for the minimum time of flight is 12.9 %.

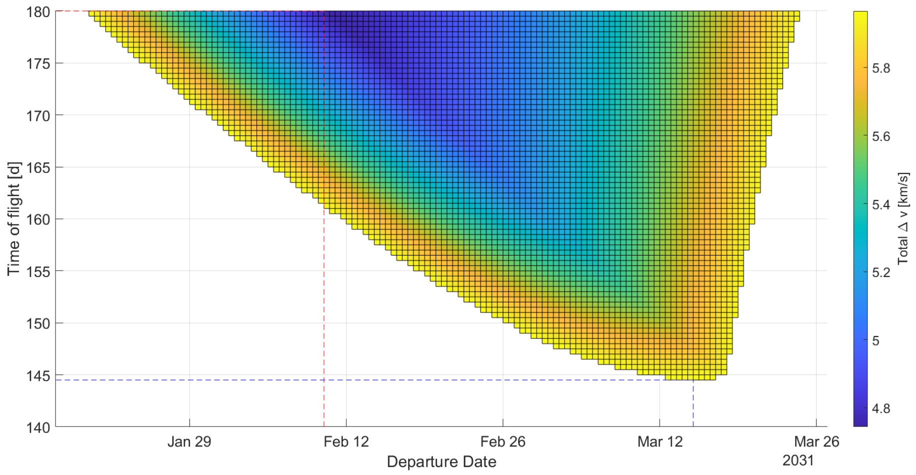

Figure 66: Porkchop plot displaying the values of Δv for a transfer in the 2031 launch opportunity. The value for m_p was set to 800 t. The red, dashed line indicates the minimum Δv trajectory, the blue, dashed line the minimum possible time of flight trajectory.

As in the 2029 launch opportunity, the reduction of the propellant mass causes a almost perfect linearly correlated penalty of the maximum payload mass of about 26 t, which is slightly higher than for 2029. The analysis shows that the minimum time of flight follows a quadratic behavior as pointed out in 6.5.1. This time, the describing equation is:

$$\Psi_t = 3 \cdot 10^{-5}\,\frac{\mathrm{d}}{\mathrm{t}^2} \cdot m_p^2 - 0.1058\,\frac{\mathrm{d}}{\mathrm{t}} \cdot m_p + 80.6\,\mathrm{d}$$

Next up is the 2033 launch opportunity, for which I will do the same analysis as for the last two opportunities.

6.5.3 2033 launch opportunity

For the 2033 launch opportunity, the nominal values for the minimum time of flight and the maximum payload mass are 99 d and 305.4 t, respectively. In figure 67, a porkchop plot for a reduced propellant mass of 1100 t, i.e. a reduction by 100 t, is displayed.

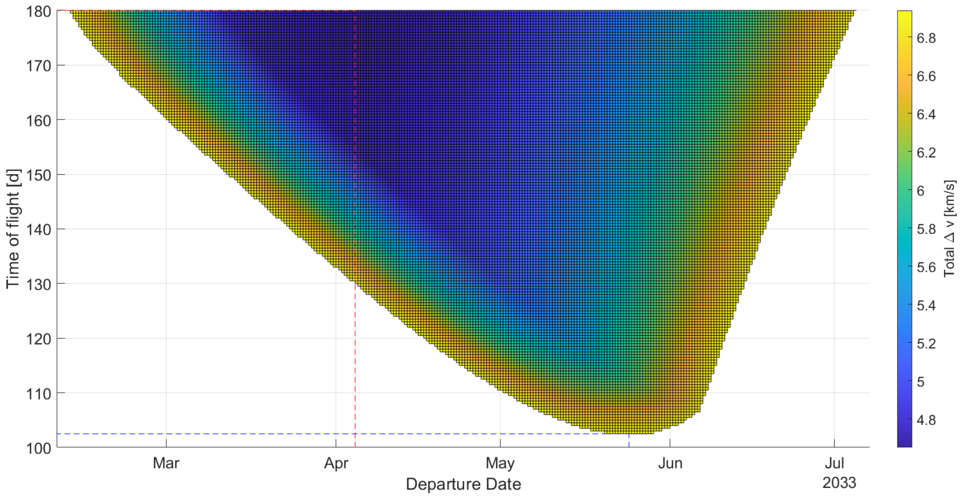

Figure 67: Porkchop plot displaying the values of Δv for a transfer in the 2033 launch opportunity. The value for m_p was set to 1100 t. The red, dashed line indicates the minimum Δv trajectory, the blue, dashed line the minimum possible time of flight trajectory.

This reduction causes an increase of the minimum time of flight to 102.5 d and a decrease of the maximum payload mass to 279.4 t. This is a reduction by 26.0 t, a penalty of −8.5 %, caused by the reduction of the propellant mass by 100 t. The penalty for the minimum time of flight is 3.5 %.
In figure 68, a porkchop plot for a reduction of the propellant mass by 200 t to 1000 t. The minimum time of flight increases to 105.5 d while the maximum payload mass decreases to 252.4 t. This is a reduction by 52.1 t, caused by the reduction of the propellant mass by 200 t. This is a penalty of −17.4 %, the penalty for the minimum time of flight is 6.6 %. In figure 69, the porkchop plot for a reduction of the propellant mass to 900 t is shown. The reduction of the propellant mass by 300 t causes an increase of the minimum time of flight to 109 d and a decrease of the maximum payload mass to 224.4 t. This is a reduction by 81.0 t, displaying a penalty of −26.5 %. The penalty for the minimum time of flight is 10.1 %.

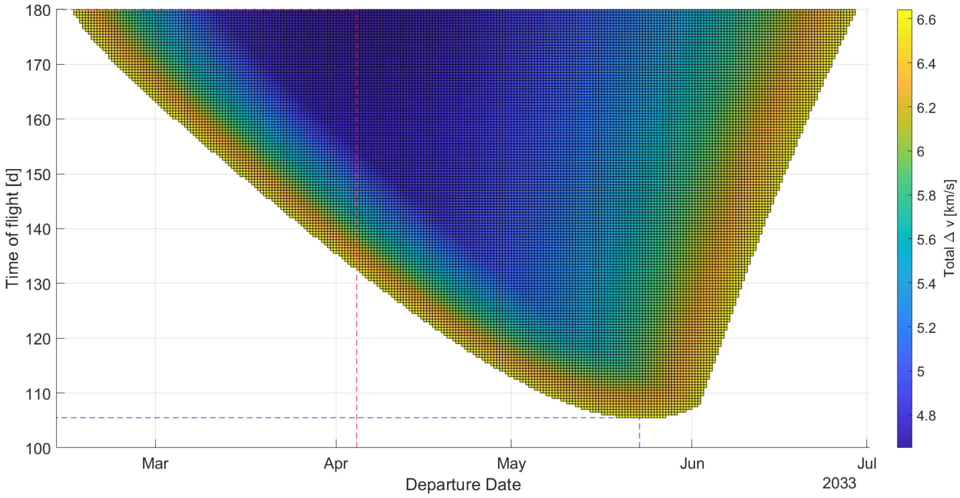

Figure 68: Porkchop plot displaying the values of Δv for a transfer in the 2033 launch opportunity. The value for m_p was set to 1000 t. The red, dashed line indicates the minimum Δv trajectory, the blue, dashed line the minimum possible time of flight trajectory.

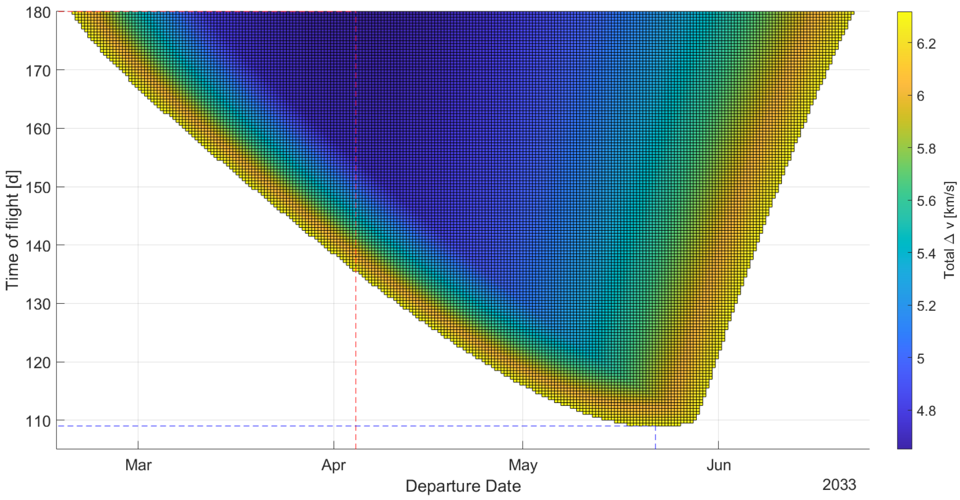

Figure 69: Porkchop plot displaying the values of Δv for a transfer in the 2033 launch opportunity. The value for m_p was set to 900 t. The red, dashed line indicates the minimum Δv trajectory, the blue, dashed line the minimum possible time of flight trajectory.

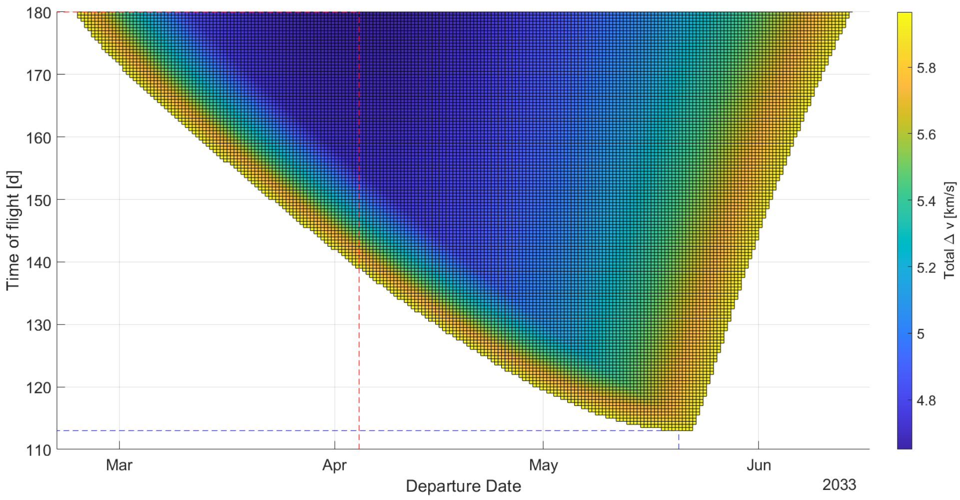

Figure 70: Porkchop plot displaying the values of Δv for a transfer in the 2033 launch opportunity. The value for m_p was set to 800 t. The red, dashed line indicates the minimum Δv trajectory, the blue, dashed line the minimum possible time of flight trajectory.

In figure 70, a porkchop plot for a reduction of the propellant mass to 800 t is shown. This reduction of the propellant mass by 400 t causes an increase of the minimum time of flight to 113 d and a decrease of the maximum payload mass to 195.2 t. This is a reduction of the maximum payload mass by 110.2 t, a penalty of −36.1 %. The penalty for the minimum time of flight is 14.1 %.
The penalty for the maximum payload mass shows a steeper increase for smaller propellant masses than in previous launch opportunities. It can be described with the following formula.

$$\Psi_{m_{P/L}} = 7 \cdot 10^{-5}\,\frac{1}{\mathrm{t}} \cdot m_p^2 - 0.4068 \cdot m_p + 393.66\,\mathrm{t}$$

For a rule of thumb, it can still be said that per 100 t of saved propellant mass, the system experiences a penalty of about 26 t in terms of payload mass that can be brought to Mars. The minimum time of flight experiences a penalty that can be described with the following formula.

$$\Psi_t = 1 \cdot 10^{-5}\,\frac{\mathrm{d}}{\mathrm{t}^2} \cdot m_p^2 - 0.0559\,\frac{\mathrm{d}}{\mathrm{t}} \cdot m_p + 51.8\,\mathrm{d}$$

This is a less quadratic behavior as for the previous launch opportunities, the mean increase during this launch opportunity is 3.5 days per a 100 t decrease in propellant mass.

6.5.4 2035 launch opportunity

Now, I will take a look at the sensitivity behavior of transfers within the 2035 launch opportunity with regard to the propellant mass. The nominal values are 90.5 d for the minimum time of flight and 297.3 t for the maximum payload mass. In figure 71, the porkchop plot for a reduction of the propellant mass by 100 t to 1100 t is shown.

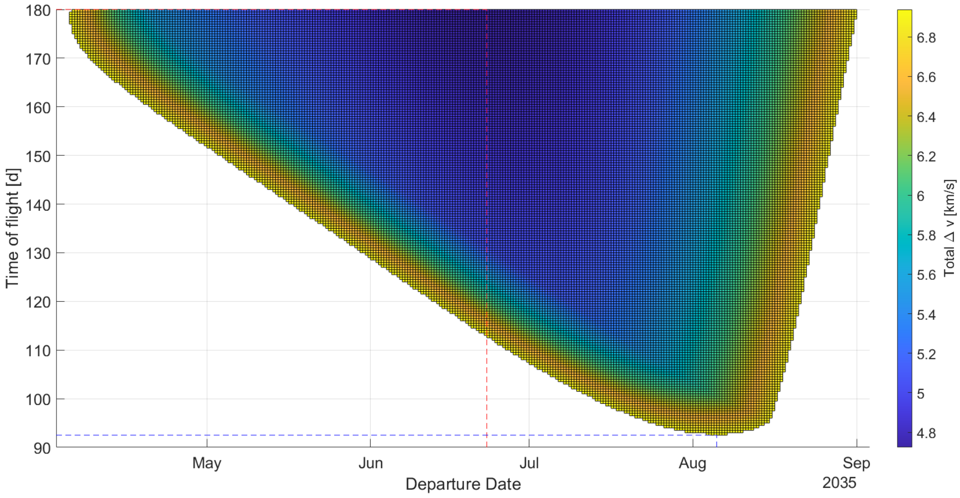

Figure 71: Porkchop plot displaying the values of Δv for a transfer in the 2035 launch opportunity. The value for m_p was set to 1100 t. The red, dashed line indicates the minimum Δv trajectory, the blue, dashed line the minimum possible time of flight trajectory.

The reduction of the propellant mass causes an increase of the minimum time of flight to 92.5 d and a decrease of the maximum payload mass to 271.7 t. This is a reduction by 25.6 t and, hence, a penalty of −8.6 %. The penalty for the minimum time of flight is 2.2 %.
In figure 72, the porkchop plot for a reduction to 1000 t is displayed.

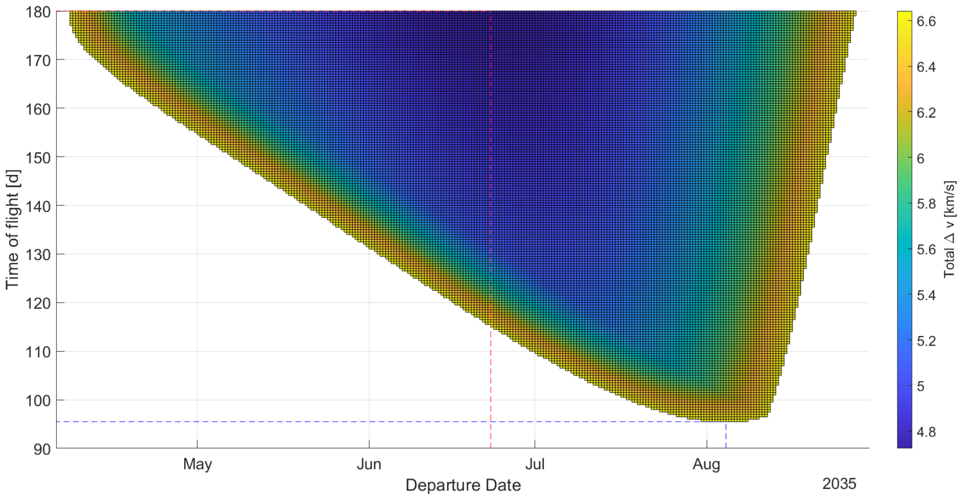

Figure 72: Porkchop plot displaying the values of Δv for a transfer in the 2035 launch opportunity. The value for m_p was set to 1000 t. The red, dashed line indicates the minimum Δv trajectory, the blue, dashed line the minimum possible time of flight trajectory.

This reduction by 200 t leads to an increase of the minimum time of flight to 95.5 d and a decrease of the maximum payload mass to 245.1 t. This is a reduction by 52.2 t, a penalty of −17.6 %. For the minimum time of flight, a penalty of 5.0 % is caused.

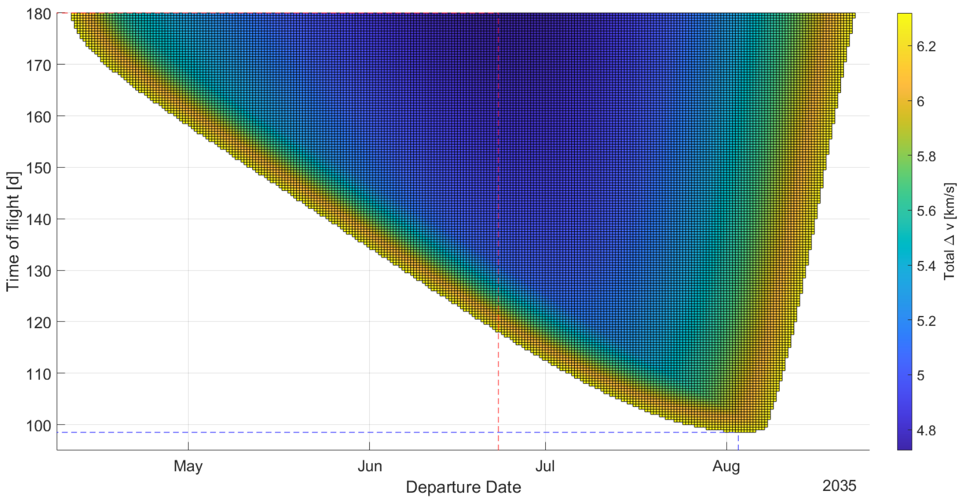

Figure 73: Porkchop plot displaying the values of Δv for a transfer in the 2035 launch opportunity. The value for m_p was set to 900 t. The red, dashed line indicates the minimum Δv trajectory, the blue, dashed line the minimum possible time of flight trajectory.

In figure 73, a porkchop plot for a reduction of the propellant mass by 300 t to 900 t is displayed. The reduction causes an increase of the minimum time of flight to 98.5 d and a decrease of the maximum payload mass to 217.5 t. This is a reduction by 79.8 t and therefore a penalty of −26.8 %. The penalty for the minimum time of flight is 8.0 %. In figure 74, a porkchop plot for the reduction of the propellant mass by 400 t to 800 t is shown. The reduction causes an increase of the minimum time of flight to 12.0 d and a decrease of the maximum payload mass to 188.8 t. This is a reduction of the maximum payload mass by 108.5 t, which is a penalty of −36.5 %. For the minimum time of flight, the penalty is 13.3 %.
The analysis shows that the penalty for the maximum payload mass is again following a quadratic behavior, but the incline is less steep than in 2033. The analytic equation that describes the penalty related to the propellant mass is found below.

$$m_{P/L,penalty} = 5 \cdot 10^{-5} \, \frac{1}{\mathrm{t}} \cdot m_p^2 - 0.3741 \cdot m_p + 374.82 \, \mathrm{t}$$

Also the penalty for the minimum time of flight follows a quadratic behavior. For smaller propellant masses, the penalty grows more rapid than in 2033. The formula can be found below.

$$t_{penalty} = 3 \cdot 10^{-5} \, \frac{\mathrm{d}}{\mathrm{t}^2} \cdot m_p^2 - 0.0871 \, \frac{\mathrm{d}}{\mathrm{t}} \cdot m_p + 63.4 \, \mathrm{d}$$

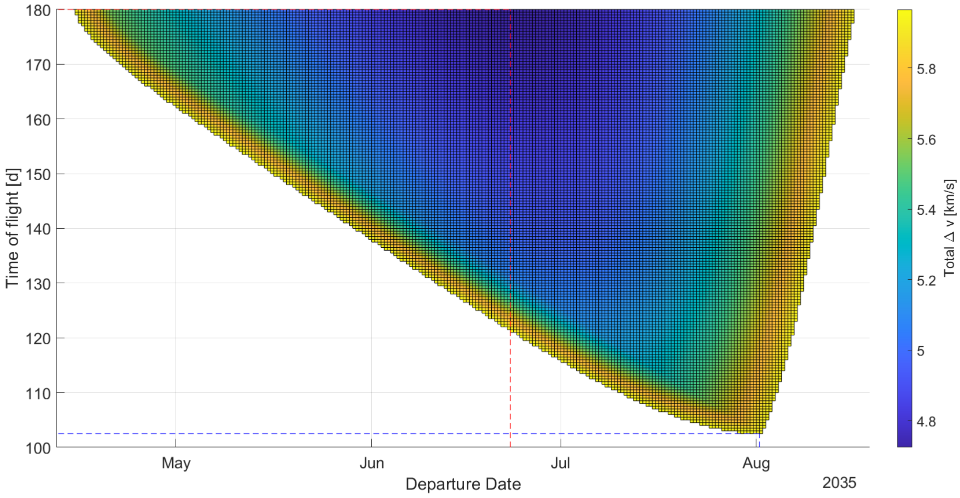

Figure 74: Porkchop plot displaying the values of Δv for a transfer in the 2035 launch opportunity. The value for m_p was set to 800 t. The red, dashed line indicates the minimum Δv trajectory, the blue, dashed line the minimum possible time of flight trajectory.

6.5.5 2037 launch opportunity

As before, the last launch opportunity that I will discuss, is the 2037 one. Here, the nominal values are 115.5 d for the minimum time of flight and 264.3 t for the maximum payload mass. In figure 75, a porkchop plot for a reduction by the propellant mass by 100 t to 1100 t is displayed.

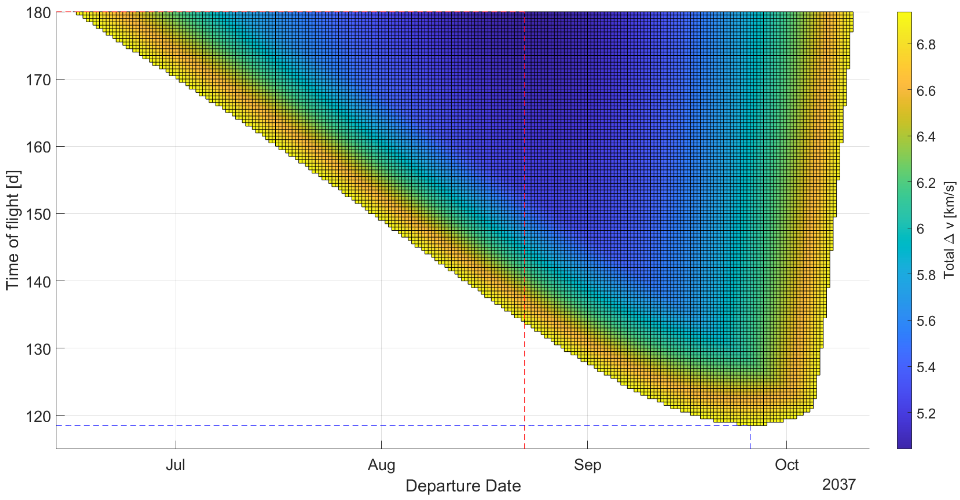

Figure 75: Porkchop plot displaying the values of Δv for a transfer in the 2037 launch opportunity. The value for m_p was set to 1100 t. The red, dashed line indicates the minimum Δv trajectory, the blue, dashed line the minimum possible time of flight trajectory.

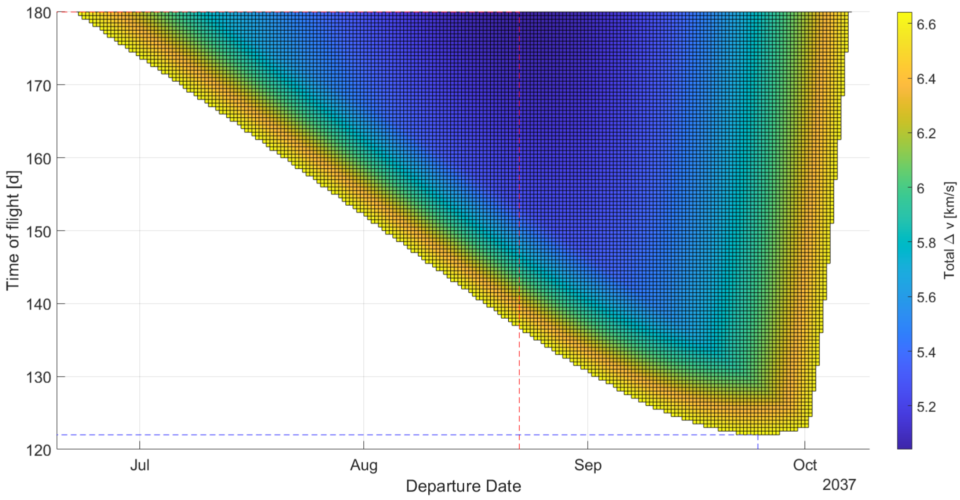

Figure 76: Porkchop plot displaying the values of Δv for a transfer in the 2037 launch opportunity. The value for m_p was set to 1000 t. The red, dashed line indicates the minimum Δv trajectory, the blue, dashed line the minimum possible time of flight trajectory.

This reduction causes an increase of the minimum time of flight to 118.5 d and a decrease of the maximum payload mass to 240.2 t. This is a reduction by 24.1 t and, hence, a penalty of −9.1 %. The penalty for the minimum time of flight is 2.6 %. In figure 76, a porkchop plot for a reduction to 1000 t is displayed. The reduction of the propellant mass by 200 t causes an increase of the minimum time of flight to 122.0 d and a decrease of the maximum payload mass to 215.3 t. This is a reduction by 49.0 t and therefore a penalty of −18.5 %. The penalty for the minimum time of flight is at 5.6 %. In figure 77, a porkchop plot for a reduction of the propellant mass by 300 t to 900 t is shown. The reduction causes an increase of the minimum time of flight to 126.0 d and a decrease of the maximum payload mass to 189.6 t. This is a reduction by 74.7 t and therefore a penalty of −28.3 %. The penalty for the minimum time of flight is 9.1 %. In figure 78, a porkchop plot for a reduction of the propellant mass to 800 t is shown. This reduction by 400 t causes an increase of the minimum time of flight to 131.0 d and a decrease of the maximum payload mass to 162.8 t. This is a reduction of the maximum payload mass by 101.5 t and, hence, a penalty of −38.4 %. The penalty for the minimum time of flight is 13.4 %. The analysis shows that the penalty for the maximum payload mass is again following a quadratic behavior, but the incline is less steep than in 2035. The analytic equation that describes the penalty related to the propellant mass is found below.

$$\Psi_{m_{P/L}} = 4 \cdot 10^{-5}\,\frac{1}{\mathrm{t}} \cdot m_p^2 - 0.3422 \cdot m_p + 346.86\,\mathrm{t}$$

Also the penalty for the minimum time of flight follows a quadratic behavior. For smaller propellant masses, the penalty grows more rapid than in 2035. The formula can be found below.

$$\Psi_t = 3 \cdot 10^{-5}\,\frac{\mathrm{d}}{\mathrm{t}^2} \cdot m_p^2 - 0.1028\,\frac{\mathrm{d}}{\mathrm{t}} \cdot m_p + 77.1\,\mathrm{d}$$

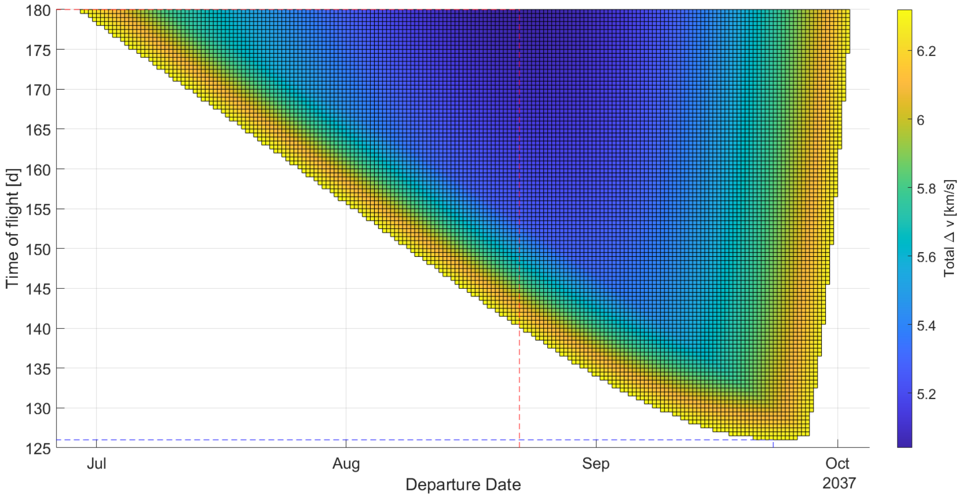

Figure 77: Porkchop plot displaying the values of Δv for a transfer in the 2037 launch opportunity. The value for m_p was set to 900 t. The red, dashed line indicates the minimum Δv trajectory, the blue, dashed line the minimum possible time of flight trajectory.

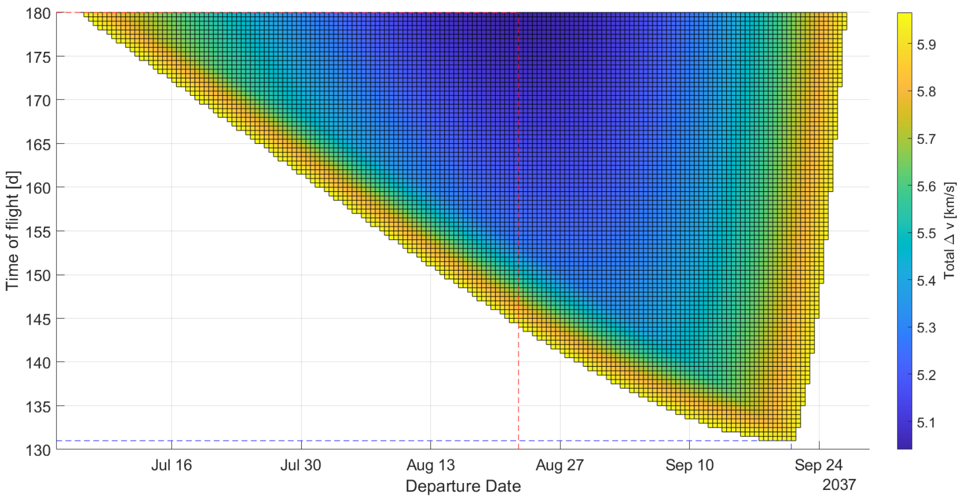

Figure 78: Porkchop plot displaying the values of Δv for a transfer in the 2037 launch opportunity. The value for m_p was set to 800 t. The red, dashed line indicates the minimum Δv trajectory, the blue, dashed line the minimum possible time of flight trajectory.

6.5.6 Summary

It has been shown that both the penalty for the maximum payload mass and the minimum possible time of flight show a quadratic behavior for a reduction of the propellant mass. The steepness of the quadratic functions varies over the different launch opportunities, but the differences are small in the observed frame of propellant masses between 800 t and 1200 t. In general, the maximum payload mass decreases by 24.0 t to 27.0 t for 100 t of reduced propellant mass. For larger reductions of 400 t, the decrease of the payload mass rises to 100.0 t to 110.0 t. The linear assumption of a decrease of 25.0 t per 100.0 t reduction of the propellant mass gives a good estimate considering the early stage of analysis.
For the minimum time of flight, the decrease is between 2.0 d and 3.5 d for a reduction of the propellant mass by 100 t. For larger reductions of 400 t, the decrease is between 12.0 d and 18.5 d and therefore more strongly depending on the launch opportunity.

6.6 Maturity of the system

This chapter deals with the combined impact of the aforementioned parameters on the system performance. Starship and its components, most notably the Raptor engine, have yet to perform a flight in a space environment. Therefore, it is recommended to apply a certain margin on the system's parameters. In this case, a margin is equivalent to a reduction in performance of three parameters of the system. These three parameters are the specific impulse of the Raptor engine, the structural mass of Starship and the propellant mass. I considered three approaches, ranging from aggressive to conservative, where the aggressive approach assumes a margin of 5 %, the mean approach a margin of 10 % and the conservative approach a margin of 20 %. For all approaches, a porkchop plot for a transfer in 2029 is compiled and compared with the nominal plot as it can be seen in figure 18.
It should be noted ahead of the comparison that these three parameters are strongly influencing the maximum Δv that Starship is able to provide as of equation (1). Therefore, it is expected to see a reduction of possible trajectories, which will result in a narrowing of the launch opportunity and an increase in the minimum possible time of flight. Furthermore, the maximum payload mass that can be brought to Mars will be reduced.

6.6.1 Aggressive approach

In the aggressive approach, the values of the aforementioned parameters are as follows: $I_{sp} = 359\,\mathrm{s}$, $m_s = 105\,\mathrm{t}$ and $m_p = 1140\,\mathrm{t}$. This means that the maximum possible Δv in this case is $\Delta v_{max} = 6623\,\mathrm{m\,s^{-1}}$ for a payload mass of 100 t. In the following two figures, first the porkchop plot for a nominal transfer, i.e. with parameter values as in table 7, is shown. In figure 80, the porkchop plot with values as described by the aggressive margin approach, is shown. The comparison between the two figures proves the expected influence of the margins on the shape of the porkchop plot. The launch opportunity gets more narrow and the minimum time of flight increases. For the nominal transfer, the minimum time of flight is 147.5 days and for the aggressive approach it is 155.5 days. Also, the launch opportunity opens about five days later and closes five days earlier.

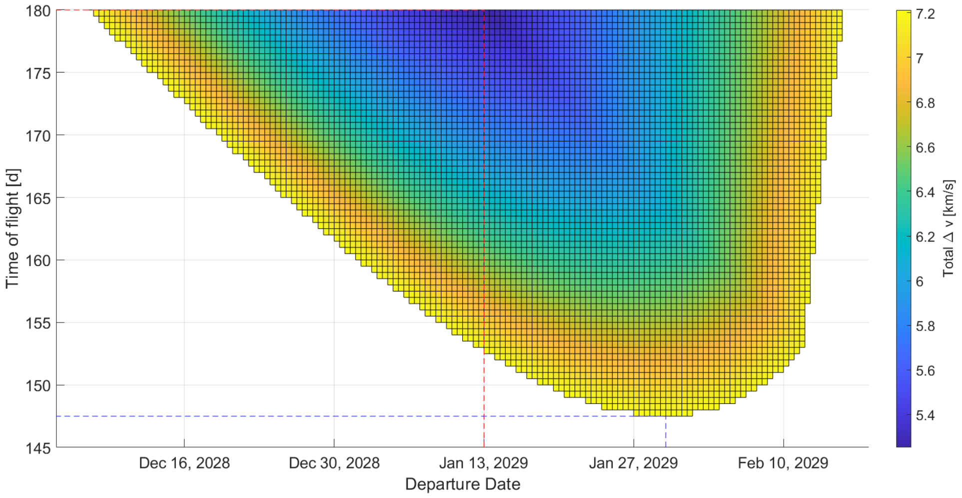

Figure 79: Porkchop plot for the nominal transfer. The red, dashed line indicates the minimum Δv trajectory, the blue, dashed line the minimum possible time of flight trajectory.

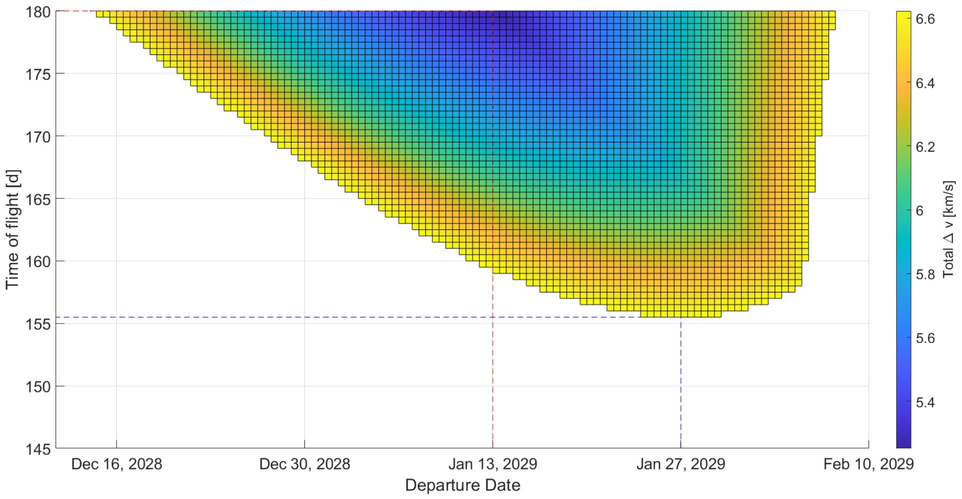

Figure 80: Porkchop plot for the transfer considering an aggressive margin approach. The red, dashed line indicates the minimum Δv trajectory, the blue, dashed line the minimum possible time of flight trajectory.

6.6.2 Mean approach

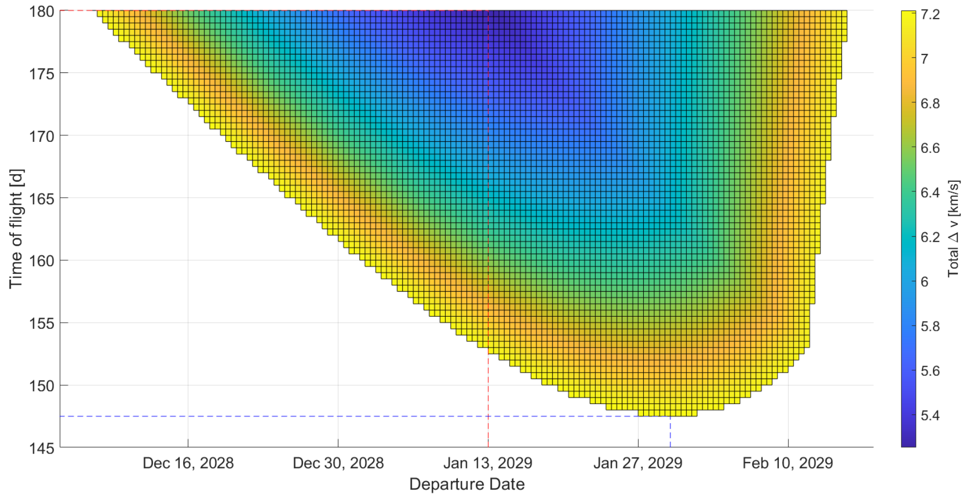

Figure 81: Porkchop plot for the nominal transfer. The red, dashed line indicates the minimum Δv trajectory, the blue, dashed line the minimum possible time of flight trajectory.

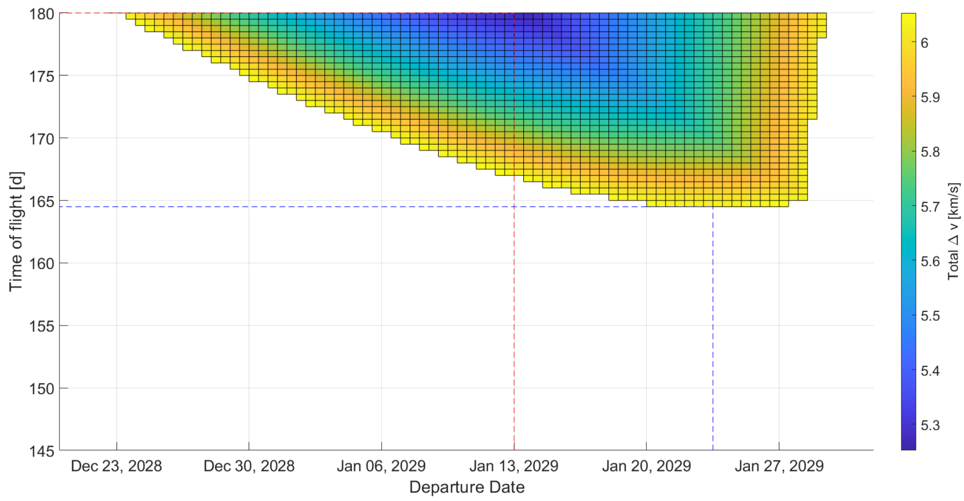

Figure 82: Porkchop plot for the transfer considering a mean margin approach. The red, dashed line indicates the minimum Δv trajectory, the blue, dashed line the minimum possible time of flight trajectory.

In the mean approach, the values of the aforementioned parameters are as follows: $I_{sp} = 340\,\mathrm{s}$, $m_s = 110\,\mathrm{t}$ and $m_p = 1080\,\mathrm{t}$. This means that the maximum possible Δv in this case is $\Delta v_{max} = 6053\,\mathrm{m\,s^{-1}}$ for a payload mass of 100 t. The two figures 81 and 82 display the nominal porkchop plot (figure 81) and the porkchop plot for parameter values as of the mean approach (figure 82). The expected effects can be observed here at a larger scale as for the aggressive approach. The launch opportunity gets even more narrow and the minimum possible time of flight increases to 164.5 days.

6.6.3 Conservative approach

In the conservative approach, the values of the aforementioned parameters are as follows: $I_{sp} = 302\,\mathrm{s}$, $m_s = 120\,\mathrm{t}$ and $m_p = 960\,\mathrm{t}$. This means that the maximum possible Δv in this case is $\Delta v_{max} = 4974\,\mathrm{m\,s^{-1}}$ for a payload mass of 100 t. The two figures 83 and 84 display the nominal porkchop plot and the porkchop plot for parameter values as of the mean approach. In this case, the margin approach results in such an increase of the minimum possible time of flight that no flight time of less than 180 days is possible. The conservative approach allows for flight times of 188 days or more.

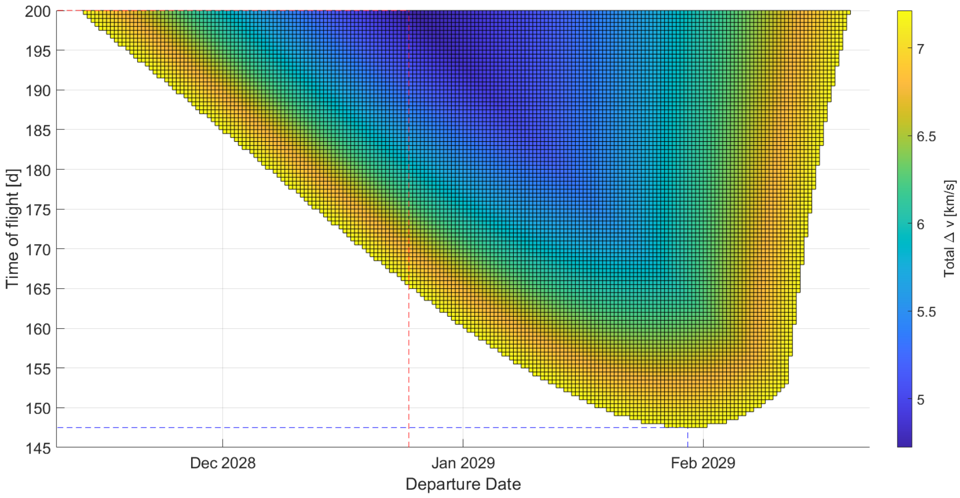

Figure 83: Porkchop plot for the nominal transfer. The time of flight was extended to 200 days to enable a comparison. The red, dashed line indicates the minimum Δv trajectory, the blue, dashed line the minimum possible time of flight trajectory.

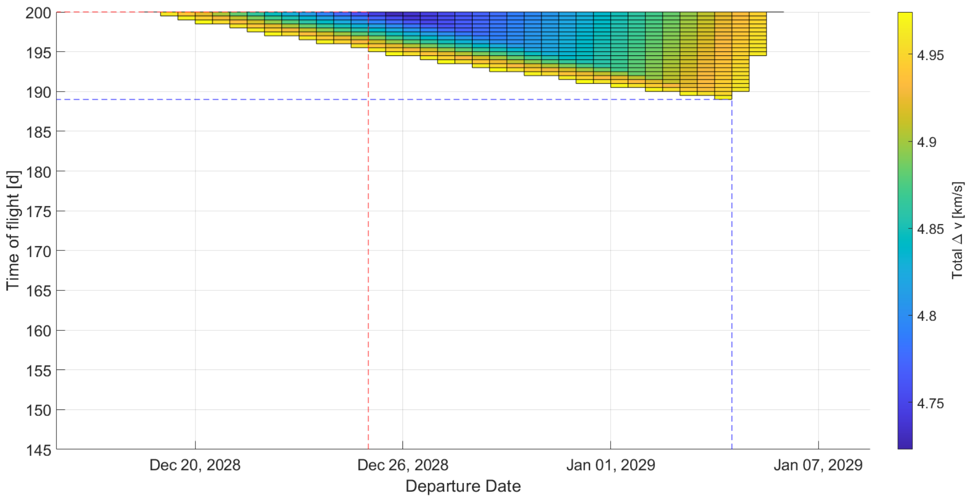

Figure 84: Porkchop plot for the transfer considering a conservative margin approach. The red, dashed line indicates the minimum Δv trajectory, the blue, dashed line the minimum possible time of flight trajectory.

6.6.4 Summary

In the last chapter, the influence of the different margin approaches on the general shape of the porkchop plots has been presented. Another possibility to examine the influence of the margin approaches is to analyse the penalty of the maximum payload mass for a respective approach and launch opportunity combination. These results are presented in table 52.

Table 52: Overview over the influence of the different margin approaches on the maximum payload mass, presented for all considered launch opportunities. The dashes indicate that no transfer is possible which fulfills the minimum requirements (I.e. a payload mass of at least 100 t while the flight time does not exceed 180 d).

Maximum payload mass	**Aggressive approach**	**Penalty to nominal**	**Mean approach**	**Penalty to nominal**	**Conservative approach**	**Penalty to nominal**
2029 launch opportunity	200.4 t	−17.8 %	158.5 t	−35.0 %	-	-
2031 launch opportunity	248.9 t	−15.7 %	203.8 t	−31.0 %	118.2 t	−60.0 %
2033 launch opportunity	258.5 t	−15.4 %	212.8 t	−30.3 %	126.0 t	−58.7 %
2035 launch opportunity	250.8 t	−15.6 %	205.6 t	−30.8 %	119.8 t	−59.7 %
2037 launch opportunity	219.7 t	−16.9 %	176.5 t	−33.2 %	-	-

By looking at the table, a more or less uniform pattern can be observed across all launch opportunities. For the aggressive approach, i.e. a margin of 5 % on the parameters, one observes a penalty between 15 % and 18 % on the system performance. For the mean approach, i.e. a

margin of 10 % on the parameters, the penalty on the system performance ranges from 30 % to 35 %. And for the conservative approach, i.e. a margin of 20 %, a penalty of about 60 % is observed. While for the aggressive and the mean approach, only a reduction of the payload mass is observed, the conservative approach leads to scenarios in which not even the minimum desired performance can be achieved.
Considering this as well as the impact on the minimum time of flight as described in chapters 6.6.1 to 6.6.3, it became evident that a operation of Starship outside of its nominal operation causes a big decrease in the system performance. Especially the margins of the conservative approach would lead to decreases in the system performance which require changes in the mission baseline. The likelihood that such an increase, resp. decrease, of these parameters will occur is not high. Especially a reduction of the specific impulse by about 75 s will not occur. Therefore, this consideration only serves as a extreme case of the analysis. Smaller reductions of the specific impulse can be considered not completely unrealistic and it has been shown that this would negatively affect the system performance. Looking at the structural mass, an increase is more likely to happen. The same accounts for a lower propellant mass, the reasons for this have also been described in 6.5.
Concluding, it should be noted that these analysed margin approaches do not represent realistic scenarios, especially not in the simultaneous decrease in performance of all parameters. This analysis provides a first estimate of the influence of a subpar system performance on the mission. The mentioned penalty values can be extrapolated and adapted to fit the respective scenario.

7 Feasibility assessment

Considering the results described in chapters 5 and 6, I will now try to assess the feasibility of SpaceX mission plans for Starship with respect to the mission analysis domain.
The analysis of the performance of Starship under nominal conditions, i.e. all technical parameters as described by SpaceX, was carried out in chapter 5. There, it was shown that the desired flight times by SpaceX (as shown in table 6) can not be achieved with Starship in its current configuration. All of the desired flight times are missed by at least 7.5 days, for a flight in the 2031 launch opportunity, the desired flight time is missed by 18 days, the maximum deviation during the considered time span. In general, it became evident that trip times under 90 days are not feasible in the current configuration, the declared aim by SpaceX is 80 days.
In chapter 5.9, the feasibility of Elon Musk's declared aim to achieve flight times of 30 days in the future was analysed. It became evident that there is no realistic situation in which Starship's components could be improved in such way that a flight time of 30 days becomes possible. As this analysis was carried out under the assumption that there would be no payload on board, in a realistic operational scenario, where it is necessary to bring payload to the Mars, it is even more unrealistic to achieve this goal.
Considering the payload capacities, it was shown that Starship is capable of (theoretically) bringing payloads with a mass of over 300 t to the surface of Mars with flight times of 180 days. This is dependant on the launch opportunities, but payload masses in extent of 250 t can be brought to Mars with a single flight regardless of the launch opportunity.
The sensitivity analysis performed in chapter 6 showed that an operation of Starship outside of the nominal operation range would result in a non-neglectable impact on the system performance. Given the current mission plans by SpaceX, which feature human flights to Mars in 2029, they showed to be vulnerable with respect to deviations in the analysed parameters. The general "quality" of the 2029 is low compared with all other observed launch opportunities. This means that it is also way more susceptible for the influences of deviations in the parameters. Also, it is more likely that Starship will have technical problems at the beginning of its operational phase than at later stages. The key risk factor here is a delay in the departure date, which may occur due to bad weather or technical problems either with the refuelling in orbit or in general. A delay of 30 days can cause a situation in which a transfer becomes impossible and can only be resolved with unloading payload from Starship. Which would then again result in further delays. The sensitivity analysis of the other parameters showed to be influencing in particular the payload capacities, but not in such a manner that a transfer would become impossible. Still, the results of this analysis indicates that Starship should not be used at the boundaries of its technical capabilities.
Of particular interest in this regard is chapter 6.6, which analyses the potential negative consequences of the low maturity of Starship. Considering that it is yet to fly in space, it can be doubted that it will actually fly in 2029 as the current technical specifications say. A decrease of the technical parameters by 5 % in quality will result in a decrease of the system performance by about 15 %. If the development of Starship would show a even larger decrease in the quality of the technical specifications, the system performance will suffer even more.
Another point of interest is the availability of Starships for consecutive launch opportunities. In chapter 5.8, it was described that the current technical design of Starship does not allow to use them in to consecutive launch opportunities. Based on the refuelling times considered by NASA, there is no possibility that they will be flown to Mars, refuelled and flown back to Earth in the 26 months between two launch opportunities. And in this consideration, additional delays for maintenance, etc. was not yet considered. Therefore, assuming flights of four Starships per launch opportunity, SpaceX needs to at least operate eight Starships simultaneously. Not only

does this mean a duplication of the building costs, but with this associated are increased costs for maintenance and operations as well as larger facilities that are needed for building, testing, maintenance and storage.
To sum up, I would say that the minimum desired performance by Starship will be achieved in any scenario. The more severe problems that can arise would come from the mission plans of the colonization of Mars. If Starship is used to constantly deliver the Mars base with supplies, materials, etc., I would assume that 100 t payload mass per flight is not sufficient. And then, the sensitivity analysis shows indication that Starship can not achieve the desired performance.

8 Outlook and future work

In this document, a detailed analysis of the possible trajectories for future SpaceX Starship missions to Mars was developed and presented. This analysis is based on the most up-to-date technical data that is available as of October 2022. Speaking of this, it is very likely that some technical data of Starship changes over the next years until the first manned flight to Mars in 2029. The presented model could then be easily adapted to the new data and again present the results as it was done here. As described earlier, results can be further improved using ephemeris data, but at the cost of significantly longer processing time.
The combination of this study with studies focusing on other aspects of SpaceX mission plans would provide a deeper understanding of the feasibility of these plans. For example, if the exact payload demands would be known or derived, the results of this study could be used to assess whether the described plans are realistic. Another interesting view could be obtained with a financial analysis of the mission plans, in particular against the background of the increased needed number of Starships.

List of Figures

1 Artist's render of a Raptor engine. (Source: [1]) 10
2 Footage of Starship SN15 during flight. (Source: [1]) 11
3 Overview of the potential landing sites for a SpaceX Mars mission. (Source: [9]) 12
4 Schematic of a Earth-Mars-Earth conjunction-class trajectory. (Source: [10]) . . 13
5 Schematic of a 2-year free return trajectory. (Source: [10]) 13
6 Mission schematic of one Starship flight to Mars and back to Earth. (Source: [11]) 15
7 Schematic of the TCM of the Mars 2020 mission. (Source: [12]) 16
8 Δv-budget of a Starship mission according to SpaceX. (Source: [21], slide 37) . . 19
9 Δv required for landing on Mars depending on the payload mass. The dotted line represents a linear regression line to best fit the values. In the box, the linear equation for the regression line is given together with the determination coefficient. 19
10 The concept is same as in figure 9, but this time includes the value from the animation [19]. 20
11 Schematic of Starship's reentry into Earth's atmosphere and landing. (Source: [4], Fig. 2-3) 23
12 Mission plans of SpaceX. (Source: [27], Slide 31) 24
13 Different trajectories between two positions. The blue vector is at a position of $\begin{pmatrix}4\,\text{LU} & 0 & 0\end{pmatrix}^\top$ and the orange vector is at $\begin{pmatrix}0 & 6\,\text{LU} & 0\end{pmatrix}^\top$ (LU indicates an arbitrary length unit). The green trajectory-ellipses have a semi-major axis of 4.5 LU and the red ones have one of 8 LU. 25
14 Geometry of the Lambert's Problem 28
15 Maximum Δv that can be applied by Starship, depending on the payload mass. . 35
16 Minimum Δv for different departure date stepsizes. Richardson extrapolation used to determine suitable stepsize. 36
17 Minimum time of flight for different time of flight stepsizes. Richardson extrapolation used to determine suitable stepsize. 36
18 Porkchop plot for a Mars transfer in the 2028/2029 launch opportunity (Type A trajectory). The red, dashed line indicates the minimum Δv trajectory, the blue, dashed line the minimum possible time of flight trajectory. 38
19 Porkchop plot for a Mars transfer in the 2028/2029 launch opportunity (Type B trajectory). The red, dashed line indicates the minimum Δv trajectory, the blue, dashed line the minimum possible time of flight trajectory. 39
20 Comparison of trajectory types for a Mars transfer in the 2028/2029 launch opportunity in terms of needed Δv 41
21 Porkchop plot indicating the maximum payload masses that can be brought to Mars for a transfer in the 2028/2029 launch opportunity. 41
22 Porkchop plot displaying the values of ΔP from equation (14). Indicates the possibilities of performing a free-return trajectory for all possible Earth-Mars trajectories in the 2028/2029 launch opportunity. 42
23 Porkchop plot for a Mars transfer in the 2031 launch opportunity (Type A trajectory). The red, dashed line indicates the minimum Δv trajectory, the blue, dashed line the minimum possible time of flight trajectory. 43
24 Porkchop plot for a Mars transfer in the 2031 launch opportunity (Type B trajectory). The red, dashed line indicates the minimum Δv trajectory, the blue, dashed line the minimum possible time of flight trajectory. 44

25 Comparison of trajectory types for a Mars transfer in the 2031 launch opportunity. The left figure displays the values for a Type A trajectory, the right figure for a Type B trajectory. 46
26 Porkchop plot indicating the maximum payload masses that can be brought to Mars for a transfer in the 2031 launch opportunity. The left figure displays the values for a Type A trajectory, the right figure for a Type B trajectory. 46
27 Porkchop plot displaying the values of ΔP from equation (14). Indicates the possibilities of performing a free-return trajectory for all possible Earth-Mars trajectories in the 2031 launch opportunity. 47
28 Porkchop plot for a Mars transfer in the 2033 launch opportunity (Type A trajectory). The red, dashed line indicates the minimum Δv trajectory, the blue, dashed line the minimum possible time of flight trajectory. 48
29 Porkchop plot for a Mars transfer in the 2033 launch opportunity (Type B trajectory). The red, dashed line indicates the minimum Δv trajectory, the blue, dashed line the minimum possible time of flight trajectory. 49
30 Comparison of trajectory types for a Mars transfer in the 2033 launch opportunity. The left figure displays the values for a Type A trajectory, the right figure for a Type B trajectory. 50
31 Porkchop plot indicating the maximum payload masses that can be brought to Mars for a transfer in the 2033 launch opportunity. The left figure displays the values for a Type A trajectory, the right figure for a Type B trajectory. 51
32 Porkchop plot displaying the values of ΔP from equation (14). Indicates the possibilities of performing a free-return trajectory for all possible Earth-Mars trajectories in the 2033 launch opportunity. 51
33 Porkchop plot for a Mars transfer in the 2035 launch opportunity (Type A trajectory). The red, dashed line indicates the minimum Δv trajectory, the blue, dashed line the minimum possible time of flight trajectory. 52
34 Porkchop plot for a Mars transfer in the 2035 launch opportunity (Type B trajectory). The red, dashed line indicates the minimum Δv trajectory, the blue, dashed line the minimum possible time of flight trajectory. 54
35 Comparison of trajectory types for a Mars transfer in the 2035 launch opportunity. The left figure displays the values for a Type A trajectory, the right figure for a Type B trajectory. 55
36 Porkchop plot indicating the maximum payload masses that can be brought to Mars for a transfer in the 2035 launch opportunity. The left figure displays the values for a Type A trajectory, the right figure for a Type B trajectory. 56
37 Porkchop plot displaying the values of ΔP from equation (14). Indicates the possibilities of performing a free-return trajectory for all possible Earth-Mars trajectories in the 2035 launch opportunity. 56
38 Porkchop plot for a Mars transfer in the 2037 launch opportunity (Type A trajectory). The red, dashed line indicates the minimum Δv trajectory, the blue, dashed line the minimum possible time of flight trajectory. 57
39 Porkchop plot for a Mars transfer in the 2037 launch opportunity (Type B trajectory). The red, dashed line indicates the minimum Δv trajectory, the blue, dashed line the minimum possible time of flight trajectory. 58
40 Comparison of trajectory types for a Mars transfer in the 2037 launch opportunity. The left figure displays the values for a Type A trajectory, the right figure for a Type B trajectory. 59

41 Porkchop plot indicating the maximum payload masses that can be brought to Mars for a transfer in the 2037 launch opportunity. The left figure displays the values for a Type A trajectory, the right figure for a Type B trajectory. 60
42 Porkchop plot displaying the values of ΔP from equation (14). Indicates the possibilities of performing a free-return trajectory for all possible Earth-Mars trajectories in the 2037 launch opportunity. 60
43 Porkchop plot for a return flight from Mars to Earth in 2030 and 2031. The red line marks the minimum Δv trajectory and the blue line marks the minimum time of flight trajectory. 63
44 Porkchop plot for a return flight from Mars to Earth in 2033. The red line marks the minimum Δv trajectory and the blue line marks the minimum time of flight trajectory. 63
45 Porkchop plot for a return flight from Mars to Earth in 2035. The red line marks the minimum Δv trajectory and the blue line marks the minimum time of flight trajectory. 64
46 Porkchop plot for a return flight from Mars to Earth in 2037. The red line marks the minimum Δv trajectory and the blue line marks the minimum time of flight trajectory. 65
47 Porkchop plot for a return flight from Mars to Earth in 2039. The red line marks the minimum Δv trajectory and the blue line marks the minimum time of flight trajectory. 65
48 Porkchop plot displaying the values of Δv for a transfer in the 2029 launch opportunity. The maximum value for $v_{p,M}$ was set to $7\,\mathrm{km\,s^{-1}}$. The red, dashed line indicates the minimum Δv trajectory, the blue, dashed line the minimum possible time of flight trajectory. 81
49 Porkchop plot displaying the values of Δv for a transfer in the 2029 launch opportunity. The maximum value for $v_{p,M}$ was set to $6.5\,\mathrm{km\,s^{-1}}$. The red, dashed line indicates the minimum Δv trajectory, the blue, dashed line the minimum possible time of flight trajectory. 82
50 Porkchop plot displaying the values of Δv for a transfer in the 2031 launch opportunity. The maximum value for $v_{p,M}$ was set to $7\,\mathrm{km\,s^{-1}}$. The red, dashed line indicates the minimum Δv trajectory, the blue, dashed line the minimum possible time of flight trajectory. 83
51 Porkchop plot displaying the values of Δv for a transfer in the 2031 launch opportunity. The maximum value for $v_{p,M}$ was set to $6.5\,\mathrm{km\,s^{-1}}$. The red, dashed line indicates the minimum Δv trajectory, the blue, dashed line the minimum possible time of flight trajectory. 84
52 Porkchop plot displaying the values of Δv for a transfer in the 2033 launch opportunity. The maximum value for $v_{p,M}$ was set to $7\,\mathrm{km\,s^{-1}}$. The red, dashed line indicates the minimum Δv trajectory, the blue, dashed line the minimum possible time of flight trajectory. 85
53 Porkchop plot displaying the values of Δv for a transfer in the 2033 launch opportunity. The maximum value for $v_{p,M}$ was set to $6.5\,\mathrm{km\,s^{-1}}$. The red, dashed line indicates the minimum Δv trajectory, the blue, dashed line the minimum possible time of flight trajectory. 86
54 Porkchop plot displaying the values of Δv for a transfer in the 2035 launch opportunity. The maximum value for $v_{p,M}$ was set to $7\,\mathrm{km\,s^{-1}}$. The red, dashed line indicates the minimum Δv trajectory, the blue, dashed line the minimum possible time of flight trajectory. 87

55 Porkchop plot displaying the values of Δv for a transfer in the 2035 launch opportunity. The maximum value for $v_{p,M}$ was set to $6.5\,\mathrm{km\,s^{-1}}$. The red, dashed line indicates the minimum Δv trajectory, the blue, dashed line the minimum possible time of flight trajectory. 88
56 Porkchop plot displaying the values of Δv for a transfer in the 2037 launch opportunity. The maximum value for $v_{p,M}$ was set to $7\,\mathrm{km\,s^{-1}}$. The red, dashed line indicates the minimum Δv trajectory, the blue, dashed line the minimum possible time of flight trajectory. 89
57 Porkchop plot displaying the values of Δv for a transfer in the 2037 launch opportunity. The maximum value for $v_{p,M}$ was set to $6.5\,\mathrm{km\,s^{-1}}$. The red, dashed line indicates the minimum Δv trajectory, the blue, dashed line the minimum possible time of flight trajectory. 90
58 Maximum possible Δv_{max} that can be applied by Starship for a varying propellant mass m_p. 92
59 Porkchop plot displaying the values of Δv for a transfer in the 2029 launch opportunity. The value for m_p was set to 1100 t. The red, dashed line indicates the minimum Δv trajectory, the blue, dashed line the minimum possible time of flight trajectory. 93
60 Porkchop plot displaying the values of Δv for a transfer in the 2029 launch opportunity. The value for m_p was set to 1000 t. The red, dashed line indicates the minimum Δv trajectory, the blue, dashed line the minimum possible time of flight trajectory. 93
61 Porkchop plot displaying the values of Δv for a transfer in the 2029 launch opportunity. The value for m_p was set to 900 t. The red, dashed line indicates the minimum Δv trajectory, the blue, dashed line the minimum possible time of flight trajectory. 94
62 Porkchop plot displaying the values of Δv for a transfer in the 2029 launch opportunity. The value for m_p was set to 800 t. The red, dashed line indicates the minimum Δv trajectory, the blue, dashed line the minimum possible time of flight trajectory. 95
63 Porkchop plot displaying the values of Δv for a transfer in the 2031 launch opportunity. The value for m_p was set to 1100 t. The red, dashed line indicates the minimum Δv trajectory, the blue, dashed line the minimum possible time of flight trajectory. 96
64 Porkchop plot displaying the values of Δv for a transfer in the 2031 launch opportunity. The value for m_p was set to 1000 t. The red, dashed line indicates the minimum Δv trajectory, the blue, dashed line the minimum possible time of flight trajectory. 96
65 Porkchop plot displaying the values of Δv for a transfer in the 2031 launch opportunity. The value for m_p was set to 900 t. The red, dashed line indicates the minimum Δv trajectory, the blue, dashed line the minimum possible time of flight trajectory. 97
66 Porkchop plot displaying the values of Δv for a transfer in the 2031 launch opportunity. The value for m_p was set to 800 t. The red, dashed line indicates the minimum Δv trajectory, the blue, dashed line the minimum possible time of flight trajectory. 97

67 Porkchop plot displaying the values of Δv for a transfer in the 2033 launch opportunity. The value for m_p was set to 1100 t. The red, dashed line indicates the minimum Δv trajectory, the blue, dashed line the minimum possible time of flight trajectory. 98
68 Porkchop plot displaying the values of Δv for a transfer in the 2033 launch opportunity. The value for m_p was set to 1000 t. The red, dashed line indicates the minimum Δv trajectory, the blue, dashed line the minimum possible time of flight trajectory. 99
69 Porkchop plot displaying the values of Δv for a transfer in the 2033 launch opportunity. The value for m_p was set to 900 t. The red, dashed line indicates the minimum Δv trajectory, the blue, dashed line the minimum possible time of flight trajectory. 99
70 Porkchop plot displaying the values of Δv for a transfer in the 2033 launch opportunity. The value for m_p was set to 800 t. The red, dashed line indicates the minimum Δv trajectory, the blue, dashed line the minimum possible time of flight trajectory. 100
71 Porkchop plot displaying the values of Δv for a transfer in the 2035 launch opportunity. The value for m_p was set to 1100 t. The red, dashed line indicates the minimum Δv trajectory, the blue, dashed line the minimum possible time of flight trajectory. 101
72 Porkchop plot displaying the values of Δv for a transfer in the 2035 launch opportunity. The value for m_p was set to 1000 t. The red, dashed line indicates the minimum Δv trajectory, the blue, dashed line the minimum possible time of flight trajectory. 101
73 Porkchop plot displaying the values of Δv for a transfer in the 2035 launch opportunity. The value for m_p was set to 900 t. The red, dashed line indicates the minimum Δv trajectory, the blue, dashed line the minimum possible time of flight trajectory. 102
74 Porkchop plot displaying the values of Δv for a transfer in the 2035 launch opportunity. The value for m_p was set to 800 t. The red, dashed line indicates the minimum Δv trajectory, the blue, dashed line the minimum possible time of flight trajectory. 103
75 Porkchop plot displaying the values of Δv for a transfer in the 2037 launch opportunity. The value for m_p was set to 1100 t. The red, dashed line indicates the minimum Δv trajectory, the blue, dashed line the minimum possible time of flight trajectory. 103
76 Porkchop plot displaying the values of Δv for a transfer in the 2037 launch opportunity. The value for m_p was set to 1000 t. The red, dashed line indicates the minimum Δv trajectory, the blue, dashed line the minimum possible time of flight trajectory. 104
77 Porkchop plot displaying the values of Δv for a transfer in the 2037 launch opportunity. The value for m_p was set to 900 t. The red, dashed line indicates the minimum Δv trajectory, the blue, dashed line the minimum possible time of flight trajectory. 105
78 Porkchop plot displaying the values of Δv for a transfer in the 2037 launch opportunity. The value for m_p was set to 800 t. The red, dashed line indicates the minimum Δv trajectory, the blue, dashed line the minimum possible time of flight trajectory. 105

79 Porkchop plot for the nominal transfer. The red, dashed line indicates the minimum Δv trajectory, the blue, dashed line the minimum possible time of flight trajectory. 107
80 Porkchop plot for the transfer considering an aggressive margin approach. The red, dashed line indicates the minimum Δv trajectory, the blue, dashed line the minimum possible time of flight trajectory. 107
81 Porkchop plot for the nominal transfer. The red, dashed line indicates the minimum Δv trajectory, the blue, dashed line the minimum possible time of flight trajectory. 108
82 Porkchop plot for the transfer considering a mean margin approach. The red, dashed line indicates the minimum Δv trajectory, the blue, dashed line the minimum possible time of flight trajectory. 108
83 Porkchop plot for the nominal transfer. The time of flight was extended to 200 days to enable a comparison. The red, dashed line indicates the minimum Δv trajectory, the blue, dashed line the minimum possible time of flight trajectory. . 109
84 Porkchop plot for the transfer considering a conservative margin approach. The red, dashed line indicates the minimum Δv trajectory, the blue, dashed line the minimum possible time of flight trajectory. 110

List of Tables

2 Overview of the required Δv for the TCM of different Mars lander missions . . . 17
3 Overview of the achieved landing accuracy of different Mars lander missions . . . 17
4 Δv required for landing on Mars depending on the payload mass 18
5 Comparison of the different methods for modelling the planets' movement 26
6 Trip times for an Earth-Mars transfer proposed by SpaceX 34
7 Overview over the parameters for the flight from Earth to Mars 37
8 Δv values for the different maneuvers (Minimum Δv in 2029, Type A) 38
9 Δv values for the different maneuvers (Minimum TOF in 2029, Type A) 39
10 Δv values for the different maneuvers (Minimum Δv in 2029, Type B) 40
11 Δv values for the different maneuvers (Minimum TOF in 2029, Type B) 40
12 Δv values for the different maneuvers (Minimum Δv in 2031, Type A) 43
13 Δv values for the different maneuvers (Minimum TOF in 2031, Type A) 44
14 Δv values for the different maneuvers (Minimum Δv in 2031, Type B) 45
15 Δv values for the different maneuvers (Minimum TOF in 2031, Type B) 45
16 Δv values for the different maneuvers (Minimum Δv in 2033, Type A) 48
17 Δv values for the different maneuvers (Minimum TOF in 2033, Type A) 49
18 Δv values for the different maneuvers (Minimum TOF in 2033, Type B) 50
19 Δv values for the different maneuvers (Minimum Δv in 2035, Type A) 53
20 Δv values for the different maneuvers (Minimum TOF in 2035, Type A) 53
21 Δv values for the different maneuvers (Minimum TOF in 2035, Type B) 54
22 Δv values for the different maneuvers (Minimum Δv in 2037, Type A) 57
23 Δv values for the different maneuvers (Minimum TOF in 2037, Type A) 58
24 Δv values for the different maneuvers (Minimum TOF in 2037, Type B) 58
25 Overview over the performance parameters for the different launch opportunities 61
26 Overview over the fixed parameters for the return flight 62
27 Performance parameters for different delays in the 2029 launch opportunity . . . 69
28 Performance parameters for different delays in the 2031 launch opportunity . . . 70
29 Performance parameters for different delays in the 2033 launch opportunity . . . 71
30 Performance parameters for different delays in the 2035 launch opportunity . . . 71
31 Performance parameters for different delays in the 2037 launch opportunity . . . 72
32 Performance parameters for different time of flights during the 2029 launch opportunity 73
33 Performance parameters for different time of flights during the 2031 launch opportunity 74
34 Performance parameters for different time of flights during the 2033 launch opportunity 74
35 Performance parameters for different time of flights during the 2035 launch opportunity 75
36 Performance parameters for different time of flights during the 2037 launch opportunity 75
37 Performance parameters for different specific impulses in the 2029 launch opportunity 77
38 Performance parameters for different specific impulses in the 2031 launch opportunity 78
39 Performance parameters for different specific impulses in the 2033 launch opportunity 78

40 Performance parameters for different specific impulses in the 2035 launch opportunity 79
41 Performance parameters for different specific impulses in the 2037 launch opportunity 80
42 Comparison of key performance parameter values for a maximum hyperbolic periapse velocity $v_{p,M,max} = 7\,\mathrm{km\,s^{-1}}$ with the nominal velocity for a transfer during the 2029 launch opportunity. 82
43 Comparison of key performance parameter values for a maximum hyperbolic periapse velocity $v_{p,M,max} = 6.5\,\mathrm{km\,s^{-1}}$ with the nominal velocity for a transfer during the 2029 launch opportunity. 83
44 Comparison of key performance parameter values for a maximum hyperbolic periapse velocity $v_{p,M,max} = 7\,\mathrm{km\,s^{-1}}$ with the nominal velocity for a transfer during the 2031 launch opportunity. 84
45 Comparison of key performance parameter values for a maximum hyperbolic periapse velocity $v_{p,M,max} = 6.5\,\mathrm{km\,s^{-1}}$ with the nominal velocity for a transfer during the 2031 launch opportunity. 85
46 Comparison of key performance parameter values for a maximum hyperbolic periapse velocity $v_{p,M,max} = 7\,\mathrm{km\,s^{-1}}$ with the nominal velocity for a transfer during the 2033 launch opportunity. 86
47 Comparison of key performance parameter values for a maximum hyperbolic periapse velocity $v_{p,M,max} = 6.5\,\mathrm{km\,s^{-1}}$ with the nominal velocity for a transfer during the 2033 launch opportunity. The red, dashed line indicates the minimum Δv trajectory, the blue, dashed line the minimum possible time of flight trajectory. 87
48 Comparison of key performance parameter values for a maximum hyperbolic periapse velocity $v_{p,M,max} = 7\,\mathrm{km\,s^{-1}}$ with the nominal velocity for a transfer during the 2035 launch opportunity. 88
49 Comparison of key performance parameter values for a maximum hyperbolic periapse velocity $v_{p,M,max} = 6.5\,\mathrm{km\,s^{-1}}$ with the nominal velocity for a transfer during the 2035 launch opportunity. 88
50 Comparison of key performance parameter values for a maximum hyperbolic periapse velocity $v_{p,M,max} = 7\,\mathrm{km\,s^{-1}}$ with the nominal velocity for a transfer during the 2037 launch opportunity. 89
51 Comparison of key performance parameter values for a maximum hyperbolic periapse velocity $v_{p,M,max} = 6.5\,\mathrm{km\,s^{-1}}$ with the nominal velocity for a transfer during the 2037 launch opportunity. 90
52 Overview over the influence of the different margin approaches on the maximum payload mass, presented for all considered launch opportunities. The dashes indicate that no transfer is possible which fulfills the minimum requirements (I.e. a payload mass of at least 100 t while the flight time does not exceed 180 d). 110

References

[1] SpaceX. (2022). Starship. SpaceX [Website]. Retrieved May 30, 2022, from https://www.spacex.com/vehicles/starship/

[2] Sesnic, T. (2021, August 11). Starbase tour and interview with Elon Musk. Everyday Astronaut. Retrieved May 30, 2022, from https://everydayastronaut.com/starbase-tour-and-interview-with-elon-musk/

[3] Seedhouse, E. (2022). Chapter 9: Starship. In *SPACEX: Starship to Mars - the first 20 years* (pp. 171 - 180). SPRINGER NATURE.

[4] SpaceX. (2019). Chapter 2.1: Proposed Action. In *Draft Environmental Assessment for the SpaceX Starship and Super Heavy Launch Vehicle at Kennedy Space Center (KSC)*. National Aeronautics and Space Administration - Public NEPA Documents. Retrieved May 20, 2022 from https://netspublic.grc.nasa.gov/main/20190801_Final_DRAFT_EA_SpaceX_Starship.pdf

[5] Bibring, J.-P., Langevin, Y., Poulet, F., Gendrin, A., Gondet, B., Berthé, M., Soufflot, A., Drossart, P., Combes, M., Bellucci, G., Moroz, V., Mangold, N., Schmitt, B. & the OMEGA team. (2004). Perennial water ice identified in the south polar cap of Mars. Nature, 428(6983), 627 - 630. https://doi.org/10.1038/nature02461

[6] Vincendon, M., Forget, F. & Mustard, J. (2010). Water ice at low to Midlatitudes on Mars. Journal of Geophysical Research, 115(E10). https://doi.org/10.1029/2010je003584

[7] Bougher, S. W., Pawlowski, D., Bell, J. M., Nelli, S., McDunn, T., Murphy, J. R., Chizek, M. & Ridley, A. (2015). Mars global ionosphere-thermosphere model: Solar cycle, seasonal, and diurnal variations of the Mars Upper Atmosphere. Journal of Geophysical Research: Planets, 120(2), 311 - 342. https://doi.org/10.1002/2014je004715

[8] Rafkin, S. C. R. & Banfield, D. (2020). On the problem of a variable Mars atmospheric composition in the determination of temperature and density from the adiabatic speed of sound. Planetary and Space Science, 193, 105064. https://doi.org/10.1016/j.pss.2020.105064

[9] Golombek, M., Williams, N., Wooster, P., McEwen, A., Putzig, N., Bramson, A., Jead, J., Heldmann, J., Marinova, M. & Beaty, D. (2021). SpaceX Starship Landing Sites on Mars. 52nd Lunar and Planetary Science Conference.

[10] Wooster, P., Braun, R., Ahn, J. & Putnam, Z. (2007). Mission Design Options for Human Mars Missions. MARS. https://doi.org/10.1555/mars.2007.0002

[11] SpaceX. (2022). Mars & Beyond. SpaceX. Retrieved June 3, 2022, from https://www.spacex.com/human-spaceflight/mars/

[12] Jesick, M., Wong, M., Wagner, S., Kangas, J. & Kruizinga, G. (2022). Mars 2020 trajectory correction maneuver design. Journal of Spacecraft and Rockets, 1 - 12. https://doi.org/10.2514/1.a35263

[13] Martin - Mur, T. J., Kruizinga, G. L. & Wong, M. C. (2012). Mars Science Laboratory interplanetary navigaton analysis. Journal of Aerospace Engineering, Sciences and Applications, 4(2), 107 - 120. https://doi.org/10.7446/jaesa.0402.10

[14] Chung, M. - K., Hahn, Y., Halsell, A., McCandless, S., Sklyanskiy, E. & Wallace, M. (2019). Maneuver Design Overview of the 2018 Insight Mars Lander Mission. *29th Annual AAS/AIAA Space Flight Mechanics Meeting, 19-232*.

[15] Vaughan, R., Kallemeyn, P., Spence, D. & Braun, R. (1999). Navigation Flight Operations for Mars pathfinder. Journal of Spacecraft and Rockets, 36(3), 340 - 347. https://doi.org/10.2514/2.3476

[16] DAmario, L. A. (2006). Mars exploration rovers navigation results. The Journal of the Astronautical Sciences, 54(2), 153 - 155. https://doi.org/10.1007/bf03256481

[17] Mendeck, G. F. & Craig McGrew, L. C. (2014). Entry guidance design and postflight performance for 2011 Mars Science Laboratory Mission. Journal of Spacecraft and Rockets, 51(4), 1094 - 1105. https://doi.org/10.2514/1.a32737

[18] DAmario, L. A. (2006). Mars exploration rovers navigation results. The Journal of the Astronautical Sciences, 54(2), 169 - 171. https://doi.org/10.1007/bf03256481

[19] SpaceX. (2017, October 14). Vehicle Landing [Video]. YouTube. Retrieved May 20, 2022 from https://youtu.be/5seefpjMQJI

[20] Pezzella, G., Viviani, A. & Lu, Y. (2020). Chapter 3: Aerocapture, Aerobraking, and Entry for Robotic and Human Mars Missions. In *Mars exploration: A step forward.* (pp. 33 - 52). IntechOpen.

[21] SpaceX. (2016). Making life multiplanetary - 2016. [Online PDF]. SpaceX. Retrieved May 30, 2022 from https://www.spacex.com/media/making_life_multiplanetary_2016.pdf

[22] Zubrin, R. M., Muscatello, A. C. & Berggren, M. (2013). Integrated Mars in situ Propellant Production System. Journal of Aerospace Engineering, 26(1), 43 - 56. https://doi.org/10.1061/(asce)as.1943-5525.0000201

[23] Mellerowicz, B., Zacny, K., Palmowski, J., Bradley, B., Stolov, L., Vogel, B., Ware, L., Yen, B., Sabahi, D., Ridilla, A., Nguyen, H., Faris, D., van Susante, P., Johnson, G., Putzig, N. E. & Hecht, M. (2022). Redwater: Water Mining System for Mars. New Space, 10(2), 166 - 186. https://doi.org/10.1089/space.2021.0057

[24] Heldmann, J. L., Marinova, M. M., Lim, D. S. S., Wilson, D., Carrato, P., Kennedy, K., Esbeck, A., Colaprete, T. A., Elphic, R. C., Captain, J., Zacny, K., Stolov, L., Mellerowicz, B., Palmowski, J., Bramson, A. M., Putzig, N., Morgan, G., Sizemore, H. & Coyan, J. (2022). Mission architecture using the spacex starship vehicle to enable a sustained human presence on Mars. New Space. https://doi.org/10.1089/space.2020.0058

[25] Polsgrove, T. P., Percy, T., Rucker, M. & Thomas, H. (2019). Update to mars ascent vehicle design for human exploration. 2019 IEEE Aerospace Conference. https://doi.org/10.1109/aero.2019.8741709

[26] Larson, W. J. & Wertz, J. R. (2005). Chapter 18.2: Launch System Selection Process. In *Space mission analysis and design* (3rd ed., p. 722). Kluwer Academic Publishers.

[27] SpaceX. (2017). Making life multiplanetary - 2017. [Online PDF]. SpaceX. Retrieved July 09, 2022 from https://www.spacex.com/media/making_life_multiplanetary-2017.pdf

[28] Musk, E. (2022, May 30). 2029 feels like a pivotal year. I'd be surprised if we don't have AGI by then. hopefully, people on Mars too. Twitter. Retrieved June 21, 2022, from https://twitter.com/elonmusk/status/1531328534169493506?ref_src=twsrc%5Etfw%7Ctwcamp%5Etweetembed%7Ctwterm%5E1531328534169493506%7Ctwgr%5E%7Ctwcon%5Es1_&ref_url=https%3A%2F%2Fwww.techtimes.com%2Farticles%2F276107%2F20220530%2Felon-musk-2029-pivotal-year-E28094agi-people-mars-spacex-mission.htm

[29] Davies, P. (2022, May 9). Elon Musk's SpaceX COO says manned missions will reach Mars by 2030. NASA says otherwise. euronews. Retrieved June 21, 2022, from https://www.euronews.com/next/2022/05/09/elon-musk-s-spacex-coo-says-manned-missions-will-reach-mars-by-2030-nasa-says-otherwise

[30] Portree, D. S. F. (2001). Chapter 3: EMPIRE and After. In *Humans to Mars: Fifty Years of Mission Planning, 1950-2000* (p. 18). NASA History Division, Office of Policy and Plans, NASA Headquarters.

[31] Vallado, D. A. & McClain, W. D. (2013). Chapter 7.6: Two Position Vectors and Time - Lambert's Problem. In *Fundamentals of astrodynamics and applications* (4. Edition, p. 467). Microcosm Press.

[32] Prussing, J. E. & Conway, B. A. (1993). Chapter 4.4.: Properties of the Solutions to Lambert's Equation. In *Orbitals Mechanics* (1. Edition, pp. 70 - 75). Oxford University Press.

[33] Vallado, D. A. & McClain, W. D. (2013). Chapter 7.6.1: Lambert - Minimum Energy. In *Fundamentals of astrodynamics and applications* (4. Edition, pp. 470 - 475). Microcosm Press.

[34] Vallado, D. A. & McClain, W. D. (2013). Fundamentals of astrodynamics and applications (4. Edition). Microcosm Press.

[35] Vallado, D. A. & McClain, W. D. (2013). Chapter 7.6.5.: Lambert Solution - Battin Method. In *Fundamentals of astrodynamics and applications* (4. Edition, pp. 493 - 497). Microcosm Press.

[36] Battin, R. H. & Vaughan, R. M. (1984). An elegant Lambert algorithm. Journal of Guidance, Control, and Dynamics, 7(6), 662 - 670. https://doi.org/10.2514/3.19910

[37] Seidelmann, P. K. (1992). Chapter 5.8.: Keplerian elements for the positions of the major planets. In *Explanatory supplement to the astronomical almanac* (1. Edition, pp. 315 - 316). University Science Books.

[38] Vallado, D. A. & McClain, W. D. (2013). Chapter 12.2.: Patched Conic Trajectories. In *Fundamentals of astrodynamics and applications* (4. Edition, pp. 944 - 954). Microcosm Press.

[39] European Space Agency. (2012). Chapter 2.3: Delta-V margins. In *Margin philosophy for science assessment studies.* [Online PDF]. European Space Agency. Retrieved June 18, 2022 from https://sci.esa.int/documents/34375/36249/1567260131067-Margin_philosophy_for_science_assessment_studies_1.3.pdf

[40] Musk, E. (2016). IAC 2016 - Late Breaking News: Making Humans a Multiplanetary Species. YouTube. Retrieved June 21, 2022, from https://www.youtube.com/watch?v=WVacRKN1tAo

[41] Aerojet Rocketdyne. (2022). RL10 PROPULSION SYSTEM [Online PDF]. Retrieved July 16, 2022, from https://www.rocket.com/sites/default/files/documents/RL10_data_sheet.pdf

[42] Polk, J. E., Kakuda, R. Y., Anderson, J. R., Brophy, J. R., Rawlin, V. K., Sovey, J. & Hamley, J. (2000). In-flight performance of the NSTAR Ion Propulsion System on the Deep Space one mission. 2000 IEEE Aerospace Conference. Proceedings (Cat. No.00TH8484). https://doi.org/10.1109/aero.2000.878373

Appendix A1: Solving Kepler's equation with Halley's method

```
function E = KeplerHalley(e,M)
%  Halley's method to solve Kepler's equation
%  Input
%  e is the eccentricity of the orbit
%  M is the mean anomaly
%  Output
%  E is the eccentric anomaly
%  Calculations
    x0 = 0;
    x1 = M;
    while abs(x1 - x0) > 10^-12
        x0 = x1;
        fx = x0 - e * sin(x0) - M;  % Kepler's equation
        dfx = 1 - e * cos(x0);      % Derivative of Kepler's equation
        d2fx = e * sin(x0);         % Second derivative of Kepler's equation
        x1 = x0 - ((2*fx*dfx)/((2*(dfx^2))-(fx*d2fx))); % Halley's method
    end
    E = x1;
end
```

Published with MATLAB® R2022a

Appendix A2: Lambert solver

```
function [dv_A,dv_B,a,mpl_A,mpl_B,dve,dvm] =
 LambertBattin(r1,r2,TOF,ve,vm,rp_e,rp_m,mpl,Isp,ms)
%  Lambert solver implementation according to Vallado2013, Algorithm 59, p.
 494f.
%  Based on Battin's method
%  Input
%  r1 is position vector of earth at departure in astronomic units
%  r2 is position vector of mars at arrival in astronomic units
%  TOF is desired time of flight in days
%  ve is the velocity of Earth at departure relative to the Sun in kilometers
 per second
%  vm is the velocity of Mars at arrival relative to the Sun in kilometers per
 second
%  rp_e is the altitude of the parking orbit around Earth in kilometers
%  rp_m is the periapsis altitude of the arrival hyperbola at Mars in
 kilometers
%  mpl is the payload that should be brought to Mars in metric tons
%  Isp is the specific impulse of the Raptor engine in seconds
%  ms is the structural mass of Starship in metric tons
%  Output
%  dv_A is total delta-v required for mission on a Type A trajectory
%  dv_B is total delta-v required for mission on a Type B trajectory
%  a is the semi-major axis of the transfer ellipse
%  mpl_A is the maximum payload to Mars on a Type A trajectory
%  mpl_B is the maximum payload to Mars on a Type B trajectory
%  dve is the required delta v for the TOI
%  dvm is the required delta v for the MOI
%  Calculations
    mu = 1.32712440018*10^11; % [km^3.s^(-2)]
    r1 = AU2km(r1); % [km]
    r2 = AU2km(r2); % [km]
    u1 = r1/norm(r1);
    u2 = r2/norm(r2);
    TOF = TOF * (24*60*60); % [s]
    r0 = norm(r1);
    r = norm(r2);
    delta = finddelta(u1,u2);
% The following equations are described in Vallado2013, Algorithm 59, p. 494f.
    cdv = cos(delta);
    c = sqrt(r0^2+r^2-2*r0*r*cdv);
    s = (r0 + r + c)/2;
    eps = (r-r0)/r0;
    tan22w = (eps^2/4)/(sqrt(r/r0)+(r/r0)*(2+sqrt(r/r0)));
    rop = sqrt(r0*r)*(cos(delta/4)^2+tan22w);
    if delta < pi
        l = (sin(delta/4)^2+tan22w)/(sin(delta/4)^2+tan22w+cos(delta/2));
    else
        l = (sin(delta/4)^2+tan22w-cos(delta/2))/(sin(delta/4)^2+tan22w);
    end
    m = (mu*TOF^2)/(8*rop^3);
```

```
    x_prev = l-1;
    x = l;
    for n = 5:1:6
        c_eta(n-4) = n^2/((2*n)^2-1);
    end
    for nu = 0:1:10
        if mod(nu,2) == 0 % even
            c_U(nu+1) = (2*(3*nu+1)*(6*nu-1))/(9*(4*nu-1)*(4*nu+1));
        else % odd
            c_U(nu+1) = (2*(3*nu+2)*(6*nu+1))/(9*(4*nu+1)*(4*nu+3));
        end
    end
    while (x/x_prev > 1+10^-6 || x/x_prev < 1-10^-6)
        eta = x/(sqrt(1+x)+1)^2;
        xi = (8*(sqrt(1+x)+1)/(3+(1/(5+eta+((9/7)*eta)/(1+((16/63)*eta)/
(1+(c_eta(1)*eta)/(1+(c_eta(2)*eta)/(1))))))));
        h1 = ((l+x)^2*(1+3*x+xi))/((1+2*x+l)*(4*x+xi*(3+x)));
        h2 = (m*(x-l+xi))/((1+2*x+l)*(4*x+xi*(3+x)));
        B = (27*h2)/(4*(1+h1)^3);
        U = B/(2*(sqrt(1+B)+1));
        K = (1/3)/(1+(c_U(1)/(1+c_U(2)/(1+c_U(3)/(1+c_U(4)/(1+c_U(5)/
(1+c_U(6)/(1+c_U(7)/(1+c_U(8)/(1+c_U(9)/(1+c_U(10)/(1+c_U(11))))))))))));
        y = ((1+h1)/3)*(2+((sqrt(1+B))/(1+2*U*K^2)));
        x_prev = x;
        x = sqrt(((1-l)/2)^2+(m/y^2))-(1+l)/2;
    end
    a = (mu*TOF^2)/(16*rop^2*x*y^2);
    if a > 0
        beta_e = 2*asin(sqrt((s-c)/(2*a)));
        if delta > pi
            beta_e = -beta_e;
        end
        amin = s/2;
        tmin = sqrt(amin^3/mu)*(pi-beta_e+sin(beta_e));
        alpha_e = 2*asin(sqrt(s/(2*a)));
        if TOF > tmin
            alpha_e = 2*pi - alpha_e;
        end
        dE = alpha_e - beta_e;
        f = 1-(a/r0)*(1-cos(dE));
        g = TOF - sqrt(a^3/mu)*(dE-sin(dE)); % [s]
        gdot = 1-(a/r)*(1-cos(dE));
    else
        alpha_h = 2*asinh(sqrt(s/(-2*a)));
        beta_h = 2*asinh(sqrt((s-c)/(-2*a)));
        dH = alpha_h - beta_h;
        f = 1-(a/r0)*(1-cosh(dH));
        g = TOF - sqrt((-a^3)/mu)*(sinh(dH)-dH);
        gdot = 1-(a/r)*(1-cosh(dH));
    end
    v1 = (r2-f*r1)/g;   % Needed velocity at Earth on the transfer ellipse
    v2 = (gdot*r2-r1)/g;% Needed velocity at Mars on the transfer ellipse
    dv1 = v1 - ve;
    dv2 = vm - v2;
```

```
    [dv_A,dv_B,mpl_A,mpl_B,dve,dvm] =
 PatchedConics(rp_e,rp_m,norm(dv1),norm(dv2),mpl,Isp,ms);
end
```

Published with MATLAB® R2022a

Appendix A3: Implementation of the patched conics approach

```
function [dv_A,dv_B,mpl_A,mpl_B,dve,dvm] =
 PatchedConics(rp_e,rp_m,v1,v2,mpl,Isp,ms)
% This function computes the required delta v for the mission with the
% patched conics approach
%  Input
%  rp_e is the altitude of the parking orbit around Earth in kilometers
%  rp_m is the periapsis altitude of the arrival hyperbola at Mars in
 kilometers
%  v1 is the needed velocity at Earth on the transfer ellipse according to
 lambert's problem
%  v2 is the needed velocity at Mars on the transfer ellipse according to
 lambert's problem
%  mpl is the payload that should be brought to Mars in metric tons
%  Isp is the specific impulse of the Raptor engine in seconds
%  ms is the structural mass of Starship in metric tons
%  Output
%  dv_A is total delta-v required for mission on a Type A trajectory
%  dv_B is total delta-v required for mission on a Type B trajectory
%  mpl_A is the maximum payload to Mars on a Type A trajectory
%  mpl_B is the maximum payload to Mars on a Type B trajectory
%  dve is the required delta v for the TOI
%  dvm is the required delta v for the MOI
%  Calculations
    mu_e = 3.986004418*10^5; % Gravitational parameter of Earth [km^3/s^2]
    mu_m = 4.282837*10^4;    % Gravitational parameter of Mars [km^3/s^2]

    mp = 1200; % Propellant mass onboard Starship at departure

    v_lim = 7.5; % Maximum allowable hyperbolic periapse velocity at Mars

    % At Earth
    vp = sqrt(v1^2 + 2*mu_e/(6378+rp_e)); % Required hyperbolic periapse
 velocity at Earth departure
    vc = sqrt(mu_e/(6378+rp_e));          % Circular velocity in Earth orbit
    dve = vp - vc;                      % Required delta v at Earth

    % At Mars
    vp_hyp = sqrt(v2^2 + 2*mu_m/(3390+rp_m)); % Required hyperbolic periapse
 velocity at Mars arrival
    if vp_hyp > v_lim   % Only aerobraking at Mars is not sufficient
        dvm = vp_hyp - v_lim; % Required delta v at Mars
    else                % Only aerobraking at Mars is sufficient
        dvm = 0;              % Required delta v at Mars (= 0)
    end
    dv_landing = ((2.088 * mpl + 367.53)/1000); % Required delta v for landing
 on Mars
    dv_TCM = 0.2; % Required delta v for TCM
```

```
    dv_A = 1.05*(dve + dvm + dv_landing) + 2*dv_TCM; % Total delta v including
 margins
    dvmax = Tsiolkowski(mpl,Isp,ms,mp); % Maximum obtainable delta v by
 Starship
    if dv_A > dvmax % Exclusion of impossible trajectories
        dv_A = NaN;
        mpl_A = NaN;
    else
        mpl_A = Payload(Isp,ms,dve,dvm,dv_TCM,mp); % Maximum possible payload
 mass to Mars
    end
    % Type B trajectories
    if vp_hyp > v_lim
        dv_B = NaN;
        mpl_B = NaN;
    else
        dv_B = dv_A;
        mpl_B = mpl_A;
    end
    % Only for return of values
    dve = 1.05 * dve;
    dvm = 1.05 * dvm;
end
```

Published with MATLAB® R2022a